Volume 70C
Number 3
July–Sept. 1966

Engineering and Instrumentation

U.S. DEPARTMENT OF COMMERCE

SECTION C

JOURNAL OF RESEARCH

NATIONAL BUREAU OF STANDARDS

Journal of Research

of the

National Bureau of Standards

C. Engineering and Instrumentation

July–Sept. • 1966

VOLUME • 70C

NUMBER • 3

Editor: Martin Greenspan

Associate Editors: G. F. Montgomery, R. V. Smith, and A. Schmidt

Publication dates:
Feb. 15, May 15, Aug. 15, Nov. 15, 1966

JOURNAL OF RESEARCH

The National Bureau of Standards Journal of Research reports research and development in the fields of activity shown at right. Also included from time to time are survey articles on topics closely related to the Bureau's scientific and technical program.

The Journal is published in three separate sections as follows:

A. Physics and Chemistry

Contains papers of interest primarily to scientists working in these fields. Issued six times a year. Annual subscription: domestic, $5.00; foreign, $6.00. Single copy, $1.00.

B. Mathematics and Mathematical Physics

Presents studies and compilations designed mainly for the mathematician and the theoretical physicist. Issued quarterly. Annual subscription: domestic, $2.25; foreign, $2.75. Single copy, 75¢.

C. Engineering and Instrumentation

Reports research and development results of interest chiefly to the engineer and the applied scientist. Issued quarterly. Annual subscription: domestic, $2.75; foreign, $3.50. Single copy, 75¢.

The National Bureau of Standards is a principal focal point in the Federal Government for assuring maximum application of the physical and engineering sciences to the advancement of technology in industry and commerce. Its responsibilities include development and maintenance of the national standards of measurement, and the provisions of means for making measurements consistent with those standards; determination of physical constants and properties of materials; development of methods for testing materials, mechanisms, and structures, and making such tests as may be necessary, particularly for government agencies; cooperation in the establishment of standard practices for incorporation in codes and specifications; advisory service to government agencies on scientific and technical problems; invention and development of devices to serve special needs of the Government; assistance to industry, business, and consumers in the development and acceptance of commercial standards and simplified trade practice recommendations; administration of programs in cooperation with United States business groups and standards organizations for the development of international standards of practice; and maintenance of a clearinghouse for the collection and dissemination of scientific, technical, and engineering information. The scope of the Bureau's activities is suggested in the following listing of its three Institutes and their organizational units.

Institute for Basic Standards. Applied Mathematics. Electricity. Metrology. Mechanics. Heat. Atomic Physics. Physical Chemistry. Laboratory Astrophysics.* Radiation Physics. Radio Standards Laboratory:* Radio Standards Physics; Radio Standards Engineering. Office of Standard Reference Data.

Institute for Materials Research. Analytical Chemistry. Polymers. Metallurgy. Inorganic Materials. Reactor Radiations. Cryogenics.* Materials Evaluation Laboratory. Office of Standard Reference Materials.

Institute for Applied Technology. Building Research. Information Technology. Performance Test Development. Electronic Instrumentation. Textile and Apparel Technology Center. Technical Analysis. Office of Weights and Measures. Office of Engineering Standards. Office of Invention and Innovation. Office of Technical Resources. Clearinghouse for Federal Scientific and Technical Information.**

*Located at Boulder, Colo. 80302.
**Located at 5285 Port Royal Road, Springfield, Va. 22151.

U.S. DEPARTMENT OF COMMERCE
John T. Connor, Secretary
NATIONAL BUREAU OF STANDARDS
A. V. Astin, Director

Order all publications from the Superintendent of Documents
U.S. Government Printing Office, Washington, D.C., 20402.

Use of funds for printing this publication approved by the Director of the Bureau of the Budget (June 22, 1966).

JOURNAL OF RESEARCH of the National Bureau of Standards—C. Engineering and Instrumentation
Vol. 70C, No. 3, July–September 1966

Some Harmonic Properties of an Oscillating Fabry-Perot Interferometer

M. Gadsden* and H. M. Williams*

(March 9, 1966)

The transmission of a spectral line through an air spaced Fabry-Perot interferometer is considered. The harmonic components of the transmission when the spacing of the interferometer is oscillated are discussed and it is found that the components can be used in a servocontrol system to offset drifts in the optical thickness of the interferometer. A possible use of such a controlled system in observations of the night airglow is discussed.

Key Words: Fabry-Perot interferometer, airglow photometry.

1. Introduction

In two recent papers, Mielenz et al. [1, 2], have discussed Fabry-Perot interferometers which use plates whose separation can be controlled electrically. The spacers in these interferometers are made from a piezoelectric ceramic material, lead zirconate-titanate, and the plate separation is thus directly, and easily, controllable by the application of an electric potential across two faces of the material. Mielenz et al., (loc. cit.) present full details of the use of this material and discuss the advantages and some applications of this piezoelectric scanning technique; it is the purpose of this paper to point out that the harmonic output of such a system has some advantages in the servocontrolling of the spacing of an interferometer.

The use of oscillating piezoelectric spacers to control the spacing and parallelism of a Fabry-Perot interferometer was first described by Ramsay [3]. In Ramsay's system, two passes of the interferometer by white light are used, and equality and constancy of the path length in the interferometer along the two light beams is maintained by seeking the maximum transmission for white light. The servocontrol to seek this maximum involves a minute superposed oscillation to give an error signal. The servocontrol to be described in what follows is similar to Ramsay's system except that the control for constancy of interferometer spacing is achieved from the spectral emission being observed with the interferometer, and does not demand subsidiary white light illumination.

*Institute of Telecommunication Science and Aeronomy, Environmental Science Services Administration, Boulder Colo. Formerly the Central Radio Propagation Laboratory of the National Bureau of Standards.

2. Harmonic Analysis of the Output

As is well known [4], the transmission at normal incidence of a perfect Fabry-Perot interferometer is given by the Airy relation

$$\frac{I}{I_m}=\frac{1}{1+F\sin^2(2\pi D)} \tag{1}$$

where D = optical thickness, in wavelengths, of the interferometer i.e., half the order,
I = transmitted intensity of a spectral line, whose width is much less than the instrumental width;
I_m = transmitted intensity when $D=\frac{n}{2}$, n being any integer,
and F = a constant, dependent on the reflectivity of the coatings on the interferometer plates.

F is related to the *finesse*, $\mathscr{F}$, of the interferometer by the relation [4]

$$F=\left(\frac{2\mathscr{F}}{\pi}\right)^2.$$

If a sinusoidal potential be applied to the piezoelectric spacers of an interferometer, D in expression (1) will become $(d_0+d\cos 2\pi ft)$, where f is the frequency of the alternating potential and d is half the total excursion in length of the spacers. In these circumstances, I/I_m becomes a periodic function of time, t, with a period equal to $1/f$. The function, I/I_m, will contain a series of harmonics of f; we shall direct our attention to the amplitudes of the zeroth, first and second harmonics in what follows, with the convention that the nth harmonic has the frequency nf.

The harmonic amplitudes and phases contained in I/I_m will vary as $2d_0$ is an integer or not. This is readily seen from figure 1, in which is sketched, from top to bottom,

(i) The variation of I/I_m as a function of plate separation, d_0;

(ii) two spacer oscillations, (A) and (B), with $d=1/2$ and d_0 at the positions indicated;

(iii) the outputs resulting from the applied spacer oscillations, and

(iv) two more outputs resulting from spacer oscillations with $d=1/2$ and d_0 at the marked positions, (C) and (D).

It is readily seen that the second harmonic predominates in (A) and (B) and that the first harmonic predominates in (C) and (D). Photographs of oscilloscope traces showing approximations to these conditions are shown in figure 2; note, in both figure 1 and figure 2, that there is a change in phase of the output between (C) and (D).

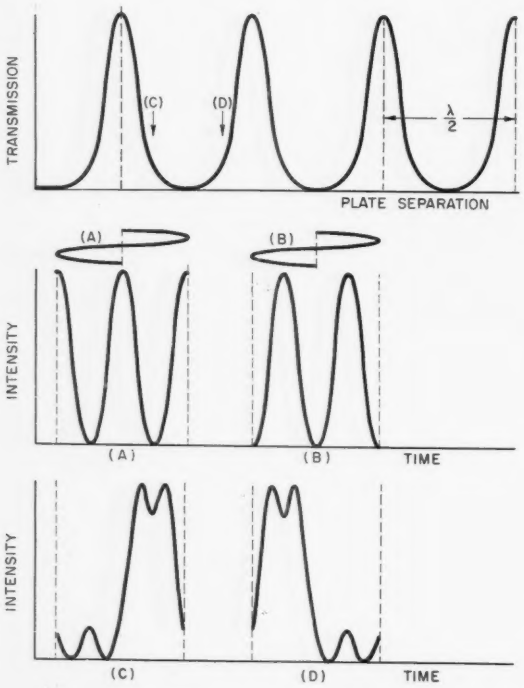

FIGURE 1. *Top: the variation in transmission of monochromatic radiation by a Fabry-Perot interferometer, as the separation of the plates is increased.*

Middle: the time variation of the transmitted intensity when the plate separation is oscillated over the ranges indicated by (A) and (B).

Bottom: the time variations resulting from spacer oscillations equal in amplitude to (A) and (B), but centered at the points (C) and (D) indicated in the top sketch.

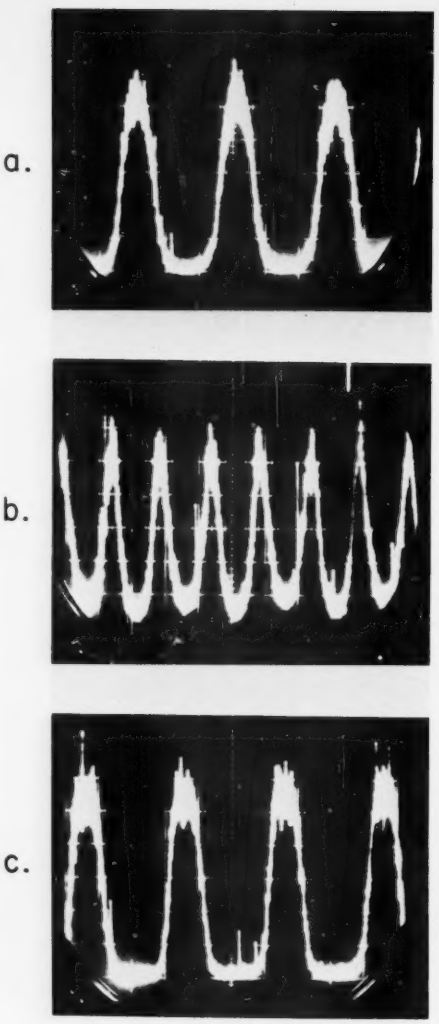

FIGURE 2. *Oscillograms of an oscillating interferometer corresponding to three settings of the mean spacing.*

Numerical harmonic analysis of I/I_m has given the results shown in figure 3. The amplitudes of the harmonics depend on whether $2d_0$ is an integer, i.e., if we write

$$d_0=\tfrac{1}{2}(n+\epsilon),$$

where $\epsilon<1$ and n is integral, all possible variations of d_0 are covered by varying ϵ. In figure 3, therefore, the abscissae are given in terms of $\epsilon/2$, with the limits $0, +0.5$.

The upper plot in figure 3 is for an interferometer with a finesse of 10, and d equal to 0.25. With this amount of driving potential, the point of interest is that the second harmonic is a maximum at the value of ϵ

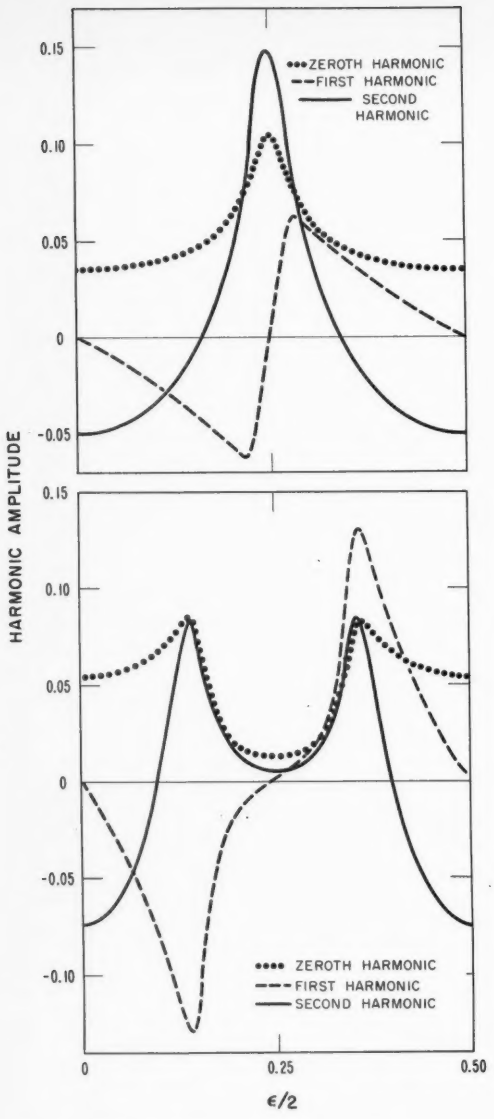

FIGURE 3. *Harmonic amplitudes of transmitted monochromatic radiation as a function of the departure of the mean spacing from an integral of half-wave lengths.*

where the first harmonic is zero (and where, also, it changes phase). This, because of the symmetry of I/I_m, holds for all values of the finesse so long as $d=0.25$. When d is either increased or decreased, the null point of the first harmonic remains at $\epsilon/2=0.25$, but the second harmonic shows two maxima at progressively increasing distances from $\epsilon/2=0.25$. (When d is increased to 0.5, then the two maxima of the second harmonic recombine at $\epsilon/2=0$, 0.5, where the first harmonic has another null point.) The lower plot in figure 3 shows the effect of reducing d to 0.15.

This property of the second harmonic going to a maximum where the first harmonic is zero and changing phase, is of immediate application in using a servosystem to control the mean optical thickness, d_0, of the interferometer. d_0 is related to the metric thickness, d^*, of the air layer between the interferometer plates by

$$d_0=\frac{\mu d^*}{\lambda_0}, \tag{3}$$

in which μ is the refractive index of the air in the interferometer and λ_0 is the wavelength in vacuo of the observed emission line. μ is, of course, dependent on the temperature and pressure of the air and, in the course of time, can be expected to show small changes; more important, however, is the temperature dependence of d^* through the thermal expansion of the spacer material. It is easy, however, to compensate for these changes in d^* and μ by arranging for a bias voltage to be applied to the spacer material from a servosystem which seeks the null of the first harmonic. With a tuned system responding to the second harmonic, one then has a controlled interferometric photometer for monitoring the radiance in a spectral line.

In this connection, it is intuitively obvious that there will be a particular value for the finesse that gives the most output in the second harmonic. If the finesse is very high, the proportion of the cycle during which the spectral line is passed by the interferometer will be small, relatively more of the available signal appearing in the higher harmonics. As the finesse is decreased, the output signal will tend to become more and more sinusoidal, although with a finesse equal to zero—i.e., with no interferometer—there will be no second harmonic. Somewhere, therefore, there will be a maximum in the curve of the second harmonic amplitude *versus* finesse; figure 4 shows this maximum to be close to a finesse of six.

In the above analysis, it has been assumed that the interferometer is 'perfect,' with I/I_m given by (1). In practice, the performance of an interferometer falls short of perfection due to surface imperfections in the plates, lack of perfect adjustment in parallelism, and the use of a finite scanning aperture in the plane of the fringes. Measurements we have made using a prototype system, with a finesse equal to approximately five, have shown that the amplitude and phase relationships between the harmonics, derived above, hold for a practical system.

It has also been found, during these measurements, that the ceramic material shows a 'damped' response to the application of a potential, such that if a potential be switched on, the majority of the strain appears very rapidly but the final strain appears only after the lapse of a few seconds. This implies that the voltage excursion required to produce a given excursion in length of the spacers will be a function of the frequency of an applied alternating potential, and will

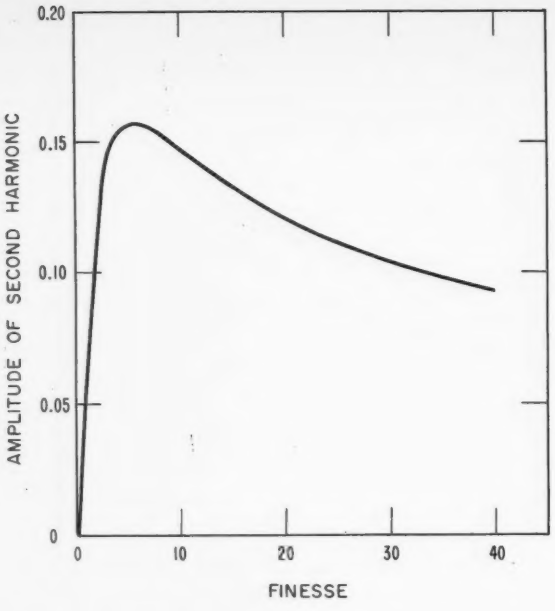

FIGURE 4. *Change of the maximum of the second harmonic with change in the finesse of the interferometer.*

be somewhat greater than that indicated from quasi-static measurements. Since the first harmonic null point is independent of the amplitude of the alternating driving potential, a practical procedure of setting the bias and driving potentials is to set first the bias potential to give zero first harmonic and then to vary the amplitude of the superposed alternating potential to maximize the second harmonic. We have found, using our prototype system, that this procedure is quick and reliable.

3. Airglow Photometry

The problem basic to photometric determination of the night airglow is that of observing an atomic emission line spectrally embedded in a continuum and emission bands. Two basic techniques are in use to eliminate, or take account of, the radiation spectrally surrounding an emission line. The most frequently used is that of 'two-filter' photometry, in which interference filters are used either to measure the radiance of the continuum in a spectral region free of atomic lines so that the contamination of the atomic line measurement may be estimated (Roach and Barbier [5]) or, in a method due to Barbier [6], to make two measurements centered on the emission line with differing proportions of background contamination. The first of these methods suffers from the uncertainty in knowledge of the spectral distribution of the background radiation (Truttse [7, 8]); both 'two-filter' methods use pairs of observations sequential in time, and are thus inherently unsuited for use in observations involving dynamic scanning of the sky. In this case, one uses the second basic technique of extracting an atomic emission line from the continuum, which is to use either a birefringent filter (Koomen et al. [9]), or a rocking interference filter (Filosofo et al., [10]). The calibration of a birefringent-filter photometer presents some difficulties although these are not insuperable (Smith and Alexander [11]; Dandekar et al., [12]).

Let us consider the basic problem. When a photometer is pointed at the night sky, the response, R, consists of two parts

$$R = R_b + R_e, \tag{4}$$

where R_b, the response to the background continuum, is given by

$$R_b = W \cdot I_b \cdot S \tag{5}$$

(W = equivalent width of the filter, I_b = specific spectral radiance of the continuum and S = spectral response of the photocell). Similarly, R_e, the response to the emission line, is given by

$$R_e = T_e \cdot I_e \cdot S \cdot \tag{6}$$

(T_e = transmission of the filter at the wavelength of the emission line and I_e = radiance of the line.)

If we now take an oscillating interferometer as the filter in the photometer, then T_e, given by (6) above, becomes of the form I/I_m discussed above; particularly, the first harmonic in R_e can be used to compensate for thermal changes in the spacer length and the second harmonic used to determine I_e. Under these conditions, the contamination of the measurement by R_b, eq (5), can become extremely small: first, by making W very small, as is easily done with an air-spaced interferometer, and, second, because the second harmonic in R_b will depend only on the derivatives of $(I_b \cdot S)$, taken at the emission wavelength, of even degree. These derivatives will be appreciable only if the emission line lies in a fraunhofer line in the continuum, or is close to emission band structure.

This result is seen by expanding I_b in Taylor's series, ignoring the variations of S with λ:

$$I_b(\lambda_0 + \Delta\lambda \cos \text{wt}) = I_b(\lambda_0) + \Delta\lambda \cos \text{wt} \left(\frac{dI_b}{d\lambda}\right)_{\lambda=\lambda_0} + \Delta\lambda^2 \cos^2 \text{wt} \left(\frac{d^2I_b}{d\lambda^2}\right)_{\lambda=\lambda_0} + \cdots$$

where $(\lambda_0 + \Delta\lambda \cos \text{wt})$ expresses the oscillating wavelength of the transmission peak of the interferometer pass-band. (It is to be noted that the coefficient of cos 2 wt contains only $\frac{d^2I_b}{d\lambda^2}, \frac{d^4I_b}{d\lambda^4}, \cdots$ etc.)

It should be noted that the presence of appreciable odd derivatives in $(I_b \cdot S)$ will give a contribution to the first harmonic signal, causing the servosystem to seek a null point away from the peak of the second harmonic. In the presence of a serious background continuum, therefore, it would be best to make W as small as convenient.

4. Conclusions

A system such as the one outlined above offers the possibility of continual control of the spacing, while observations of a feeble spectral line are in progress. The use of three small spectral line sources, sampling the interferometer at three separated positions, is an obvious extension of this monitoring to the control of parallelism. In this case, we have a system closely resembling that of Ramsay [3], but one which does not demand an optical system, with close tolerances, to return the sampling light for a second pass through the interferometer.

5. References

[1] Mielenz, K. D., R. B. Stephens, and K. F. Nefflen, J. Res. NBS **68C** (Engr. and Instr.) No. 1, 1, (1964).
[2] Mielenz, K. D., J. Res. NBS **68C** (Engr. and Instr.) No. 2, 73, (1964).
[3] Ramsay, J. V., Appl. Optics **1**, 411 (1962).
[4] Born, M. and E. Wolf, Principles of Optics (Pergamon, New York, 1964).
[5] Roach, F. E. and D. Barbier, Trans. Amer, Geophys. Union **31**, 7, (1950).
[6] Barbier, D., The Airglow and the Aurorae, ed. E. B. Armstrong and A. Dalgarno (Pergamon, New York, 1955).
[7] Truttse, Yu. L., Section 4, No. 10, p. 5, IGY Program, Moscow (1963).
[8] Truttse, Yu. L., Section 4, No. 10, p. 8, IGY Program, Moscow (1963).
[9] Koomen, M. J., C. Lock, D. M. Packer, R. Scolnik, and R. Tousey, J. Opt. Soc. Amer. **44**, 827, (1954).
[10] Filosofo, I., J. A. Greenspan, and C. M. Groom, Appl. Optics **4**, 215 (1965).
[11] Smith, L. L. and R. B. Alexander, IQSY Instruction Manual No. 5, Airglow. p. 25; IQSY Secretariat, London, 1963.
[12] Dandekar, B. S., J. C. Pomalaza, and W. F. Bellew, Appl. Optics **4**, 295 (1965).

(Paper 70C3–226)

JOURNAL OF RESEARCH of the National Bureau of Standards—C. Engineering and Instrumentation
Vol. 70C, No. 3, July–September 1966

Precise Reflection Coefficient Measurements With an Untuned Reflectometer

W. E. Little* and D. A. Ellerbruch*

Institute for Basic Standards, National Bureau of Standards, Boulder, Colo.

(March 9, 1966)

The precision tuned reflectometer technique of reflection coefficient measurement is, at present, the most accurate technique available. Utilization of the technique requires the use of tuners and sliding terminations to eliminate or reduce the inherent errors of a directional coupler.

This paper describes a reflection coefficient measurement technique that approaches the accuracy of the tuned reflectometer. Instead of tuners, the technique uses an ideal one-quarter wavelength waveguide section to eliminate the measurement error introduced by finite directional coupler directivity and to reduce to second order the error introduced by an equivalent generator mismatch.

A comparison of the quarter-wave technique with the tuned reflectometer technique through the measurement of the reflection coefficient of three 9/16 inch coaxial waveguide terminations is also included.

Key Words: Microwave, impedance, measurements, reflectometer.

1. Introduction

The reflectometer technique for microwave reflection coefficient measurements is now widely used [1].[1] The measurement accuracy of a basic reflectometer (a simple directional coupler coupled to the reflected wave) depends on the directivity of the directional coupler and the equivalent generator mismatch. The best known method of improving the measurement accuracy of the basic reflectometer requires the use of tuners, tuning procedures, and auxiliary equipment [2, 3]. The result of this tuning is an increase in the effective directivity of the coupler and a matched equivalent generator. At present, the most accurate measurements are achieved with this tuned reflectometer.

The purpose of this paper is to present another method of improving the measurement accuracy of the basic reflectometer technique. This method utilizes a quarter-wavelength waveguide section. Proper use of the quarter-wave section during the measurement procedure will, in theory, eliminate the error caused by a finite directivity and will reduce the error caused by a mismatched equivalent generator to second order.

No detailed error analysis is included in this paper; however, a laboratory measurement comparison with the tuned reflectometer indicates that the total measurement error is small. Such an error analysis may be given at a later date, depending on results of further laboratory experiments with the method.

2. Theory

The operation of a reflectometer is discussed in detail elsewhere [3]. Therefore, only a brief review will be presented here as a starting point for the discussion of the quarter wavelength technique. The side-arm output, b_3, of a directional coupler connected to sample the reflected wave (see fig. 1) can be expressed as

$$b_3 = kb_G \frac{\frac{1}{K} + \Gamma_T}{1 - \Gamma_{2i}\Gamma_T}, \tag{1}$$

where b_G is the component of the incident wave furnished by the generator, Γ_{2i} and k are both functions of the scattering coefficients of the directional coupler and reflection coefficients of the generator and detector, and Γ_T is the reflection coefficient of the terminating element. The symbol Γ_{2i} represents the equivalent source reflection coefficient presented to the reflector under study at the reference plane. The symbol K is approximately equal to the directivity ratio of the directional coupler.

The desired performance of the directional coupler is realized when $\Gamma_{2i}=0$ and $1/K=0$. Equation (1) then reduces to

$$b_3 = kb_G\Gamma_T. \tag{2}$$

Hence, inspection of (1) shows that the terms involving $1/K$ and Γ_{2i} introduce first order errors in Γ_T, when Γ_T is determined according to (2) from a measurement of

* Radio Standards Engineering Division. National Bureau of Standards, Boulder, Colo.

[1] Figures in brackets indicate the literature references at the end of this paper.

the side-arm output, b_3, of an untuned ($1/K$ and $\Gamma_{2i} \neq 0$) directional coupler. Reference 3 discusses the minimization of these errors by proper use of tuners.

It is possible to eliminate the term $1/K$ and simultaneously reduce the error arising from a finite Γ_{2i} to second order by a measurement procedure utilizing an ideal waveguide section that is one-quarter wavelength long. The theoretical basis for the method is as follows:

If the unknown is connected directly to the reference plane of the untuned reflectometer shown in figure 1, the side-arm output, $b_{1\mu}$, is

$$b_{1\mu} = kb_G \frac{\frac{1}{K} + \Gamma_\mu}{1 - \Gamma_{2i}\Gamma_\mu} \tag{3}$$

where Γ_μ is the reflection coefficient of the unknown.

Interposing a precision quarter-wavelength waveguide section between the reflectometer and Γ_μ adds a 180° phase shift to the argument of the impedance appended to the reference plane, causing the reflection coefficient at this plane to be $-\Gamma_\mu$. With the quarter-wavelength section inserted between the reference plane and the unknown, as shown in figure 2, the side-arm output, $b_{2\mu}$, is

$$b_{2\mu} = kb_G \frac{\frac{1}{K} - \Gamma_\mu}{1 + \Gamma_{2i}\Gamma_\mu}. \tag{4}$$

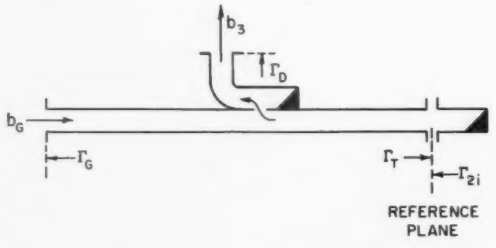

FIGURE 1. *A basic reflectometer.*

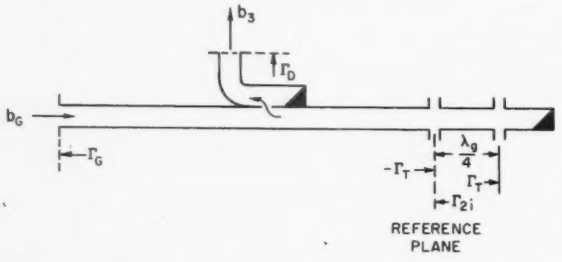

FIGURE 2. *A basic reflectometer with a quarter-wave section connected.*

The difference between $b_{1\mu}$ and $b_{2\mu}$ is then

$$b_{1\mu} - b_{2\mu} = 2kb_G\Gamma_\mu \frac{1 + \frac{1}{K}\Gamma_{2i}}{1 - (\Gamma_{2i}\Gamma_\mu)^2}. \tag{5}$$

If the unknown is now replaced with a quarter-wavelength standard short circuit[2] whose reflection coefficient is unity and the above measurement procedure repeated, formula (5), upon substitution of $\Gamma_s = 1$ for Γ_μ, reduces to

$$b_{1s} - b_{2s} = 2kb_G \frac{1 + \frac{1}{K}\Gamma_{2i}}{1 - (\Gamma_{2i})^2}, \tag{6}$$

where b_{1s} is the sidearm output when the standard short circuit is connected directly to the reference plane, and b_{2s} is the sidearm output when the ideal quarter-wavelength section is placed between the reference plane and the short circuit.

Dividing (6) by (5) results in

$$\frac{b_{1s} - b_{2s}}{b_{1\mu} - b_{2\mu}} = \frac{1}{\Gamma_\mu} \frac{1 - (\Gamma_{2i}\Gamma_\mu)^2}{1 - \Gamma_{2i}^2}. \tag{7}$$

Note that (7) does not contain the $1/K$ factor and that Γ_{2i} occurs only to the second power. $|\Gamma_{2i}|$ is usually less than 0.05 in a practical situation; hence, $|\Gamma_{2i}|^2 \ll 1$. Therefore, the limitations of the untuned directional coupler (i.e., finite directivity and a mismatched equivalent generator) have been essentially circumvented, and the correct value of Γ_μ can be determined without tuning the coupler.

To evaluate Γ_μ by means of (7), it appears that four individual (complex) quantities have to be measured. If one is interested only in a magnitude measurement, which is usually the case, a relatively simple measurement procedure can be used to determine the ratio $|b_{1s} - b_{2s}|/|b_{1\mu} - b_{2\mu}|$ directly, in decibels.

3. Measurement Procedures for Determining the Modulus of Γ_μ

A measurement system has been constructed and used to substantiate the quarter-wave method experimentally. A block diagram of the system is shown in figure 3. The measurement procedure is as follows:

1. One end of the precision quarter-wavelength section of waveguide is connected to the reference plane and terminated with a standard short circuit. The signal from the side arm under these conditions is b_{2s} of formula (7).

[2] A quarter-wavelength standard short circuit is a quarter wavelength of precision line terminated by a shorting metal wall. If a simple shorting plate is used, $\Gamma_s = -1$ is substituted for Γ_μ in (5) and one side of (7) would be multiplied by a -1.

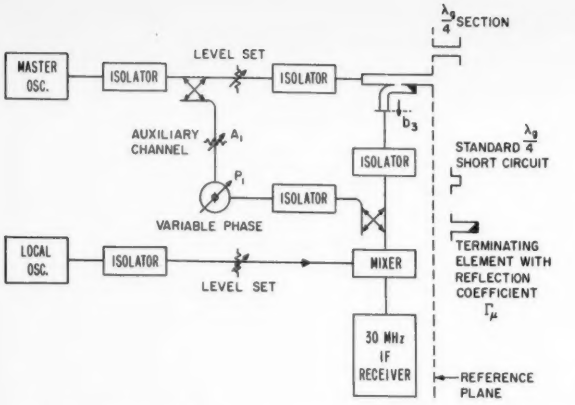

FIGURE 3. *Block diagram of quarter-wavelength measurement system.*

2. The variable phase shifter and attenuator, designated P_1 and A_1 in figure 3, are adjusted to produce a null at the 30 MHz IF receiver. This adjustment sets the signal from the auxiliary channel, b_{1A}, equal to $-b_{2s}$.

3. The ideal quarter-wavelength section is removed and the standard short circuit is connected directly to the reference plane. Under these conditions the signal from the side arm is b_{1s} of (7). Because the signal from the auxiliary channel of figure 3 was adjusted in the preceding step to produce the signal $-b_{2s}$, the receiver, which responds to the sum of the outputs of the side-arm and auxiliary channel, registers $|b_{1s}-b_{2s}|$.

4. The standard 30 MHz attenuator in the IF receiver is adjusted to produce an arbitrary reference level at the indicator.

5. The short circuit is removed from the reference plane, and the quarter-wavelength section is connected and terminated in the unknown reflection coefficient. Under these conditions the signal out of the side-arm is equal to $b_{2\mu}$ of (7).

6. The phase shifter and attenuator (P_1 and A_1) are now readjusted to again produce a null at the 30 MHz receiver. This adjustment provides that $b_{A2}=-b_{2\mu}$, where b_{A2} is the signal from the auxiliary channel.

7. The quarter-wavelength section is removed, and the unknown is connected directly to the reference plane. The signal into the 30 MHz IF receiver is again the sum of the signals from the side-arm and auxiliary channel, i.e., $|b_{1\mu}-b_{2\mu}|$. A record is made of the change (in decibels) in the setting of the standard 30 MHz attenuator in the receiver required to return the indicator to the reference level chosen in step four. This difference (in decibels) between the final attenuator setting and the setting at step four is a measure of the ratio $|b_{1s}-b_{2s}|/|b_{1\mu}-b_{2\mu}|$. Thus,

$$\text{dB(measured)} = 20 \log \left|\frac{b_{1s}-b_{2s}}{b_{1\mu}-b_{2\mu}}\right|$$

$$= 20 \log \frac{1}{|\Gamma_\mu|} \frac{|1-(\Gamma_{2i}\Gamma_\mu)^2|}{|1-\Gamma_{2i}^2|}.$$

Assuming that $|\Gamma_{2i}^2| \leq 1$, this equation reduces to approximately

$$\text{dB(measured)} = 20 \log \frac{1}{|\Gamma_\mu|},$$

whence the unknown reflection coefficient magnitude is given by

$$|\Gamma_\mu| = 10^{-\frac{\text{dB(measured)}}{20}}.$$

4. Measurement Results

The reflection coefficient magnitude of three 9/16-inch coaxial terminations were measured at 4 GHz using the quarter-wave technique. These measurements were compared with those obtained with a tuned reflectometer and those obtained with an untuned reflectometer that did not utilize a quarter-wavelength section. Table 1 summarizes the results.

The first column lists the values obtained for the three terminations when measured with a tuned reflectometer. The tolerances associated with these values include the measurement error as well as the non-repeatability obtained by rotating the termination. In the second column are listed the VSWR's corresponding to the reflection coefficients in the first column.

TABLE 1. *Tabulated measurement results*

TUNED REFLECTOMETER MEASUREMENT VALUES		VALUES OBTAINED WITH IMPERFECT COUPLER		VALUES OBTAINED WITH IMPERFECT COUPLER AND λ/4 SECTION	
$\|\Gamma\|$	VSWR	$\|\Gamma\|$	VSWR	$\|\Gamma\|$	VSWR
0.0217 ±0.0006	1.0443 ±0.0012	0.042	1.088	0.0224	1.0458
0.0902 ±0.0015	1.1983 ±0.003	0.108	1.242	0.0918	1.2022
0.3334 ±0.0028	2.000 ±0.006	0.351	2.082	0.3353	2.0089

In the third and fourth columns are listed the reflection coefficients and VSWR's obtained with an untuned directional coupler but no quarter-wavelength section. These values were obtained as follows: The standard short circuit was connected to the reference plane, and an indicator reference point

was obtained. The short circuit was then replaced by the unknown impedance, and the reflection coefficient was computed from the measured change in the signal level at the indicator. These values are subject to all the errors due to imperfections in the directional coupler. The directional coupler employed in the three systems with which the data of table 1 were obtained (including that of fig. 3), had a directivity of approximately 30 dB (this corresponds to a $1/|K|$ value of approximately 0.032) and a $|\Gamma_{2i}|$ of less than 0.02.

In the fifth and sixth columns of table 1 are listed the reflection coefficient magnitude and VSWR values obtained by using the quarter-wavelength measurement technique described in this report.

The values obtained using the quarter-wave technique are in near agreement with the values obtained using the tuned reflectometer. The values obtained with the untuned reflectometer when the quarter-wave section was not used are considerably in error.

5. Conclusions

Precise reflection coefficient measurements are possible with an untuned reflectometer if the quarter-wave measurement technique is used. The theory was verified experimentally by measuring the reflector coefficient magnitudes of several terminations with a tuned reflectometer and then remeasuring them using the quarter-wave technique with an untuned reflectometer. These same terminations were also measured directly with an untuned reflectometer without application of the quarter-wavelength technique, to demonstrate the improvement in accuracy provided by the quarter-wave method.

Relative phase data were neglected during this evaluation. No serious difficulties are anticipated in modifying the measurement system to obtain phase data so that the quarter-wave technique will then provide the complex reflection coefficient.

Use of the quarter-wave technique instead of a tuning procedure eliminates the need for variable-phase high- and low-reflection loads and shortens the required length of precision line. The most important potential application of the quarter-wave technique is in the measurement of impedance at frequencies below approximately 1 GHz. With decreasing frequency the tuned reflectometer becomes increasingly cumbersome.

6. References

[1] Ginzton, E. L., Microwave Measurements, p. 300 (McGraw-Hill Book Co., Inc., New York, N.Y., 1957).

[2] Engen, G. F., and R. W. Beatty, Microwave reflectometer techniques, IRE Trans. MTT **MTT-7,** No. 3, 351–355 (July 1959).

[3] Anson, Wilbur J., A Guide to the use of the modified reflectometer technique of VSWR measurement, J. Res. NBS **65C** (Engr. and Instr.) No. 4, 217 (Oct.-Dec. 1961).

(Paper 70C3–227)

JOURNAL OF RESEARCH of the National Bureau of Standards—C. Engineering and Instrumentation
Vol. 70C, No. 3, July–September 1966

A Versatile Ratio Instrument for the High Ratio Comparison of Voltage or Resistance

Alfred E. Hess*

Institute for Basic Standards, National Bureau of Standards, Boulder, Colo.

(April 12, 1966)

A 9-dial resistance ratio instrument capable of precise high ratio comparison of voltage or resistance (from 1/1 to 10^7/1) is described. Also described is the modification of a 6-dial universal ratio set to permit its additional use as a versatile ratio instrument. Paramount to the accuracy of these high ratio instruments is the carefully adjusted "common point" junction which is briefly discussed.

Key Words: DRRS (direct reading ratio set); junction; precision measurements; ratio, resistor, four-terminal; resistance decade; transresistance; URS (universal ratio set); VERI (versatile ratio instrument).

1. Introduction

Because of a need to make accurate high ratio d-c resistance comparisons and an inability to do so with existing ratio instruments such as the DRRS (direct reading ratio set) and the URS (universal ratio set), [1, 2, 3][1] a versatile ratio instrument (abbreviated VERI) was developed. With the VERI an arbitrary voltage or resistance ratio from 1/1 to 10^7/1 (or 1/10^7) may be measured with a dial resolution of 1 part in 10^8 or better. (Permissible generator voltage and detector sensitivity may further limit the actual resolution attainable.) This instrument may be used to calibrate ratio devices—potentiometers, voltage dividers, volt boxes, the ratio arms of Wheatstone bridges, etc. Also, the individual fixed resistors of the VERI may be used as 4-terminal resistance standards, and the incremental resistance section may be used as a 9-dial, 2- or 4-terminal resistance decade.

A 6-dial URS may be modified as described in section 3 to permit its additional use as a 6-dial VERI having a ratio range from 1/1 to 2×10^4/1. Its normal function as a URS is not impaired by the modification.

The accuracy of the VERI depends directly upon the design and adjustment of the "common point" junction [4]. The transresistances[2] of the junctions used in the described instruments are less than $10^{-8}\ \Omega$. This causes a worst-case uncertainty in ratio of less than 1 part in 10^7.

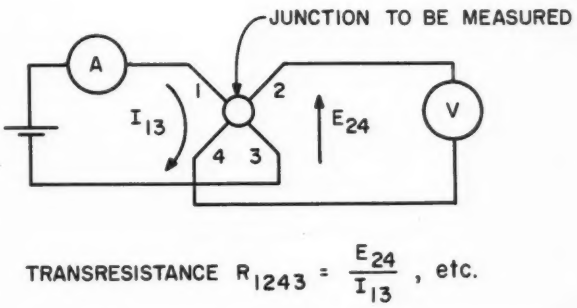

FIGURE 1. *Basic setup for measuring junction transresistance.*

2. Versatile Ratio Instrument

Figure 2 is a schematic diagram of the VERI. It consists basically of a precision resistance decade section and several precision fixed resistors of decimal values connected at a common point by a "zero" transresistance junction. The resistance decade section shown consists of 9 decades which may be varied in 0.001 Ω steps to a total resistance of 1,111,111.111 Ω. The seven fixed resistors have decimal values from 0.1 to 100 kΩ. The "outside" ends of each of the resistors have dual terminals, so they may be connected as 4-terminal resistors to permit the elimination of the terminal and external lead resistances. The "common-point" junction shown is a

*Radio Standards Engineering Division, National Bureau of Standards, Boulder, Colo.

[1] Figures in brackets indicate the literature references at the end of this paper.

[2] Transresistance: The ratio of the voltage induced at one pair of junction terminals to the current through another terminal pair, i.e., $R_{1243} = \frac{E_{24}}{I_{13}}$, see figure 1.

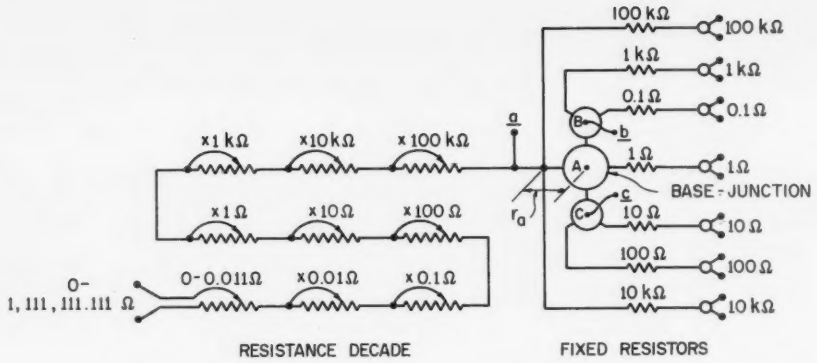

FIGURE 2. *Schematic diagram of a versatile resistance ratio instrument.*

composite junction consisting of three tetrajunctions,[3] A, B, and C. This is necessary because a junction may have a maximum of only four electrically symmetrical terminals [4]. Junction A is the base junction to which all resistance and ratio measurements are referred. It is adjusted to have less than 10^{-8} Ω transresistance. Because of their relatively large resistance, the 10 kΩ and 100 kΩ fixed resistors, and the 0–1 MΩ resistance decade section may be connected to a common terminal of the base juction without introducing significant error (assuming r_a is less than 0.001 Ω). Terminals a, b, and c are needed for the calibration and use of the VERI since the potential terminal used for a ratio measurement should not be common to either of the resistors being used in the VERI. The switches used in the resistance decades have low resistance variation (less than 0.001 Ω per switch).

This instrument when fully calibrated may be used in a variety of ways, including:

(1) 4-terminal fixed resistance standards, 0.1, 1, 10, 100, 1k, 10k, and 100 kΩ;

(2) a 2- or 4-terminal, 9-dial decade resistor, 0.000 to 1, 111, 111.111 Ω;

(3) a 0.01 ppm resolution direct reading ratio set for precise 1 to 1 comparisons;

(4) fixed ratio standards with nominal ratios to 10^6/1; and

(5) an incremental ratio standard having continuous ratio adjustability from 1/1 to 10^7/1 with 9-dial resolution.

Calibration of the instrument may be accomplished by measuring one of the fixed resistors, and then making 10/1 [5] and/or 100/1 step-up or step-down (ratio) calibrations of the remaining fixed resistors using the technique reported by Hamon [6] and further analyzed by Page [7] or, each of the fixed resistors may be measured and the ratios between them calculated. The latter has the disadvantage that the uncertainty of the calculated ratios will include the uncertainty in the values of the individual resistors. The decade resistors are calibrated as a 4-terminal resistance box with direct checks of the x1 and x10 dial settings against the fixed resistors.

3. URS Modified to a VERI

A universal ratio set may be modified to permit its additional use as a versatile ratio instrument. A minor modification of a URS for use as a DRRS has been described by Ramaley and Shafer [8]. Figure 3 is a photograph of a URS which has been altered as shown by the schematic diagram of figure 4. As modified, it may be used as:

(1) a conventional 6-dial URS;

(2) 4-terminal fixed resistance standards, 0.1, 1, 10, 100, and 1000 Ω;

(3) a 2- or 4-terminal 6-dial decade resistor, 0.001, to 2111.110 Ω;

(4) a 1 ppm resolution direct reading ratio set for 1/1 comparisons;

(5) fixed ratio standards with nominal ratios to 10^4/1; and

(6) an incremental ratio standard having continuous ratio adjustability from 1/1 to 2×10^4/1 with 6-dial resolution.

The modifications to the URS consist of the following:

(1) Replacing the x100 Ω switch (top decade) with a switch having very low contact resistance variation (less than 0.001 Ω).

(2) Adding 12 terminals to the front panel, making a total of 17 as seen in figure 3.

(3) Mounting a tetrajunction (a ½-inch diam copper sphere having four terminals).

(4) Mounting the five additional precision resistors, 0.1, 1, 10, 100, and 1000 Ω.

(5) Wiring the resistors and terminals as shown in figure 4.

[3] A "tetrajunction" is an electrically symmetrical 4-terminal junction [4] having essentially zero transresistance.

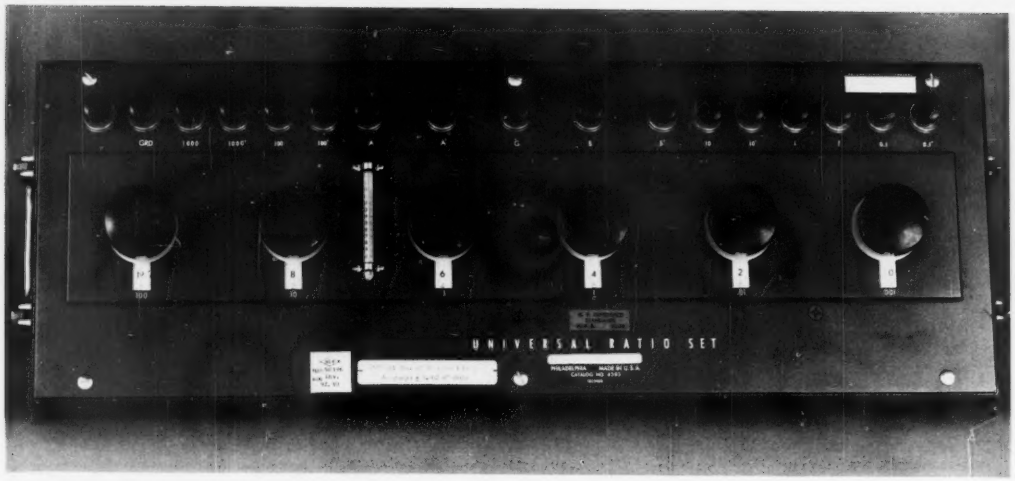

FIGURE 3. *A commercial 6-dial URS which has been modified to permit its additional use as a VERI.*

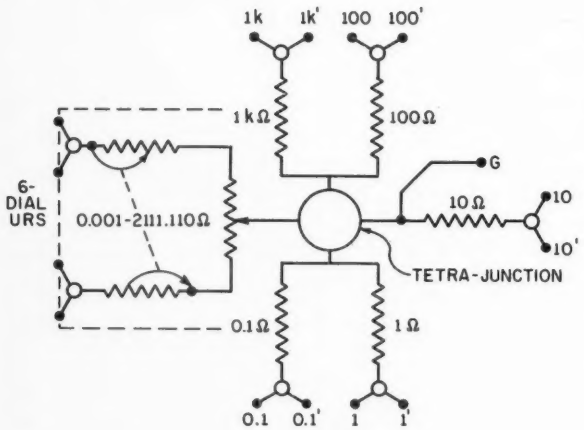

FIGURE 4. *Schematic diagram of the NBS-modified 6-dial URS to permit its additional use as a VERI.*

The spherical tetrajunction, the five added precision resistors, and some of the additional wiring can be seen in the photograph of figure 5.

4. A Typical Application of the VERI

Figure 6 shows a modified 6-dial URS used as a VERI in a setup for calibrating the ratio arms of a Wheatstone bridge. Units L_1 and L_2 are lead compensating networks which are needed when resistances of 1000 Ω or less are involved in the ratios. S_1 and S_2 are low resistance shorting wires which are used during the adjustment of the lead compensators, L_1 and L_2. Balance is achieved and the setting of the R_a dials of the URS is noted when the removal and replacement of the shorting links, S_1 and S_2, have no effect on the galvanometer null. The ratio of the Wheatstone bridge ratio arm for the circuit values shown is

$$M=\frac{R_a(1+a)}{0.1(1+b)}\approx\frac{R_a}{0.1}(1+a-b),$$

where R_a is the "R_a" reading of the URS dials, and a and b are the proportional corrections to R_a and 0.1 Ω respectively. (The right-hand expression of the equation introduces less than 1 part in 10^8 uncertainty when a and b are each less than 0.0001.)

Once the ratio arms of the Wheatstone bridge are calibrated, the standard arm, R_s, may be calibrated by measuring the fixed and decade resistances of the VERI on the "unknown" terminals of the Wheatstone bridge.

5. Conclusion

The versatile ratio instrument described permits the precise comparison of ratio from 1/1 to 10^7/1 with a dial resolution of 1 part in 10^8 or better. By comparison, a standard 6-dial universal ratio set cannot measure a ratio of 10^7/1, and will give only 3-digit resolution on a ratio of 10^4/1. A VERI modified URS, however, will give 7-digit resolution on a ratio of 10^4/1 and not less than 6-digit resolution on any ratio from 1/1 to 2 x 10^4/1. The effective resolution attainable in high ratio measurements may be limited by the maximum permissible generator (battery) voltage and detector (galvanometer) sensitivity.

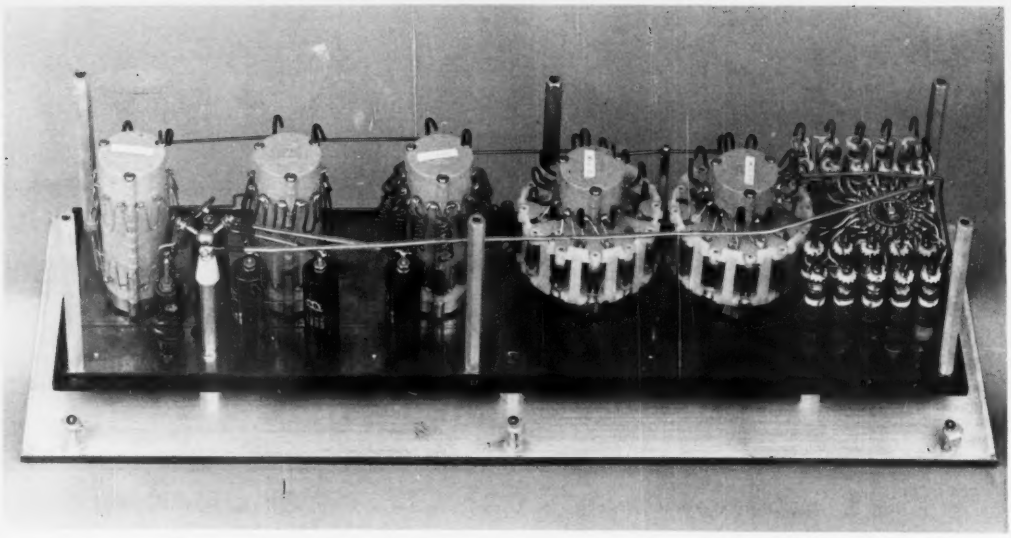

FIGURE 5. *Internal view of the commerical 6-dial URS modified by NBS to permit its additional use as a VERI.*

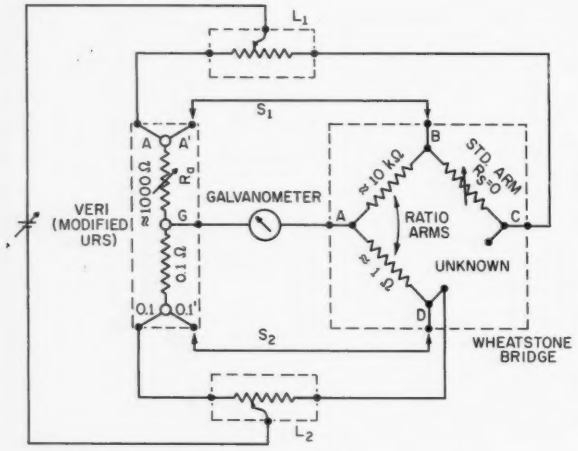

FIGURE 6. *Circuit used to calibrate the ratio arms of a Wheatstone bridge with the VERI (modified URS).*

6. References

[1] Brooks, P. P. B., Calibration procedures for direct current resistance apparatus, NBS Mono. 39 (Mar. 1962).

[2] Thomas, J. L., Precision resistors and their measurements, NBS Circ. 470 (Oct. 1948).

[3] Wenner, F., and E. Weibel, The testing of potentiometers, Scientific Paper 223, Bull. BS **11**, No. 1, 1–39 (1914).

[4] Hess, A. E., Nano-ohm junctions for accurate ratio instruments, NBS Report No. 9158 (Jan. 1966).

[5] Wenner, F., Methods, apparatus and procedures for the comparison of precision standard resistors, J. Res. NBS **25**, 229–293 (Aug. 1940).

[6] Hamon, B. V., A 1–100 Ω Build-up Resistor for the Calibration of Standard Resistors, J. Sci. Instr. **36**, 450–453 (Dec. 1954).

[7] Page, C. H., Errors in the series-parallel build-up of four-terminal resistors, J. Res. NBS **69C** (Engr. and Inst.), No. 1, 3, 181–189 (July-Sept. 1965).

[8] Ramaley, D., and J. F. Shafer, Universal ratio sets made direct reading sets, NBS Tech. News Bull. **47**, 9, 162 (Sept. 1963).

NOTE: A reprint of references [2] and [5] is also in Precision Measurement and Calibration—Electricity and Electronics, NBS Handbook 77, **1** (1961).

(Paper 70C3–228)

JOURNAL OF RESEARCH of the National Bureau of Standards—C. Engineering and Instrumentation
Vol. 70C, No. 3, July–September 1966

Console for the Rapid and Precise Comparison of Volt Boxes

Patrick H. Lowrie, Jr.*

Institute for Basic Standards, National Bureau of Standards, Boulder, Colo.

(March 24, 1966)

The comparison of volt boxes within uncertainties of ±0.01 percent or less has, in the past, been a long and difficult task at the NBS Boulder Laboratories. A console for this purpose recently put in use has reduced the time and labor to a great extent and, at the same time, has reduced the uncertainties associated with the measurement circuitry to less than 0.001 percent, thus allowing realizable calibration uncertainties of less than 0.005 percent. The console was designed as part of a system in which the operator was considered to be the decision-making link in the measurement chain. The circuitry, through the use of a contained computer and associated circuits, provides the operator with the data he requires in the form he chooses. The operator is thus freed from the need to consider minutiae, and thereby is able to concentrate on those factors requiring judgment.

Key Words: Calibration, console, electrical, measurement, ratio, standards, voltage, volt box.

1. Introduction

A volt box is a carefully constructed voltage divider having a number of fixed ratios between input and output terminals. These ratios are commonly in multiples of the integers 1 through 5. A volt box is normally used to extend the effective range of a potentiometer so that voltages up to 750 or 1500 V may be measured.

As a volt box is a ratio device, the absolute resistance of its elements is not of great importance and under ordinary circumstances need be known only in a nominal sense (i.e., 750 Ω/V, etc.). However, before a volt box may be used for accurate measurements, the actual ratio must be determined. There are two characteristics inherent in volt boxes that manifest themselves in a dependence of the ratio upon the applied voltage. One is the change in the resistance of the elements with heating. In the large "master" volt boxes fabricated in accordance with NBS RP1419 [1],[1] the changes in ratio resulting from self-heating are usually quite small, being in the order of 5 to 20 ppm (parts per million) at rated voltage. In the less complex, general purpose boxes, however, the difference between the ratio at reduced voltage (under 30% of rated) and that at rated voltage may be as great as 200 ppm. The other characteristic is the variation in the resistance of the insulating parts of the box. Even when using the new, high-resistance insulating materials, small currents across the surface of the insulator can result from surface contamination. When these currents are in parallel with resistance paths, the ratio is disturbed. These currents are not, in general, a linear function of applied voltage, and the current paths cannot be well-defined. To reduce the effects of these currents, the more complex, master boxes have guarded circuits wherein the voltage across the leakage path is reduced considerably with a corresponding reduction in leakage currents.

When these characteristics are considered, it becomes apparent that the ratio should be measured at the voltage for which the box will be used. This may be done most easily by comparing the box with another volt box having known characteristics. Two methods of comparison are described in RP1419. (The second method is discussed in appendix I of that paper.) The first method is the one used at NBS.

The recently completed console used for this measurement at the NBS Boulder Laboratories incorporates many new features that contribute to the accuracy and efficiency of the measurement. With this console, uncertainties associated with the measurement circuitry are less than 0.001 percent, which allows realizable calibration uncertainties of less than 0.005 percent. This paper describes the console and includes, as appendices, an evaluation of the uncertainties that may be expected in its use.

2. Comparison Measurement

As a comprehensive description of this measurement may be found in the literature, [2] only a brief treatment will be undertaken here. The circuit is shown in figure 1. In the course of the measurement, the values of v_3, v_2, v_1, and v_4 are measured in microvolts. (v_3 is normally measured first because it is the voltage most sensitive to changes in ratio caused by heating and to wrong connections in the measuring circuit.) When these values and the supply voltage, V, are known, it can be shown [3] that the corrected ratio of the box

*Radio Standards Laboratory, National Bureau of Standards, Boulder, Colo.

[1] Figures in brackets indicate the literature references on page 180.

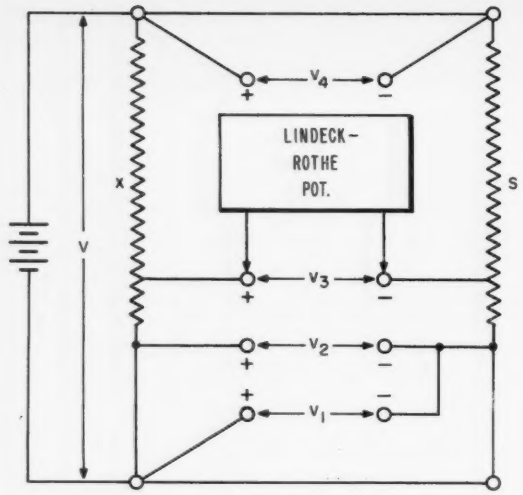

FIGURE 1. *Basic volt box measurement circuit.*

undergoing comparison (within the limits of uncertainty in the measurement) is

$$X = X_n\left[1+\left(\mu_s+\frac{v_4-v_1}{V}+\frac{v_2-v_3}{V/S_n}\right)10^{-6}\right], \qquad (1)$$

where X_n is the nominal ratio of the unknown,

μ_s is the correction to the ratio of the standard volt box in ppm,
S_n is the nominal ratio of the standard volt box, and is equal to X_n,
V is the supply voltage, in volts, and
v_1, v_2, v_3, and v_4 are the measured voltages, in microvolts.

(v_1, v_2, and v_3 are considered to be positive when of the same polarity as v_4.)

3. Measuring System Requirements

In order to achieve a high degree of accuracy, the measuring system must, of course, be fabricated of stable, high-quality components and must be guarded. However, the use of good quality equipment alone is not a guarantee of highly accurate measurements. The success of the measurement is dependent to a very large extent upon the operator. Human operational factors contributing to degradation of accuracy are primarily fatigue, both muscular and nervous, and inability to copy figures indefinitely without error. In the design of the console, these factors were carefully considered, and as a result the following requirements were formulated: (1) The operator should be able to change ratios quickly and easily. This will not only reduce irritation but also will minimize the time during which no power is applied and thus reduce uncontrolled cooling of the volt boxes. It is important to minimize this cooling because volt boxes are calibrated under temperature equilibrium conditions. (2) Controls should be centralized as much as possible. (3) The digital form of indication is to be preferred over the analog form. (4) All readings and settings should be capable of being checked. (5) As much of the computing as possible should be done automatically. (In the calibration of a volt box eq (1) may have to be calculated as many as 32 times.) (6) Recopying of data should be reduced to a minimum.

In addition to the requirements listed above, the fact that voltages as high as 1500 V dc may be present during calibration dictates the use of adequate safety measures.

4. Features

The console was designed from the human engineering viewpoint to as great an extent as was technically and economically practical. The operator was treated as a decision maker, and the console was designed to automatically handle those functions not requiring decision and to supply the operator with the appropriate data in a clear and concise form (fig. 2). As a result of this viewpoint, and of the requirements listed above, the following features were included. (1) A plug-panel was designed to allow the operator to quickly change ratios on the standard volt box. (2) All controls are grouped in front of the operator. During the measurement of a given ratio, the operator does not need to leave his seat, and no control is more than 18 in. away. However, the operator does need

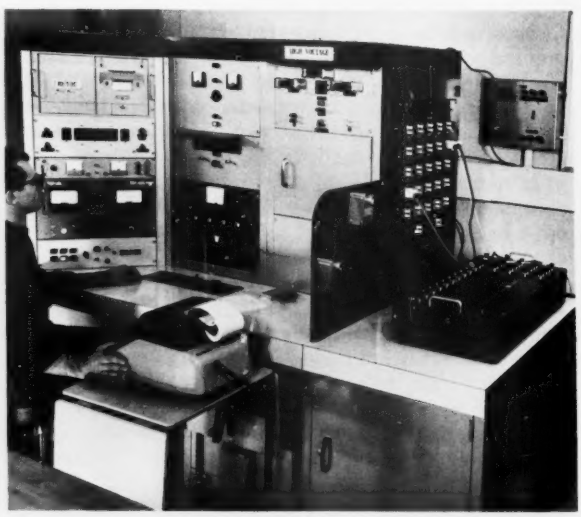

FIGURE 2. *The volt box calibration console at the NBS Boulder Laboratories, now at NBS laboratories, Gaithersburg, Md.*

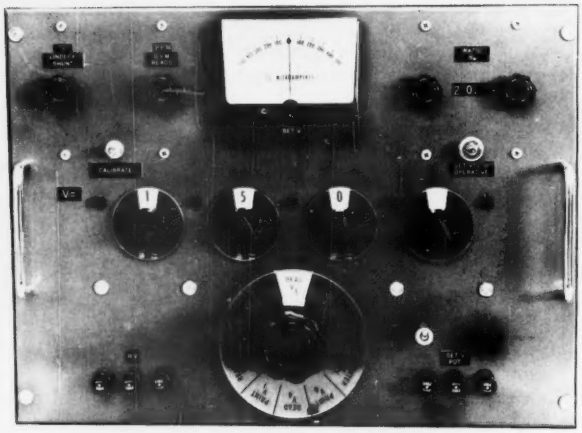

A

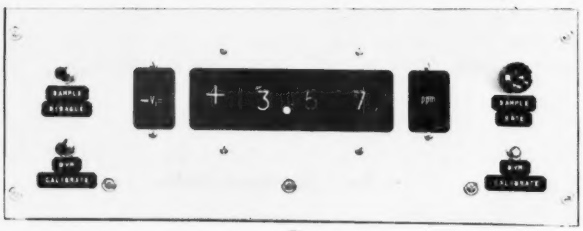

B

FIGURE 3. A. *Main control panel*; B. *Output display panel.*

to get up and move around the end of the console to change ratios. (3) All important control settings and displays are in digital form (fig. 3). (4) The basic measuring circuit includes provision for reducing the measured voltage to parts per million continuously and automatically. The value, in ppm, is recorded by the operator on an adding machine. (5) The tape from the adding machine, when complete, is cut into appropriate lengths and photographically reproduced on $8\frac{1}{2} \times 11$ inch sheets which become the permanent records. Thus the data need be recopied by hand only once, onto the summary sheet from which the Report of Calibration is typed. To comply with the safety requirements, the area in which the high voltage is exposed is protected by a two-stage photoelectric fence. If the illumination to either of two photocells is interrupted, the high voltage is disconnected. Also, a prominently mounted, high-voltage sign is illuminated whenever the high voltage circuit is energized. To provide an indication of high voltage even if all other safety circuits were to fail, two neon bulbs are connected, in series with suitable dropping resistors, across the high voltage leads. One of these is mounted on the front panel, and the other is mounted at the top of the plug-panel in the high-voltage area.

Initially a digital printer was connected to print the position of every control on the main control panel and the output from the measuring circuit. The tape from the printer was to be used to check the validity of the recorded data. However, the action of the printer adversely affected the measuring circuit, and it proved to be impractical to reduce this circuit interaction to a tolerable level. The use of the printer was therefore discontinued. The checking of recorded data is accomplished by the making of multiple measurements.

5. Measurements Procedure

In the measurement of a given range of a volt box, the operator first connects the box as shown in figure 2. The main function switch (the large, rotary switch in the lower center of the main control panel, fig. 3A) is rotated to the "Enter S_n" position. The operator enters the nominal value of the ratio into the console circuitry by adjusting the switches in the upper right of the main control panel. He then rotates the main function switch to the "Enter and Set V" position. (In so doing he moves the switch through the "Print S_n" position which originally caused the printer to record the values of the S_n dials. This position no longer has any meaning.) After having turned the four "V=" dials to the desired value of applied voltage (the fourth dial controls the position of the decimal point), he adjusts the high-voltage supply until a null is obtained on the Set-V meter. By rotating the main function switch to the "Read v_3" position, he makes those circuit connections necessary for the measurement of the difference voltage shown in figure 1. He records the values of V and S_n on the calculator, and then proceeds to measure v_3, then v_2, v_1, and v_4. As the measurement of each difference voltage is completed, he enters the value displayed on the output display panel (fig. 3B) into the calculator. After having completed the four measurements, he enters the correction to the standard into the calculator. By depressing the totaling key, he completes the calculations.

6. Computer Principle

If eq (1) is rewritten as shown in eq (2), the correction to the ratio of the box undergoing calibration is seen to be the sum of five terms, each of which is in parts per million, provided the conditions listed under eq (1) are met.

$$X = X_n \left[1 + \left(\mu_s + \frac{v_4}{V} - \frac{v_1}{V} + \frac{S_n v_2}{V} - \frac{S_n v_3}{V} \right) 10^{-6} \right]. \quad (2)$$

As only multiplication and division are needed to convert the measured voltage to parts per million, an electrical analog is easily constructed. Considering the v_3 term of eq (2),

$$V_{3(\text{ppm})} = v_{3(\mu V)} \frac{S_n}{V} \quad (3)$$

Correspondingly, in a voltage divider circuit,

$$E_0 = E\frac{R_2}{R_1}, \qquad (4)$$

where R_2 is the portion of R_1 across which E_0 appears. It remains only to determine the circuit that allows the relationship

$$\frac{E_0}{E} = \frac{R_2}{R_1} = \frac{S_n}{V} \qquad (5)$$

to hold, considering that V and S_n are independent parameters.

If R_2 is allowed to vary in such a way as not to change the value of R_1, the two values will be independent and eq (5) may be realized in fact. This is done as is explained in section 7.3. The result is a simple, completely passive computer, the accuracy of which is limited only by the accuracy of the contained resistors.

In the actual design, no attempt was made to retain the decimal point in the voltage divider circuit, as that would require excessive voltages in the computer. Instead, a separate switching circuit is used to place the decimal point.

7. Circuit

7.1. Block Diagram

Figure 4 shows a block diagram of the circuit. The output from the 0–1500 V supply is monitored by the set-volts potentiometer. This potentiometer is also used to enter the significant figures of the value of V (eq (2)) into the computing potentiometer such that R_1 of eq (5) is proportional to V. The significant figure of S_n is similarly entered by adjusting the value of R_2 in eq (5) appropriately. Decimal information is supplied to the decimal point computer as shown. (The value of V may be anywhere between 0 and 1500 V, to three significant figures. That of S_n may lie anywhere between $1.\times10^0$ and $9.\times10^4$, but in practice it does not exceed 1×10^4.) The four difference voltages (v_1, v_2, v_3, and v_4) to be measured are connected to the computing potentiometer by means of a relay switching circuit. The output from the computing potentiometer is connected to a digital volt-meter which has been modified to read only significant figures. The decimal information proceeds directly to the digital display from the decimal point computer. The printer monitored both the computing potentiometer (which included, for the purpose of printing, the settings on the set-volts and S_n dials) and the digital display. The printer output included codes indicating the nature of the display (ppm, microvolts, etc.) as well as the value and sign.

7.2. Set-Volts Potentiometer

a. Significant Figures Section

The set-volts potentiometer circuit is shown in figure 5. The significant figures section comprises a one-volt zener source supplying a Kelvin-Varley voltage divider. Each decade of the divider is 1000 Ω per step with 2500 Ω resistors used for compensation. This type of design allows all decades to be of a high (and easily procured) resistance which reduces the

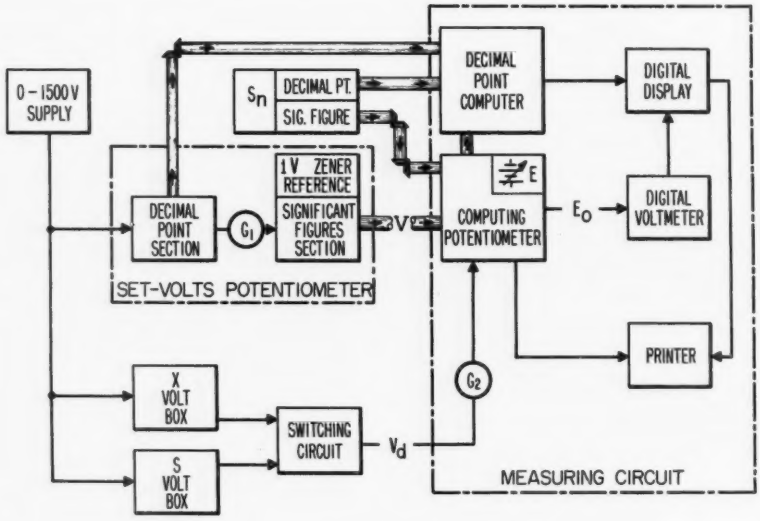

FIGURE 4. *Block diagram of console circuit.*

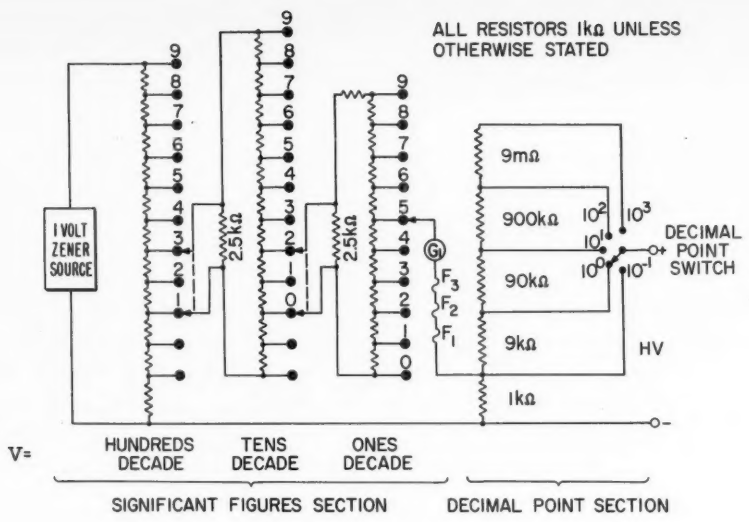

FIGURE 5. *The set-volts potentiometer.*

effect of contact resistance. Each decade is physically ganged to, but guarded and shielded from, a corresponding decade in the computing potentiometer. Thus, as the value of V is set on the three decades in the set-volts potentiometer, the value of R_1 in eq (5) is simultaneously adjusted to be proportional to V. It should be noted that the significant figures of the lowest value that can be set on the set-volts potentiometer dials are 100. This is necessitated by the need, in the computer, for $R_{1(\min)} = 10\ \text{k}\Omega > R_{2(\max)} = 9\ \text{k}\Omega$. A more detailed explanation is given in section 7.3.

It will be noted that the galvanometer, G_1 (which is of the chopper-amplifier type), is protected by three fuses (f_1, f_2, and f_3) in series. The possibility, however remote, of the operator inadvertently applying 1500 V directly across the galvanometer circuit necessitated this, and the fusing system has been found to be entirely adequate.

b. Decimal Point Section

The decade voltage divider connected across the high-voltage terminals divides that voltage by integral powers of ten. The switch used for this purpose is the fourth switch to the right in the "$V=$" section on the main control panel (fig. 3). This switch also enters the appropriate power of ten in the Decimal-Point computer and lights the appropriate decimal point light on the main control panel (fig. 3). The relationship between the decimal point section of figure 5 and the "$V=$" dials of figure 3 is as follows. The 10^{-1} position causes the decimal point light preceding the first significant figure to light; hence the reading of the $V=$ section, as shown in the figure, would be *.150*. The 10^0 position causes the light between the first and second significant figures to light; hence the reading would be *1.50*, etc. When the decimal point switch is rotated to the 10^3 position, a zero appears in the fourth window of the $V=$ section and the decimal point light to the right of that window will light. With the switch in this position the reading would be *1500*. If a potential of 1500 V was now impressed across the decimal-point-section divider, the voltage to the right of G_1 would be

$$\frac{1500.(10^3)}{10^7} = 0.150 \text{ volt}, \tag{6}$$

which is equal to the voltage to the left, and the galvanometer would be at null.

The possible errors introduced by the circuits in the set-volts potentiometer are discussed in appendix A.

7.3. Computing Potentiometer

The computing potentiometer (fig. 6) is basically a modified Lindeck-Rothe circuit connected to a voltage divider. The ammeter normally used as an indicator has been replaced by a 10 kΩ resistor. Hence the output from the potentiometer is a voltage rather than a meter deflection. As is explained below, this voltage is operated on by the voltage divider comprising R_1 and R_2 such that

$$E_0 = \frac{R_2}{R_1} M \cdot v_d, \tag{7}$$

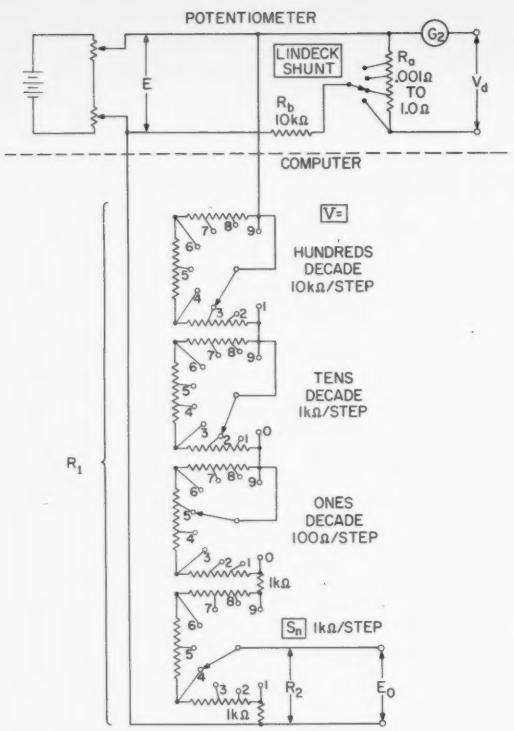

FIGURE 6. *Computing potentiometer.*

where v_d is the voltage to be measured by the potentiometer, and M is a multiplier determined by the values of R_a and R_b.

The three decades shown under "$V=$" in figure 6 are ganged to the corresponding decades in the set-volts potentiometer. It will be noted that when these decades are adjusted to the minimum value ($V=100$) there is still 10 kΩ of resistance in the circuit. It is this feature that allows R_2 of eq (5) to vary independently of R_1.

When both the "$V=$" and "S_n" decades are adjusted to minimum, the circuit is as shown in figure 7a. If the "$V=$" dials are adjusted to 325, for example, the resistance of R_1 becomes 32.5 kΩ and the result is shown in figure 7b. The value of E_0 in figure 7b is equal to that of figure 7a divided by 325 (ignoring the decimal point). Thus the "$V=$" value is entered as a divisor. If the S_n decade is adjusted to 4, the circuit is as shown in figure 7c, and E_0 is four times that of figure 7b. Thus the value of S_n is entered as a multiplier, and the circuit of figure 6 meets the requirement of eq (5).

The errors associated with the computing potentiometer are discussed in appendix B.

7.4. Decimal Point Computer

The decimal point is placed by means of the circuit shown in figure 8. Placement is determined by three switches, as shown. It will be noted that as the value of the Lindeck shunt selected is increased, the decimal point moves to the right. This is true also when the S_n decimal point switch is changed to select a larger value. If the decimal point switch on the set-volts potentiometer is adjusted to a larger value, however, the decimal point on the digital display will move to the left. Thus the Lindeck shunt and S_n decimal point switches serve to multiply by powers of 10, and the set-volts decimal point switch divides by powers of 10. In the actual circuit, provision is included for bypassing the S_n switch when v_1 and v_4 are being measured.

7.5. Switching Circuit

The measuring circuit is connected to the voltages v_1, v_2, v_3, and v_4 by means of double-pole, single-throw relays, as shown in figure 9. It will be noted that the movable and stationary contacts of any relay are separately guarded. This is necessary to minimize the effects of leakage currents flowing between the contacts when the relay is deenergized. With the circuit as shown, any leakage currents of this type flow directly from the high-voltage supply and hence have no effect on the ratio. To implement the guarding shown in figure 9, it was necessary to modify commercially available relays to the form shown in figure 10.

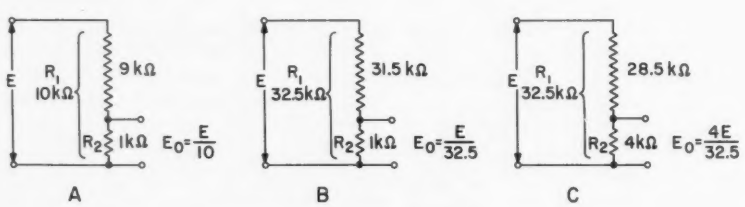

FIGURE 7. *Computer circuit showing* "V=" *and* "S_n" *adjustments.*
A: $V=100$, $S_n=1$
B: $V=325$, $S_n=1$
C: $V=325$, $S_n=4$.

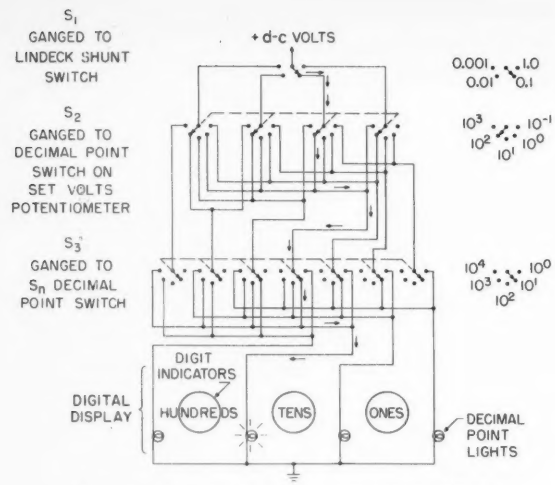

FIGURE 8. *Decimal point computer (simplified).*

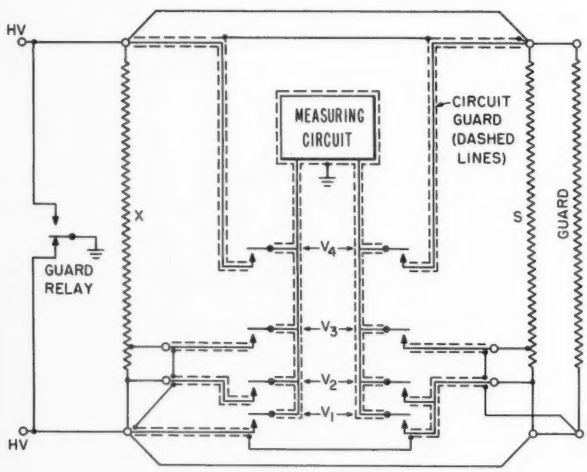

FIGURE 9. *Switching circuit showing guard configuration.*

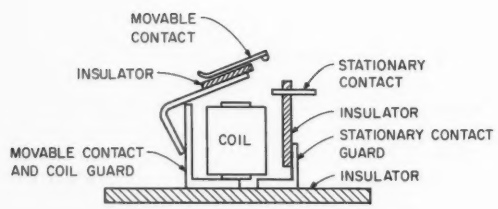

FIGURE 10. *Switching circuit relay.*

7.6. Guard Circuit

In keeping with personnel safety requirements, the cabinets of the console are connected to a low-impedance ground. Grounding the cabinets also provides the measuring circuit with shielding. The measuring circuit guard is grounded also as shown in figure 9. The power supplies are isolated; one side of the high-voltage line is grounded (see fig. 9). When v_1, v_2, or v_3 is being measured, the side connected to v_1 is grounded. When v_4 is measured, the side connected to v_4 is grounded.

8. Conclusion

The incorporation of this console into the measurement facility at the Boulder Laboratories has resulted in a significant reduction in the limits of uncertainty associated with the calibration of volt boxes. The results of measurements made on a box of the type described in RP1419 are well within the predicted worst-case uncertainty of ±8 ppm (see appendix C).

TABLE 1. *Comparison of measurements made by the self-check method with those made on the console*

A Range	Corrections in ppm				Comparison in ppm
	B Self check	Console measurements		*E* Ave of *C* & *D*	*F* *E* − *B*
		C	*D*		
3 /1.5	−2	+5	+1	+3	+5
4.5/1.5	−4	0	+1	0	+4
6 /1.5	−6	0	0	0	+6
7.5/1.5	−7	−4	−1	−2	+5
15 /1.5	−9	−8	−7	−8	+1
30 /1.5	−9	−9	−10	−10	−1
45 /1.5	−7	−6	−6	−6	+1
60 /1.5	−7	−5	−6	−6	+1
75 /1.5	−7	−4	−6	−5	+2
150 /1.5	−3	−3	−2	−2	+1
300 /1.5	−1	0	0	0	+1
450 /1.5	+2	+1	0	0	−2
600 /1.5	+1	+1	+1	+1	0
750 /1.5	+1	+3	+3	+3	+2

These results are shown in table 1. Column B shows the results of measurements made by the "self checking" technique described in appendix II of RP1419. Columns C and D are the results of two independent measurements made by comparing the unknown (previously self-checked) volt box with the standard by means of the console and, in fact, reflect not only the console uncertainties, but the uncertainties in the correction to the standard ratio and any uncertainties introduced by the operator also. The comparisons were made at 20 percent of rated voltage on each range to approximate the conditions under which the self check was made. Column E is the average of columns C and D. These conclusions are corroborated by the results of a second experiment that involved measurements of three master volt boxes in the following manner.

First V.B. 1 was measured against V.B. 2,
then V.B. 3 was measured against V.B. 1, and
finally V.B. 3 was measured against V.B. 2.

In the first and third measurements, V.B. 2 was considered the absolutely perfect standard. In the second measurement, V.B. 1 was considered the absolutely perfect standard.

If the corrections, in ppm, to V. B. 1 resulting from the first measurement are called A; those to V. B. 3 resulting from the second measurement are called B; and those to V. B. 3 resulting from the third measurement are called C, the following relationship should exist [5].

$$A+B-C=0, \tag{8}$$

provided the corrections to the three volt boxes did not change between measurements, and provided no errors are introduced by the measuring system—in this case, the console. To insure unchanging corrections in the volt boxes, measurements were made at reduced voltage. When the data from the measurements were applied to eq (8), the results were as shown in figure 14.

The author is indebted to Joseph J. Barth, who deciphered the many schematics and wiring diagrams and reduced them to operating hardware.

9. References

[1] Silsbee, F. B., and Gross, F. J., Testing and performance of volt boxes, J. Res. NBS **27**, 269–287 (Sept. 1941) RP1419.
[2] Dunfee, B. L., Method for calibrating a standard volt box, J. Res. NBS **67C** (Engr. and Instr.) No. 1, 1–3 (Jan.–Mar. 1963).
[3] Op. Cit., p. 2.
[4] Dunn, A. F., Calibration of a Kelvin-Varley Voltage Divider, 1964 IEEE International Convention Record, Part 8, Sessions on Instrumentation, pp. 213–224.
[5] Youden, W. J., Uncertainties in calibration, IRE Trans. Instr. Vol. **I–II**, Nos. 3 and 4, December 1962, pp. 134–135.

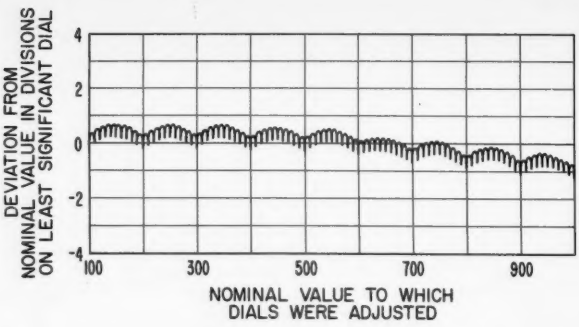

FIGURE 11. *Measured deviations of K-V divider ratio from dial settings.*

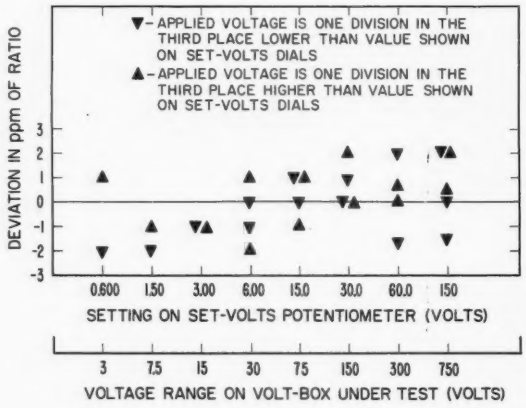

FIGURE 12. *Deviations in measured value of ratio caused by disagreement between value of applied voltage and value to which set-V dials are set.*

10. Appendix A. Evaluation of the Set-Volts Potentiometer

10.1. Kelvin-Varley Circuit (See Fig. 5)

The rigorous mathematical analysis of a Kelvin-Varley divider is quite complex, and has appeared in the literature.[4]

As the divider in the Set-Volts Potentiometer is to be used without applying corrections, the maximum effective uncertainty that will be introduced by the divider is the only thing that must be determined. Individual errors in the several sections are important only in their contribution to the overall error. As a recently calibrated digital voltmeter having combined uncertainties within 0.01 percent was available for the purpose, it was simpler and easier to measure this overall error than to calculate it. Accordingly, the 900 settings on the set-volts divider were measured against the digital voltmeter, and the data were checked at 19 points with a commercial potentiometer (in which the combined uncertainties were within 0.01%). The results of these measurements are shown in figure 11. As can be seen, the largest error introduced by the nonlinearity of the divider is roughly equal to one digit on the third (least significant) dial. When the applied voltage is adjusted to a value equal to one division in the third place higher or lower than the value to which the Set-Volt Potentiometer dials are set, the resulting difference in measured ratio, from that determined when the applied voltage and dial setting are equal, is smaller than the random errors encountered in the measurement. The results of such an experiment are shown in figure 12.

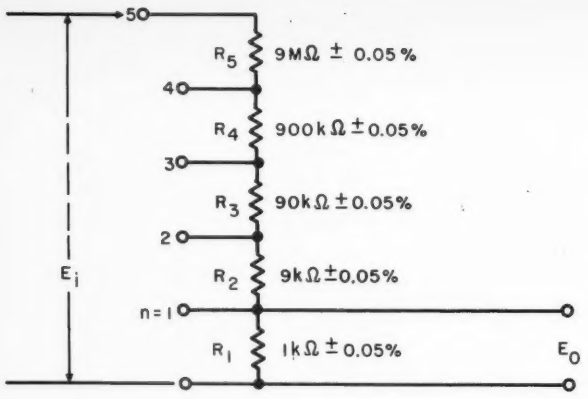

FIGURE 13. *Decimal divider in set-volts potentiometer.*

10.2. Decimal Divider

The decimal divider is shown in figure 13, which corresponds to the circuit of the Decimal Point Section in figure 5. In figure 13, the relationship of E_0 to E_i for any given switch setting, n, is

$$E_0=\left(\frac{R_1}{R_1+R_2+\ldots+R_n}\right)E_i, \tag{A1}$$

where E_0 and R_1, R_2, . . . R_n are the nominal values. The true value, E_0', however, is

$$E_0'=E_0(1+e_a)=\frac{R_1(1+r_1)E_i}{\sum_1^n R_k(1+r_k)}. \tag{A2}$$

Dividing eq (A2) by eq (A1) gives

$$1+e_a=\frac{(1+r_1)\sum_1^n R_k}{\sum_1^n R_k(1+r_k)}, \tag{A3}$$

or

$$e_a=\frac{(1+r_1)\sum_2^n R_k-\sum_2^n R_k(1+r_k)}{\sum_1^n R_k(1+r_k)}, \tag{A4}$$

which reduces to

$$e_a=\frac{\sum_2^n R_k(r_1-r_k)}{\sum_1^n R_k(1+r_k)}. \tag{A5}$$

Equation (A5) will be maximum when $n=5$ and r_2, r_3, r_4, and r_5 are opposite in sign to r_1. In this worst case, assuming the corrections to all the resistors are maximum, i.e., 0.0005,[2] e_a is found to be

$$e_a \doteq 0.001. \tag{A6}$$

11. Appendix B. Evaluation of Errors Associated With the Computing Potentiometer

As explained in the text, the milliameter of the Lindeck-Rothe potentiometer has been replaced by a resistor (R_b) of 10,000 Ω nominal value (see fig. 6). The voltage across R_b will (nominally) be 10^4, 10^5, 10^6, or 10^7 times v_d depending on which value of R_a is switched into the circuit. If this value, V_{R_b}, is applied across the divider circuit, R_1, the nominal value of voltage, E_0, applied to the digital voltmeter would be found by the relation:

$$E_0=\frac{R_2}{R_1}\frac{R_b}{R_a}v_d \tag{B1}$$

[2] The resistors used were individually measured and found to have corrections well within the limits of ± 0.0005.

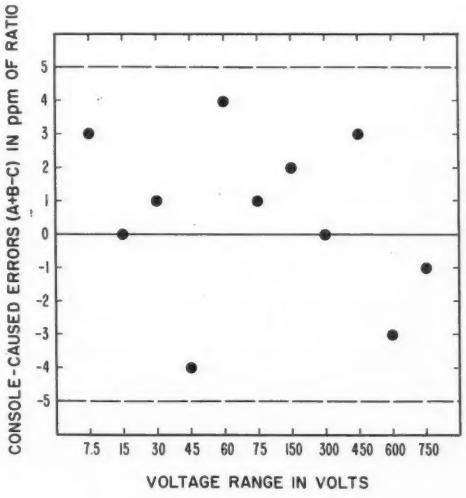

FIGURE 14. *Console-caused errors as determined by intercomparison of three master volt boxes.*

where v_d is any one of the four difference voltages (v_1, v_2, v_3, or v_4), R_1 and R_2 are the displayed (i.e., nominal) values proportional to V and S_n respectively, see eq (1), R_b is nominally 10,000 Ω, and R_a is nominally either 1, 0.1, 0.01, or 0.001 Ω as determined by the position of the Lindeck Shunt switch. However, it is not practicable to measure V_{R_b} without changing its effective value (because of the loading effect of the measuring system) and hence disturbing the ratio of multiplication, R_b/R_a. Therefore, to prevent this disturbance, the voltage is measured across R_b+R_a. With a circuit of this configuration, the voltage applied across R_1 is not V_{R_b}, but $V_{R_b}+V_{R_a}$, and the actual value, E_0', is related to v_d by the equation

$$E_0'=\frac{R_2'}{R_1'}\frac{R_b'+R_a'}{R_a'}v_d. \tag{B2}$$

In eq (B2) the primes indicate actual (as opposed to nominal) values.

As providing automatic correction for the effect of R_a in the numerator of eq (B2) would have appreciably increased the cost of the console, it was decided to treat the circuit *as though the voltage applied across* R_1 *is* V_{R_b} even though in fact this is not the case. This will, of course, introduce an error in addition to that caused by the errors in R_1, R_2, R_a, and R_b. It is the purpose of this appendix to determine the relative error (e_0) in E_0, for any given v_d, resulting both from the errors in the component values and from the presumption that eq (B1) is the circuit equation.

If the circuit of figure 6 is examined rigorously it will be found that the actual value of each of the components differs, although slightly, from the nominal value. If we consider each actual value (designated by a prime) to be comprised of the nominal value and the small difference between nominal and actual (i.e., $R_a'=R_a(1+r_a)$), the circuit equation for determining the actual output voltage for a given v_d is

$$E_0'=E_0(1+e_0)=\frac{R_2(1+r_2)}{R_1(1+r_1)}\left[\frac{R_b(1+r_b)+R_a(1+r_a)}{R_a(1+r_a)}\right]v_d \tag{B3}$$

where e_0, r_1, r_2, r_a, and r_b are the relative differences between the actual values, E_0', R_1', R_2', R_a', and R_b' and the nominal values E_0, R_1, R_2, R_a, and R_b, respectively.

Equation (B3) may be more readily analyzed if it is considered to be of the form

$$E_0(1+e_0)=T_1(1+t_1)T_2(1+t_2)v_d. \tag{B4}$$

If, in eq (B4), the following relations hold,

$$T_1(1+t_1)=\frac{R_2(1+r_2)}{R_1(1+r_1)}, \tag{B5}$$

$$T_2(1+t_2)=\frac{R_b(1+r_b)+R_a(1+r_a)}{R_a(1+r_a)}, \tag{B6}$$

$$T_1=\frac{R_2}{R_1}, \tag{B7}$$

and

$$T_2=\frac{R_b}{R_a} \tag{B8}$$

then eq (B4) may be rewritten as

$$E_0(1+e_0)=\frac{R_2}{R_1}\frac{R_b}{R_a}(1+t_1)(1+t_2)v_d. \tag{B9}$$

From a comparison of eq (B9) and eq (B1) it is immediately apparent that

$$1+e_0=(1+t_1)(1+t_2). \tag{B10}$$

It is now possible to examine each of the component errors, t_1 and t_2, individually; this possibility greatly facilitates the analysis.

Let us first determine the relative error, t_2. If we divide eq (B6) by eq (B8), the result is

$$1+t_2=\frac{R_a}{R_b}+\frac{1+r_b}{1+r_a}. \tag{B11}$$

If $|r_a|$ and $|r_b|$ are small (i.e., <0.001), eq (B11) reduces approximately[3] (i.e., to first degree terms) to

$$t_2\doteq\frac{R_a}{R_b}+r_b-r_a. \tag{B12}$$

In the circuit, the resistors R_a and R_b have been chosen such that $|r_a|<0.0004$ and $|r_b|<0.0001$. From figure 6 it will be seen that

$$\frac{R_a}{R_b}\leq 0.0001. \tag{B13}$$

Thus t_2 will be within the limits

$$|t_2|\leq\left(\frac{R_a}{R_b}\right)_{\max}+|r_a|+|r_b|=0.0006. \tag{B14}$$

The evaluation of t_1 may be handled in a similar manner. The division of eq (B5) by eq (B7) gives

$$1+t_1=\frac{1+r_2}{1+r_1}. \tag{B15}$$

[3] If $|r_a|$ and $|r_b|$ are each less than 0.001, the difference between the right-hand side of eq (B12) and the true value,

$$t_2=\frac{R_a}{R_b}+\frac{1+r_b}{1+r_a}-1, \tag{F1}$$

is

$$\left|\frac{r_a(r_b-r_a)}{1+r_a}\right|<2\times10^{-6} \tag{F2}$$

and hence is so small as to not significantly affect the value of t_2.

If $|r_1|$ and $|r_2| < 0.001$, eq (B15) becomes

$$t_1 \doteq r_2 - r_1. \tag{B16}$$

From figure 6, R_1 is seen to comprise many resistors in series. These resistors and switches have been chosen so that the actual value of the resistance added by any decade, on any position, does not differ from the nominal value by more than ± 0.03 percent. Also the two 1 kΩ resistors have been similarly chosen. Hence the circuit of R_1 may be realistically represented by eq (B17). (As R_1 is the total resistance of the network, it is represented by R_t in the following analysis.)

$$R_t(1+r_t) = \sum_{k=1}^{n} R_k(1+r_k), \tag{B17}$$

where $R_1, R_2, \ldots, R_n$ are the resistors in the S_n switch, the 1 kΩ resistors connected to either end of that switch, and all other resistors that have been switched into the circuit by the settings of the three "$V=$" dials. Equation (B17) may be rewritten in the form

$$R_t(1+r_t) = \sum_{1}^{n} R_k + \sum_{1}^{n} R_k r_k. \tag{B18}$$

Since

$$R_t = \sum_{1}^{n} R_k, \tag{B19}$$

eq (B18) may be divided by R_t to give the equation

$$r_t = \frac{1}{R_t}\sum_{1}^{n} R_k r_k = \left(\sum_{1}^{n} R_k r_k\right) \Big/ \left(\sum_{1}^{n} R_k\right). \tag{B20}$$

That is, r_t is dependent upon the sum of the differences, in ohms, between the actual and nominal values of the resistors R_k in ratio with the sum of the nominal values. If, as previously stated, all values of $|r_k|$ are within some limit, r, then the value, r, as substituted for $|r_k|$ may be factored out of eq (B20) to yield the bounds to r_t; i.e.,

$$|r_t| \leq r \frac{\sum_{1}^{n} R_k}{\sum_{1}^{n} R_k} = r. \tag{B21}$$

Therefore, the bounds to r_t (i.e., to the relative difference between the actual and nominal values of R_1 in fig. 6) are 0.0003. Similar reasoning[4] can be used to determine the bounds to the relative error of R_2 (fig. 6) with the result:

$$|r_2| \leq 0.0003. \tag{B22}$$

Hence, the bounds to t_1 are found, using eq (B16), to be

$$|t_1| \leq 0.0006. \tag{B23}$$

However, the validity of this value is questionable since the interdependence of the errors of R_1 and R_2 was not considered in the analysis. A more rigorous analysis results when the resistance network R_1 is considered to comprise the independent resistances R_3 and R_2 such that

$$R_3 + R_2 = R_1. \tag{B24}$$

If this is done, eq (B5) becomes

$$T_1(1+t_1) = \frac{R_2(1+r_2)}{R_3(1+r_3) + R_2(1+r_2)}. \tag{B25}$$

The determination of the error introduced by R_3 and R_2 may be found by operating on the relation

$$\frac{R_2}{R_3+R_2}(1+e_r) = \frac{R_2(1+r_2)}{R_3(1+r_3)+R_2(1+r_2)}. \tag{B26}$$

Dividing eq (B26) by $R_2/(R_3+R_2)$ gives

$$1+e_r = \frac{(R_3+R_2)(1+r_2)}{R_3(1+r_3)+R_2(1+r_2)}. \tag{B27}$$

If $|r_3|$ and $|r_2| < 0.001$ (this has already been demonstrated as the reasoning used in the determination of r_t applies with equal validity to r_3), eq (B27) may be approximated by (the reasoning of footnote 4 applies)

$$1+e_r \doteq \frac{R_3+R_2}{R_2+R_3(1+r_3-r_2)} \tag{B28}$$

being more than adequately accurate for the purpose intended. Subtracting 1 from both sides allows eq (B28) to be reduced to the more usable form,

$$e_r = \frac{R_3(r_2-r_3)}{R_2+R_3(1+r_3-r_2)}. \tag{B29}$$

From eq (B29), $|e_r|$ approaches the value

$$\frac{r_2-r_3}{1+r_3-r_2} \tag{B30}$$

[4] As R_3 is in parallel with the input impedance of the digital voltmeter, the actual resistance may differ from nominal by as much as 0.09 percent unless compensating techniques are used. These techniques, in the form of trimmer resistors, were used on R_2. Hence the resistances shown are the effective values including the input impedance of the digital voltmeter, adjusted to within ±0.03 percent (300 ppm).

as a maximum limit as the ratio R_3/R_2 increases without bound. Using bounds of ± 0.0003 for r_3 and r_2

$$|e_r| \leq \frac{0.0003+0.0003}{1-.0003-.0003}. \tag{B31}$$

Hence

$$|e_r| \leq 0.0006. \tag{B32}$$

A comparison of statement (B32) with statement (B23) shows that (B23) is indeed valid.

Referring again to eq (B4), the value, e_0, is quite approximately determined by the relation

$$e_0 \doteq t_1+t_2 \tag{B33}$$

provided $|t_1|$ and $|t_2|$ are < 0.001. That these values are less than 0.001 has been demonstrated. Therefore e_0 may be determined from eq (B33) (using the limits of t_1 and t_2 listed in statements (B14) and (B23)) to be

$$|e_0| \leq |0.0006|+|0.0006| = 0.0012. \tag{B34}$$

This figure, found by direct addition, is certainly the pessimistic limit in the worst case (i.e., where $R_1/R_2 \rightarrow \infty$). A more realistic appraisal might be to combine the different independent errors by the square root of the sum of the squares, as they are as likely to compensate for one another as to add. If this is done using eq (B12) and (B16), then with high probability

$$|e_0| \leq \sqrt{r_1^2+r_2^2+(R_a/R_b)^2+r_b^2+r_a^2}; \tag{B35}$$

the result is

$$|e_0| \leq 0.0006. \tag{B36}$$

The actual limits of e_0 will lie somewhere between these two extremes.

Hence the premise of eq (B1) is found to be uncertain by about ± 0.1 percent of E_0.

Total Measurement Circuit Uncertainty. An additional uncertainty of ± 0.2 percent (e_m) of the measured voltage is introduced by the digital voltmeter. Also the digital display has an inherent uncertainty of $\pm$one digit in the last place. Because of the way in which the display is used, this $\pm$one digit causes an absolute uncertainty (e_d) of ± 1 ppm of the ratio (of the unknown volt box) in the worst case for each displayed value.

12. Appendix C. Evaluation of the Measurement Uncertainty of the Volt Box Console

This evaluation does not include the effect of the uncertainties associated with the corrections to the Standard Volt Box.

The equation of correction for the unknown volt box as used by the operator of the console is

$$X_n[1+(x)10^{-6}] = X_n[1+(\mu_s+V_1+V_2+V_3+V_4)10^{-6}], \tag{C1}$$

where X_n is the nominal ratio of the unknown, x is the correction to the unknown in ppm, V_1, V_2, V_3, and V_4 are the computed results in ppm, and μ_s is the correction to the standard volt box in ppm.

The error in V_1, V_2, V_3, or V_4 is closely approximated by the relation:

$$e \approx e_v - e_V, \tag{C2}$$

where e_v is the error resulting from the computer and e_V is the error caused by the set-volts potentiometer. The difference in errors shown in eq (C2) is the reason that the zener supply for the set-volts potentiometer need only be calibrated against the digital voltmeter. If the digital voltmeter is in error (absolutely) by some value, the set-volts potentiometer will be in error by the same value, and the two errors will subtract to zero.

The uncertainties in e resulting from the dividers in the set-volts potentiometer, the resistors in the computing circuits, etc., must be considered as the signs of these uncertainties are not known.

e_v and e_V are the actual values of the errors and, of course, are not known. It is possible to determine the approximate bounds within which these values must fall.

The error, e_v, is comprised of the contributing errors e_0 (the error in the voltage measured by the digital voltmeter), e_m (the error introduced by the digital voltmeter circuits), and e_d (the uncertainty in the last digit of the display) (see appendix B). These components have been determined to have the limits

$|e_0| \leq 0.0012$ of voltage measured by the digital voltmeter

$|e_m| \leq 0.0002$ of voltage measured by the digital voltmeter

$e_d = \pm 1$ ppm of measured ratio.

The values of the limits of e_0 and e_m are functions of the voltage that is measured by the digital voltmeter and can be combined. Since e_0 and e_m are independent errors, their uncertainties can be combined by the relation:

$$|e_v'| \leq \sqrt{e_0^2+e_m^2} \tag{C3}$$

to give the highly probable limits to this portion of e_v. Thus

$$|e_v'| \leq \sqrt{(0.0012)^2+(0.0002)^2} \tag{C4}$$

$$|e_v'| \leq 0.0012. \tag{C5}$$

However, there is a possibility that the component errors could, under some circumstances, be of such sign that they would add, giving a value approximating the simple sum of the limits of uncertainty. Under these conditions

$$|e_r''| \leq 0.0014. \tag{C6}$$

The value of e_d must be treated separately.

The error e_V, is also comprised of component errors. These are e_a, the error resulting from the divider of figure 13, (see appendix A) and the errors introduced by the Kelvin-Varley divider.

The value of e_a has been determined to be within the limits ± 0.0001 of the applied voltage, V. The errors resulting from the Kelvin-Varley divider are somewhat obscure, but conservatively may be assumed to lie within the limits ± 2 ppm of the measured ratio.

The accuracies of the values of V_1, V_2, V_3, and V_4 are directly dependent upon the accuracy with which the applied voltage can be measured (see eqs (2) and (3) in the text). However, the error in the measurement of the applied voltage will be the same for each value, and, though the sign is not known, it will be the same also. Hence the uncertainty of the measured ratio will very probably lie within the limits

$$|u| \leq [(V_1 e_v'' + V_2 e_v'' + V_3 e_v'' + V_4 e_v'') + (V_1 + V_2 + V_3 + V_4)e_a + 4e_d + e_{kv}] \tag{C7}$$

where e_{kv} is the value of the limits of the error introduced by the Kelvin-Varley divider in ppm of ratio. When the limits of the different component uncertainties are substituted in eq (C7), the limits of u are found to be approximately

$$|u| \leq 8 \text{ ppm}. \tag{C8}$$

(Paper 70C3–229)

JOURNAL OF RESEARCH of the National Bureau of Standards—C. Engineering and Instrumentation
Vol. 70C, No. 3, July–September 1966

Corrosion Rates of Binary Alloys of Nickel and Iron Measured by Polarization Methods

W. J. Schwerdtfeger

Institute for Materials Research, National Bureau of Standards, Washington, D.C.

(May 6, 1966)

Specimens of ten binary alloys of nickel and iron containing 3, 5, 10, 16, 20, 30, 36, 50, 57, and 81 percent Ni and of the metals nickel and iron were immersed for 7 months in 265 gallons of city water to which had been added 3 percent by weight of sodium chloride.

Cathodic and anodic polarization curves of the specimens were obtained at about 22 periodic intervals throughout the exposure period. Corrosion currents, calculated from currents at breaks in the curves, were converted to corrosion rates expressed as weight losses by applying Faraday's law. The calculated weight losses were in reasonable agreement with the actual weight losses.

The polarization rates, $\Delta V/\Delta I$, of the specimens calculated from cathodic polarization curves (cathodic control prevailed) at several intervals throughout the exposure period were plotted on logarithmic coordinates with respect to the corrosion current densities calculated from breaks in the same curves. Similarly, the averages of these $\Delta V/\Delta I$ values were also plotted on logarithmic coordinates versus the actual corrosion rates expressed as weight losses. Both plots conformed to the theoretical slope of -1.

Key Words: Corrosion rates, Ni-Fe alloys, polarization techniques, polarization rate, polarization resistance, polarization circuits, Ni-Fe pitting.

1. Introduction

A few years ago, it was demonstrated experimentally that the corrosion rates of a series of ferrous alloys, containing chromium additions up to 18 percent and a similar series with 3 percent of silicon in addition to the chromium, exposed to a 3 percent sodium chloride solution, could be calculated from currents associated with changes of slope (breaks) in polarization curves [1].[1] The sensitivity of the method was shown by the fact that the weight loss of the 18 Cr alloy attributed to corrosion was measured satisfactorily even though the apparent area affected by corrosion was less than 1 percent of the entire surface. The polarization curves of the alloys showed that the known critical change in corrosion rate (expressed as weight loss) for this range of chromium occurred when the corrosion reaction changed from cathodic to anodic control, between 11.4 and 14.3 percent Cr.

The reason for the laboratory measurements described in this paper, using binary alloys of nickel and iron, was to explore further the practicability of polarization techniques as methods of evaluating rates of corrosion. The corrosion rates of several binary alloys between 3 and 81 percent nickel, including the unalloyed metals, were measured by the above technique and also by a method which has been called "polarization resistance" but is referred to by this writer as polarization rate $\Delta V/\Delta I$.

The significance of the slope, $\Delta V/\Delta I$, of the controlling polarization curve was observed by the author and related to the break method [2] but was never further pursued until after Skold and Larson [3] found the method favorable. They observed that a linear relationship existed when corrosion rate (expressed as weight loss) was plotted versus $\Delta V/\Delta I$ on logarithmic coordinates. Shortly thereafter, Stern provided a theoretical basis for the polarization resistance method [4]. These methods among others have also been discussed by Phelps [5]. The writer has found it desirable to use both techniques simultaneously as an aid in interpreting and checking data [6, 7] and this procedure was followed in the measurements about to be described.

2. Experimental Procedure

2.1. Preparation and Exposure of Specimens

The binary alloys were forged and heat treated by the Armco Steel Corporation. Their compositions according to analysis are shown in table 1. Forgings, 0.875 in. × 0.875 (2.2 cm × 2.2 cm) in cross section, were machined into specimens 0.625 in. (1.59 cm) diam × 12 in. (30 cm) long. A hole, 0.25 in. (6.3 mm) diam centered 0.32 in. (8.1 mm) from one end, was drilled through the specimen to permit insertion of a Nichrome wire, No. 30 B & S gage, 0.010 in. (0.25 mm) diam, which served as a loop to hold the specimen in suspension below the surface of the corrodent. All edges were

[1] Figures in brackets indicate the literature references at the end of this paper.

rounded, particularly at the hole, in order to assure accuracy in weight loss measurements. This precaution also prevented nicking of the suspension wire and provided good electrical contact as this wire also conducted the polarizing current.

The method used in suspending the specimens and the reasons therefor were previously described [1]. The Nichrome was always cathodic to the specimens, even to the nickel specimen, and galvanic action, if any, was insignificant as previously observed with the Fe-Cr alloys.

Before exposure, the specimens were degreased, scrubbed with scouring powder, rinsed, rubbed with fine-grit abrasive, scrubbed under running hot water, dried by air-blast and then weighed to the nearest 2 mg.

Twelve specimens, each of different composition (table 1) were exposed to Washington, D.C. city water to which was added 3 percent by weight of sodium chloride. The salt water was contained by an open cylindrical vat, 66 in. (16.7 dm) diam. The depth of the water was maintained at 18 in. and the volume of water about 265 gal. The specimens, about 13 in. (33 cm) apart, were staggered and suspended in two rows across the center of the vat, the tops of the specimens being 2 in. (5 cm) below the water surface. Electrical contact with a given specimen was made through a terminal strip mounted on the outside of the vat from which wires were permanently connected to the Nichrome suspension loops by battery clips. The temperature of the water was not controlled but was measured regularly during exposure.

TABLE 1. *Composition of alloys*

Specimen	Compositon, percent*	
	Iron	Nickel
1	100	0
2	97	3
3	95	5
4	91	10
5	85	16
6	81	20
7	70	30
8	64	36
9	49	50
10	43	57
11	21	81
12	0	100

*Analyzed by x-ray fluorescence techniques for iron and nickel in each specimen. Iron and nickel were determined separately. Values as measured were within ±0.5 percent and are rounded off to the nearest 1 percent. Two specimens, 1 and 11, were analyzed by a qualitative spectrochemical method for impurities, resulting in the following: Specimen 1 had Ni, Cu, Si, Ti, each between 0.01–0.1 percent, Al < 0.01 percent. Specimen 11 had Si between 0.1–1.0 percent, Cu, Co, Ti, each between 0.01–0.1 percent, Al, Mn each < 0.01 percent.

2.2. Electrical Measurements

Potentials were measured with reference to a saturated calomel half-cell. Contact between the salt water and the half-cell was by an agar-salt bridge in the form of a 5-ft (152 cm) length of flexible tubing containing a mixture of agar and potassium chloride. The electrical continuity of the agar-salt bridge was assured by a cotton cord saturated with potassium chloride. The cord extended the entire length of the tube enveloped by the agar-salt mixture. The end of the tube was placed into the water through a sleeve mounted about 6 in. (15 cm) from the wall inside of the vat. The distance between the tip of the salt-bridge and a specimen varied between 18 in. (46 cm) and 40 in. (101 cm), depending on the location of the specimen. When electrical measurements were not in progress, the salt-bridge was removed from the water. When polarization measurements were being made, auxiliary electrodes consisting of two strips of zinc sheet, 4 in. (10 cm) wide × 18 in. (46 cm) long, were hung over the wall of the vat.

Measurements were made on about 22 occasions during the exposure period of 210 days. The measurements involved corrosion potential and the running of cathodic and anodic polarization curves. For a given specimen, an interval of several hours, sometimes 24 hr, was permitted between cathodic and anodic polarization runs, not necessarily in that order, but usually so.

Corrosion potentials were measured with a high resistance voltmeter and polarization was measured and recorded with a two-pen (current and potential) strip-chart recorder. The length of time required for obtaining a polarization curve varied from about 15 to 30 min. Most of the polarization data were obtained by using the galvanodynamic method and about 25 percent using a potentiodynamic method for comparison. The schematic circuit diagrams for these methods are shown in figures 1 and 2, respectively. Both circuits incorporate the Holler bridge for balancing out undesirable voltage drop (IR) from the recorded potentials [8]. In figure 1, the polarizing current is steadily increased by varying the applied voltage at a linear rate by means of the ten-turn motor-driven potentiometer R_1 with resistor R_3 set for a predetermined range of polarizing current. In figure 2, initially the applied voltage between the specimen and the reference electrode is manually adjusted by setting R_4 to a value equal to the corrosion potential after which R_4 becomes motor-driven and sweeps the range of potential required for polarization while R_3 is set at a comparatively low value of resistance so as to not unduly limit the applied current. In viewing the recorder charts, the break in the curve is more evident on the potential plot than on the current plot with the galvanodynamic method, while the reverse is true when the potential sweep circuit (fig. 2) is used.

2.3. Removal of Corrosion Products

Following removal from the salt water, the specimens were held under running hot water and scrubbed with a stiff fiber-bristle brush. They were then placed into an ultrasonic cleaning tank (for 10 min) containing a 10 percent solution, at 150 °F, of ammonium citrate made alkaline (*p*H 9–10) by the addition of ammonium hydroxide. Then, the specimens were again brushed under running hot water, dried under an air

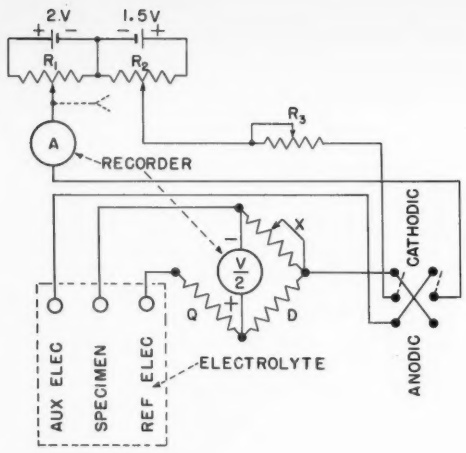

FIGURE 1. *Polarization circuit-galvanodynamic method.*
$R_1 = 25\Omega - 10$ turn (motor driven -0.2 RPM), $R_2 = 100\Omega 10$ turn, R_3, 10,000Ω, $X = 100\Omega - 10$ turn, $Q = D = 100{,}000\Omega$.

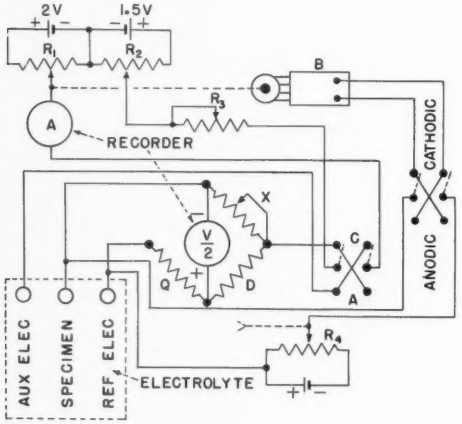

FIGURE 2. *Polarization circuit—potentiodynamic method.*
$R_1 = 50\Omega - 10$ turn (motor driven—variable speed—reversible), $R_2 = 100\Omega$ 10 turn, $R_3 = 10{,}000\Omega$, $R_4 = 25\Omega - 10$ turn (motor driven -0.2 RPM reversible), $X = 100\Omega - 10$ turn, $Q = D = 100{,}000\Omega$, $B =$ motor (controlled by voltage differential).

blast and weighed to the nearest 2 mg. After repeating this procedure the third time, there was no significant change in weight; the final weights were then subtracted from the original weights in computing the actual metal loss attributed to corrosion.

3. Results and Discussion

On the 210th day of exposure the specimens were removed from the salt water. Although the object of the experimental work was primarily that of evaluating the corrosion rate measuring techniques, the data in table 2 show how the results to be described are related to the apparent areas corroded and to the depths of the pits. Note, that all apparent corrosion on the nickel (specimen 12) seems to have been confined to one pit.

Polarization curves from data on recorder charts obtained on the 202d day of exposure are shown in figures 3 and 4 on semilogarithmic and rectangular coordinates, respectively. While such data, ordinarily, are shown on semilogarithmic coordinates, the rectangular plot helps to verify the break in the curve and the value of applied current at which it occurs. The absence of a break on the latter would place doubt on the extrapolated semilogarithmic value. The values of I_p (break in the cathodic curve) and of I_q (break in the anodic curve) chosen in calculating the corrosion currents (table 3) are marked I_p and I_q in figures 3 and 4 and are indicated by vertical dashes (where dashed lines intersect). It will be noted that there is reasonably good agreement between figures 3 and 4 for a given specimen in the values of I_p, but apparently not as good agreement in the values of I_q.

TABLE 2. *Appearance of the binary alloys of nickel and iron after cleaning which followed 210 days of exposure to salt water*

Specimen	Apparent area corroded	Remarks, pit depths
	Percent	
1 (100 Fe)	85	General corrosion (0–3 mils*).
2 (3 Ni)	70	General corrosion (0–3 mils), except for one pit (5 mils).
3 (5 Ni)	80	General corrosion (0–3 mils).
4 (10 Ni)	75	General corrosion (0–3 mils).
5 (16 Ni)	65	General corrosion (0–5 mils).
6 (20 Ni)	50	General corrosion (0–8 mils).
7 (30 Ni)	40	Lower 4.5 in. (11 cm) (opposite suspension end) of specimen length not corroded, otherwise—general corrosion (0–8 mils).
8 (36 Ni)	50	Spotty corrosion to 10-mil depths.
9 (50 Ni)	15	8 in. (20 cm) of the specimen measured from the lower end was not corroded. Spotty corrosion (8–12 mils) on the upper 4 in. (10 cm). Pits to 45 mils in depth at the top end.
10 (57 Ni)	< 1	Scattered pits (2–6 mils) in about 24 places. One pit (50 mils) at the top end.
11 (81 Ni)	< 0.05	Three pits (5–25 mils) on the surface. One pit (50 mils) inside of the mounting hole.
12 (100 Ni)	< 0.02	No corrosion, except for one pit (60 mils deep) inside the mounting hole.

*mil = 0.001 in. (25.4 μ).

The values of I_q, pertaining to these data, selected from the rectangular coordinates are considered the more significant, except for specimens 11 (81 Ni) and 12 (100 Ni). The actual values of I_p and I_q were obtained before compressing the scales (particularly the ordinates) as shown in figures 3 and 4. The data for all specimens are shown on one figure so that the reader can get an overall picture of what the curves portray for different rates of corrosion. When calculating the corrosion current (see the equation, footnote b, table 3), the smaller current, whether it be I_p or I_q, is the more significant (controlling) and fortunately can be extrapolated with the greater degree of accuracy.

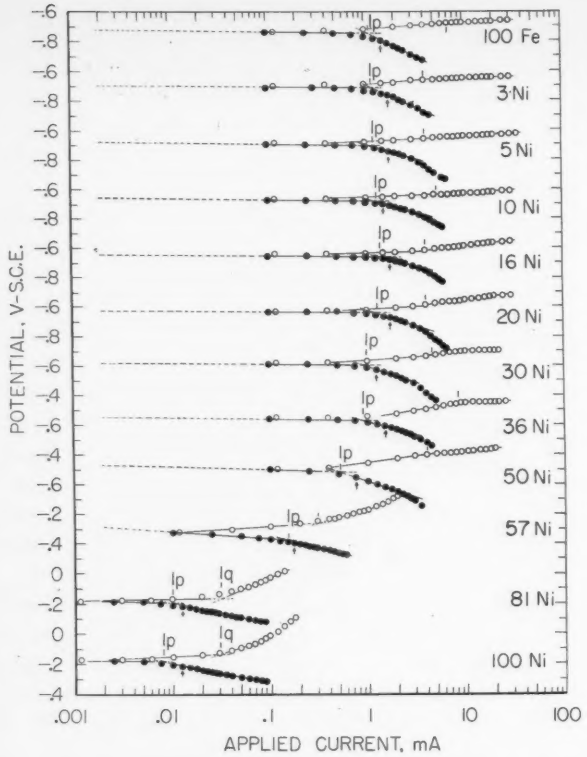

FIGURE 3. *Polarization curves of iron, nickel, and binary alloys of nickel and iron obtained on the 202d day of exposure to city water having added 3 percent by weight of sodium chloride.*

○ anodic, ● cathodic.

NOTE: Values of I_p and I_q actually used for the calculations (table 3) are marked I_p and I_q (figs. 3 and 4), for example, I_p (fig. 3) is used with I_q (fig. 4) for the 100 Fe specimen. In the case of the 100 Ni specimen, I_p and I_q of figure 3 are used, etc. The ordinates (figs. 3 and 4) are compressed to save space. In going up the scale, the potentials become less negative. Thus, for the 30 Ni specimen, the corrosion potential is about −0.58 V (see fig. 4).

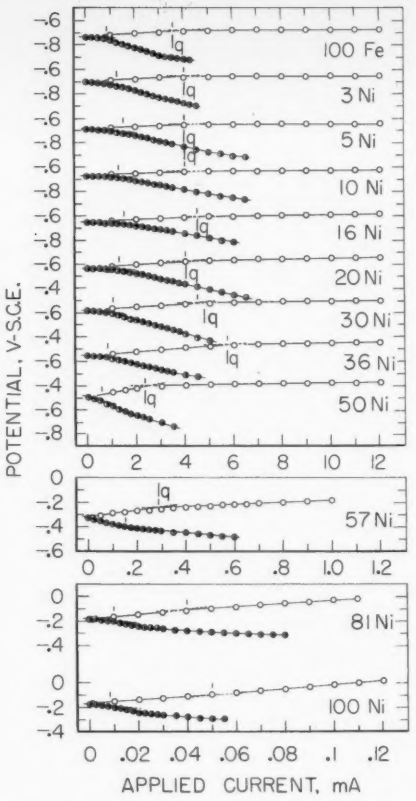

FIGURE 4. *Same data as in figure 3, plotted on rectangular coordinates.*

○ anodic, ◑ cathodic. See "Note" figure 3.

All the values of I_p and I_q, calculated corrosion currents, calculated weight losses, and actual weight losses for all specimens are tabulated in table 3. In calculating weight losses, the electrochemical equivalent for ferrous iron was chosen for the alloys with less than 50 percent of nickel, and that of nickel for the alloys having 50 percent or more of nickel. Actually, the equivalent value chosen is not significant here as the difference (about 5%) in results obtained is within the limit of accuracy with which the polarization curves can be evaluated.

In table 3, beginning with the 78th day of exposure and on through the 117th day, all data were obtained using the potentiodynamic method of polarization. It will be noted that the data pattern fits in quite well with the pattern before and after this period obtained using the galvanodynamic polarization technique. For specimens 1 through 6, the change from $I_q = 10\ I_p$ to lesser values of I_q is not believed to be significant. The potentiodynamic method offered no advantage in obtaining these data and required more instrumentation.

Figure 5 shows how the corrosion rates vary with the nickel content and how the calculated and actual values compare. The biggest reduction in corrosion rate occurred in changing from 50 Ni to 57 Ni. For the particular environment, nickel in amounts up to 20 percent seem to offer no advantage from the standpoint of corrosion resistance. Pettibone [9] demonstrated an advantage in the corrosion resistance of 36.53 Ni steel over mild steel in four sea water environments for exposure periods varying from 5 to 15 years. It has also been reported that the corrosion rate of a 26 percent Ni alloy of iron and nickel was about one-third that of wrought iron in sea water as well as in the atmosphere [10].

When specimen 8 (36 Ni) was initially exposed, the corrosion current was about one-eighth that of the specimens with lesser amounts of nickel (table 3). Between the 4th and 7th days, the corrosion potential of specimen 8 changed from −0.355 V to −0.540 V (potentials are not shown in the table) and the corrosion current increased fivefold. On specimen 9 (50 Ni), a low rate of corrosion prevailed through the 34th

TABLE 3. *Corrosion weight losses calculated from polarization data obtained on a series of alloys containing nickel and iron exposed to a 3-percent sodium chloride solution for 7 months*

Specimen	Exposure time	Polarizing current at break in curve [a]		Corrosion current [b]	Weight loss [c]	
		Cathodic I_p	Anodic I_q	i_0	Calculated cumulative	Actual
	Days	*mA*	*mA*	*mA*	*mg*	*mg*
1 (100 Fe)	4	1.8	$10I_p$ [d]	1.6	160	
	14	1.0	$10I_p$ [d]	0.91	470	
	20	0.75	$10I_p$ [d]	0.68	590	
	28	1.0	$10I_p$ [d]	0.91	750	
	34	0.93	$10I_p$ [d]	0.84	920	
	41	1.1	$10I_p$ [d]	1.0	1100	
	46	1.0	$10I_p$ [d]	0.91	1200	
	54	0.95	$10I_p$ [d]	0.86	1400	
	62	1.1	$10I_p$ [d]	1.0	1600	
	70	1.2	$10I_p$ [d]	1.1	1800	
	78	1.1	6.0	0.93	2000	
	88	1.2	8.2	1.0	2200	
	95	1.1	8.0	0.96	2400	
	102	1.3	7.3	1.1	2600	
	117	1.2	7.8	1.0	3000	
	125	1.1	9.0	0.98	3200	
	137	1.0	7.0	0.88	3400	
	145	0.80	4.7	0.68	3600	
	159	1.2	4.5	0.95	3900	
	172	1.1	4.5	0.88	4200	
	202	1.1	3.5	0.84	4800	
	210				5000	4590
2 (3 Ni)	4	1.6	$10I_p$ [d]	1.4	140	
	14	1.3	$10I_p$ [d]	1.2	460	
	20	0.95	$10I_p$ [d]	0.85	610	
	28	1.2	$10I_p$ [d]	1.1	810	
	34	1.1	$10I_p$ [d]	1.0	970	
	41	1.1	$10I_p$ [d]	1.0	1100	
	46	1.0	$10I_p$ [d]	0.91	1300	
	54	0.95	$10I_p$ [d]	0.85	1400	
	62	1.2	$10I_p$ [d]	1.1	1600	
	70	1.3	$10I_p$ [d]	1.2	1900	
	77	1.3	7.5	1.1	2100	
	88	1.3	8.0	1.1	2400	
	95	1.2	7.5	1.0	2500	
	102	1.3	6.8	1.1	2700	
	117	1.4	8.8	1.2	3200	
	125	0.95	6.0	0.82	3400	
	137	1.3	6.0	1.1	3600	
	145	1.1	4.0	0.86	3800	
	159	1.3	9.0	1.1	4200	
	172	1.2	4.0	0.92	4500	
	202	1.1	4.0	0.86	5200	
	210				5300	4660
3 (5 Ni)	4	1.6	$10I_p$ [d]	1.4	140	
	14	1.0	$10I_p$ [d]	0.91	410	
	20	0.80	$10I_p$ [d]	0.73	540	
	28	1.2	$10I_p$ [d]	1.1	720	
	34	1.1	$10I_p$ [d]	1.0	890	
	41	1.3	$10I_p$ [d]	1.2	1100	
	46	1.1	$10I_p$ [d]	1.0	1200	
	54	0.98	$10I_p$ [d]	0.89	1400	
	62	1.3	$10I_p$ [d]	1.2	1600	
	70	1.5	$10I_p$ [d]	1.4	1900	
	78	1.3	8	1.1	2100	
	88	1.2	8.3	1.0	2400	
	95	1.5	7.5	1.3	2600	
	102	1.5	7.3	1.2	2800	
	118	1.3	8.0	1.1	3300	
	125	1.1	7.0	0.96	3400	
	137	1.3	9.0	1.1	3700	
	145	1.2	5.0	0.97	3900	
	159	1.3	4.5	1.0	4300	
	172	1.2	4.2	0.93	4600	
	202	1.2	4.0	0.92	5300	
	210				5500	4860

TABLE 3. *Corrosion weight losses calculated from polarization data obtained on a series of alloys containing nickel and iron exposed to a 3-percent sodium chloride solution for 7 months*—Continued

Specimen	Exposure time	Polarizing current at break in curve [a]		Corrosion current [b]	Weight loss [c]	
		Cathodic I_p	Anodic I_q	i_0	Calculated cumulative	Actual
	Days	*mA*	*mA*	*mA*	*mg*	*mg*
4 (10 Ni)	4	1.5	$10I_p$ [d]	1.4	140	
	14	1.3	$10I_p$ [d]	1.2	470	
	20	1.0	$10I_p$ [d]	0.91	630	
	28	1.3	$10I_p$ [d]	1.2	830	
	34	1.3	$10I_p$ [d]	1.2	1000	
	41	1.1	$10I_p$ [d]	1.0	1200	
	46	1.2	$10I_p$ [d]	1.1	1300	
	55	1.2	$10I_p$ [d]	1.1	1600	
	62	1.2	$10I_p$ [d]	1.1	1800	
	70	1.3	$10I_p$ [d]	1.2	2000	
	78	1.2	7.5	1.0	2200	
	88	1.2	9.0	1.1	2500	
	95	1.2	8.0	1.0	2600	
	102	1.3	8.0	1.1	2800	
	117	1.3	7.0	1.1	3200	
	125	1.2	7.0	1.0	3400	
	137	1.5	14.0	1.4	3800	
	145	1.2	5.0	0.97	4000	
	159	1.3	4.0	0.98	4400	
	172	1.3	4.2	0.99	4700	
	202	1.3	4.0	0.98	5400	
	210				5600	4880
5 (16 Ni)	4	1.9	$10I_p$ [d]	1.7	170	
	14	1.4	$10I_p$ [d]	1.3	550	
	20	1.2	$10I_p$ [d]	1.1	720	
	28	1.5	$10I_p$ [d]	1.4	980	
	34	1.0	$10I_p$ [d]	0.90	1100	
	41	1.2	$10I_p$ [d]	1.1	1300	
	46	1.2	$10I_p$ [d]	1.1	1500	
	55	1.3	$10I_p$ [d]	1.2	1700	
	62	1.5	$10I_p$ [d]	1.4	1900	
	70	1.5	$10I_p$ [d]	1.4	2200	
	78	1.4	8.7	1.2	2500	
	88	1.5	9.0	1.3	2800	
	95	1.4	8.0	1.2	3000	
	102	1.7	7.1	1.4	3200	
	117	1.6	8.4	1.3	3700	
	125	1.4	6.0	1.1	4000	
	137	1.5	5.0	1.1	4300	
	145	1.5	4.5	1.1	4500	
	159	1.4	4.0	1.0	4900	
	172	1.5	4.0	1.1	5200	
	202	1.4	4.5	1.1	6100	
	210				6300	5350
6 (20 Ni)	5	2.0	$10I_p$ [d]	1.8	220	
	12	1.5	$10I_p$ [d]	1.4	500	
	20	1.1	$10I_p$ [d]	1.0	740	
	28	1.5	$10I_p$ [d]	1.4	990	
	34	1.2	$10I_p$ [d]	1.1	1200	
	41	1.1	$10I_p$ [d]	1.0	1400	
	46	1.1	$10I_p$ [d]	1.0	1500	
	55	1.2	$10I_p$ [d]	1.1	1700	
	62	1.1	$10I_p$ [d]	1.0	1900	
	70	1.2	$10I_p$ [d]	1.1	2100	
	77	1.2	8.3	1.0	2300	
	88	1.3	7.7	1.1	2600	
	95	1.3	7.3	1.1	2800	
	102	1.3	8.0	1.1	3000	
	117	1.5	6.8	1.2	3400	
	125	1.1	6.3	0.94	3600	
	137	1.4	6.0	1.1	3900	
	145	1.0	4.0	0.80	4100	
	159	1.3	6.0	1.1	4400	
	172	1.2	4.2	0.93	4800	
	202	1.3	4.0	0.98	5500	
	210				5700	4440

TABLE 3. *Corrosion weight losses calculated from polarization data obtained on a series of alloys containing nickel and iron exposed to a 3-percent sodium chloride solution for 7 months*—Continued

Specimen	Exposure time	Polarizing current at break in curve [a]		Corrosion current [b]	Weight loss [c]	
		Cathodic I_p	Anodic I_q	i_0	Calculated cumulative	Actual
	Days	*mA*	*mA*	*mA*	*mg*	*mg*
7 (30 Ni)	4	1.7	5.0	1.3	130	
	12	1.5	7.5	1.1	370	
	20	1.0	7.0	0.87	570	
	28	1.2	$10I_p$ [d]	1.1	760	
	34	1.1	$10I_p$ [d]	1.0	920	
	40	1.1	$10I_p$ [d]	1.0	1100	
	47	0.93	$10I_p$ [d]	0.85	1200	
	55	1.1	$10I_p$ [d]	1.0	1400	
	62	1.1	5.0	0.90	1600	
	70	1.0	6.0	0.86	1800	
	78	1.1	9.2	0.98	1900	
	88	1.2	11.5	1.1	2200	
	95	1.1	8.0	0.97	2400	
	102	1.2	9.0	1.1	2500	
	117	1.0	8.8	0.90	2900	
	125	0.95	5.3	0.81	3100	
	137	1.0	6.5	0.87	3300	
	145	0.90	4.0	0.74	3500	
	159	0.98	2.5	0.70	3700	
	172	1.1	2.5	0.76	4000	
	202	1.0	4.5	0.82	4600	
	210	.....	.....	.....	4700	4100
8 (36 Ni)	4	0.20	0.90	0.16	16	
	7	1.1	4.4	0.88	55	
	12	1.4	8.2	1.2	180	
	21	0.75	5.0	0.65	390	
	29	1.3	5.5	1.1	560	
	34	0.90	4.3	0.74	680	
	41	1.0	5.8	0.85	820	
	47	0.80	3.7	0.66	930	
	55	0.90	5.5	0.77	1100	
	62	0.90	5.0	0.76	1200	
	70	1.0	5.0	0.83	1400	
	78	1.0	5.5	0.85	1500	
	88	1.1	6.0	0.93	1800	
	95	1.2	5.0	0.97	1900	
	102	1.2	4.8	0.96	2100	
	117	1.2	5.0	0.97	2500	
	125	1.2	6.0	1.0	2600	
	137	0.90	6.5	0.79	2900	
	145	0.90	5.2	0.77	3100	
	159	1.3	6.0	1.1	3400	
	173	0.90	5.0	0.76	3700	
	202	0.90	5.7	0.78	4300	
	210	.....	.....	.....	4400	3110
9 (50 Ni)	4	0.18	0.30	0.11	12	
	7	0.11	0.11	0.055	18	
	12	0.15	0.30	0.10	28	
	18	0.32	0.14	0.097	43	
	28	0.26	0.30	0.14	75	
	34	0.29	0.25	0.13	96	
	40	1.4	3.0	0.95	180	
	46	1.3	3.0	0.91	330	
	54	0.75	2.1	0.55	480	
	62	1.0	2.5	0.71	610	
	70	1.0	6.0	0.85	780	
	78	0.90	6.0	0.78	950	
	88	0.82	6.5	0.73	1100	
	95	0.75	6.5	0.67	1300	
	102	0.88	5.9	0.76	1400	
	117	0.60	6.8	0.55	1700	
	125	0.55	2.5	0.45	1800	
	137	0.65	4.0	0.56	1900	
	145	0.60	2.8	0.49	2000	
	159	0.60	2.0	0.46	2200	
	173	0.67	2.5	0.53	2400	
	202	0.52	2.3	0.42	2700	
	210	.....	.....	.....	2800	2860

[a] See the text.
[b] $i_0 = I_p \cdot I_q / (I_p + I_q)$.
[c] Calculated weight loss (g) $= Kti$, K = electrochemical equivalent (for specimens 1–8, assumed $K = 2.8938 \times 10^{-4}$ g/coulomb; for specimens 9–12, assumed $K = 3.0409 \times 10^{-4}$ g/coulomb; i = average of corrosion currents (A) for the exposure period (t in sec) between successive readings). The values of i_0 at the beginning and end of exposure are taken as the initial and final values, respectively, as calculated.
[d] Assumed.

TABLE 3. *Corrosion weight losses calculated from polarization data obtained on a series of alloys containing nickel and iron exposed to a 3-percent sodium chloride solution for 7 months*—Continued

Specimen	Exposure time	Polarizing current at break in curve [a]		Corrosion current [b]	Weight loss [c]	
		Cathodic I_p	Anodic I_q	i_0	Calculated cumulative	Actual
	Days	*mA*	*mA*	*mA*	*mg*	*mg*
10 (57 Ni)	4	0.10	0.25	0.071	7.5	
	7	0.08	0.13	0.049	12	
	12	0.18	0.32	0.11	23	
	21	0.20	0.09	0.062	43	
	29	0.15	0.13	0.07	57	
	34	0.13	0.12	0.065	66	
	40	0.29	0.14	0.094	78	
	46	0.15	0.15	0.075	91	
	54	0.15	0.19	0.084	110	
	62	0.15	0.25	0.094	130	
	70	0.21	0.41	0.14	150	
	78	0.20	0.35	0.13	180	
	88	0.18	0.25	0.10	210	
	95	0.16	0.25	0.098	230	
	102	0.14	0.41	0.10	250	
	117	0.17	0.40	0.12	290	
	125	0.13	0.56	0.11	320	
	137	0.11	0.55	0.092	350	
	146	0.17	0.38	0.12	370	
	159	0.16	0.30	0.10	410	
	173	0.13	0.25	0.085	440	
	202	0.15	0.28	0.097	510	
	210	.....	.....	.....	530	332
11 (81 Ni)	4	0.036	0.070	0.024	2.5	
	7	0.009	0.010	0.0047	3.7	
	12	0.025	0.027	0.013	4.9	
	18	0.011	0.019	0.007	6.5	
	29	0.010	0.014	0.0059	8.4	
	34	0.0095	0.016	0.0060	9.2	
	40	0.011	0.020	0.0071	10	
	46	0.010	0.018	0.0064	11	
	54	0.012	0.022	0.0078	13	
	62	0.009	0.022	0.0064	14	
	70	0.010	0.027	0.0073	16	
	78	0.011	0.027	0.0078	17	
	88	0.012	0.033	0.0088	20	
	95	0.012	0.030	0.0086	21	
	102	0.011	0.040	0.0085	23	
	117	0.012	0.042	0.0094	26	
	125	0.0085	0.027	0.0064	28	
	137	0.0095	0.026	0.0070	30	
	145	0.011	0.026	0.0077	32	
	159	0.0082	0.025	0.0062	34	
	173	0.012	0.030	0.0086	37	
	202	0.010	0.030	0.0075	43	
	210	.....	.....	.....	45	61
12 (100 Ni)	4	0.050	0.038	0.022	2.3	
	7	0.0070	0.012	0.0044	3.3	
	12	0.010	0.025	0.0071	4.0	
	18	0.0088	0.028	0.0067	5.1	
	29	0.010	0.011	0.0052	7.8	
	34	0.0095	0.011	0.0051	8.5	
	40	0.010	0.020	0.0067	9.4	
	46	0.0075	0.020	0.0055	10	
	54	0.0060	0.020	0.0046	11	
	62	0.0090	0.020	0.0062	13	
	70	0.0090	0.022	0.0064	14	
	78	0.010	0.030	0.0075	16	
	88	0.010	0.026	0.0072	17	
	95	0.011	0.030	0.0080	19	
	102	0.011	0.030	0.0080	20	
	117	0.012	0.033	0.0088	24	
	125	0.0080	0.021	0.0058	25	
	138	0.011	0.026	0.0077	27	
	145	0.0088	0.030	0.0068	29	
	159	0.0083	0.034	0.0067	31	
	173	0.0090	0.027	0.0067	34	
	202	0.0080	0.030	0.0063	39	
	210	.....	.....	.....	40	54

NOTE: All specimens were completely submerged and exposed at the same time in an open vat containing about 265 gal of salt water. Mean solution temp., 73 °F; min, 64 °F; max, 81 °F. Area of specimen, 1/6 ft² (155 cm²).

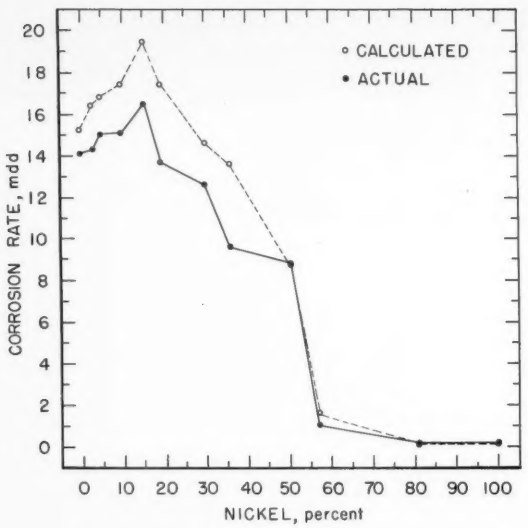

FIGURE 5. *Effect of nickel alloyed with iron on the corrosion rates of alloys exposed for 7 months to Washington, D.C. city water to which was added 3 percent by weight of sodium chloride.*

● based on the actual weight loss for 210 days.
○ based on the cumulative weight loss as calculated from the breaks in polarization curves (table 3).

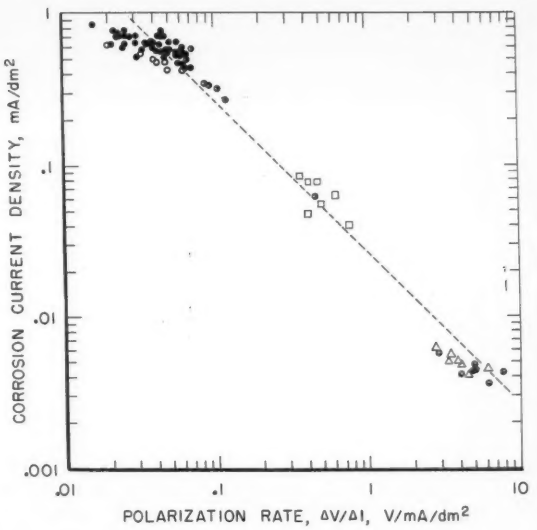

FIGURE 6. *Logarithmic relationship between the corrosion current density, calculated from breaks in cathodic and anodic polarization curves, and the controlling polarization rate (cathodic) of nickel, iron, and binary alloys of nickel and iron.*

Sublegend: Seven values are shown for each specimen based on measurements made at periodic intervals during the 210-day exposure period.

● Specimens 1 through 7,	0–30 Ni.
○ Specimen 8,	36 Ni.
◑ Specimen 9,	50 Ni.
□ Specimen 10,	57 Ni.
△ Specimen 11,	81 Ni.
◒ Specimen 12,	100 Ni.

day (table 3) after which the corrosion potential changed from −0.343 V to −0.495 V and the corrosion current increased sevenfold. The corrosion current pertaining to specimen 9 was minimum when its corrosion potential was the least active (−0.285 V) on the 7th day of exposure. For a comparison of the corrosion potentials of all alloys on the 202d day of exposure, see figure 4 (at zero current). Perhaps, the still water surrounding the specimens, where a greater chance for oxygen depletion occurred, may have prevented a continuation of the film-forming tendencies initially exhibited by the 36 and 50 Ni alloys. In moving water, the oxide films would probably have been more stable and might have prevailed.

The relationship between the two corrosion rate measuring techniques is shown in figure 6. The line through the points is drawn with a slope of −1, the theoretical basis for which was given by Stern [4]. The values of $\Delta V/\Delta I$ are based on the change in potential caused by the increase of applied current from zero to a value slightly larger than the current I_p, as indicated by arrows in figure 3 when the corrosion current is zero or negligible as indicated by the increase polarization rate. Selecting values of applied current smaller than I_p could result in erroneous values of ΔV because the changes in potential might be too small for reliable measurement. Once a relationship, as in figure 6, is established for a given environment, corrosion rates can be approximated simply by measuring $\Delta V/\Delta I$.

As the corrosion currents were controlled by the cathodic reactions, almost without exception (table 3), the values $\Delta V/\Delta I$ were calculated from the cathodic polarization curves. The relationship between the polarization rates $\Delta V/\Delta I$ and the actual corrosion rates (weight losses) of the 12 specimens is shown in figure 7, the line through the points again being drawn with slope of −1.

4. Summary

Ten binary alloys of nickel and iron (series of 3 to 81% Ni) and the metals nickel and iron, 12 specimens in all, were exposed for 210 days to about 265 gals of still Washington, D.C., tap water (64–81 °F) to which was added 3 percent by weight of sodium chloride. Corrosion currents were calculated periodically from breaks in polarization curves, averaged for each of the 22 periods and converted to cumulative weight losses by Faraday's law. The calculated weight losses differed from the actual weight losses (resulting from corrosion) by from 1 to 61 percent, averaging 22 percent for the 12 specimens. The iron lost about 85 times as much weight as did the nickel while the ratio of the respective areas apparently corroded was about 4000 to 1. Corrosion of the nickel seemed to be confined to one pit about 0.064 in. (1.6 mm) diam.

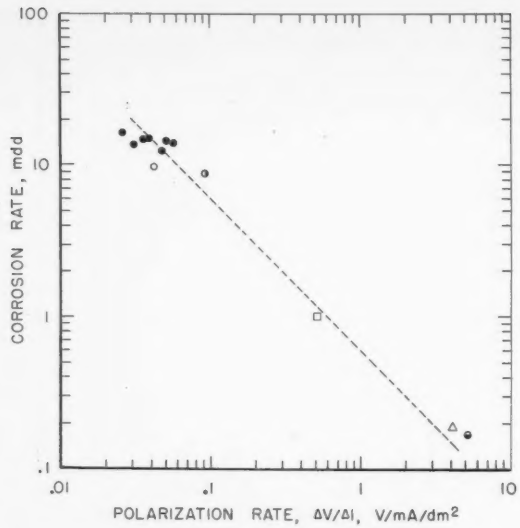

FIGURE 7. *Logarithmic relationship between corrosion rate based on actual weight loss and the controlling polarization rate of nickel, iron, and binary alloys of nickel and iron.*

Sublegend: Each point pertains to a specimen and the polarization rate is the average of seven measurements made at periodic intervals during the 210-day exposure period.

● Specimens 1 through 7,	0–30 Ni.
○ Specimen 8,	36 Ni.
◑ Specimen 9,	50 Ni.
□ Specimen 10,	57 Ni.
△ Specimen 11,	81 Ni.
◒ Specimen 12,	100 Ni.

Polarization rates, $\Delta V/\Delta I$, of the 12 specimens, referred to by most investigators as polarization resistance, were plotted on logarithmic coordinates against corrosion current densities calculated from the same curves by the break method and found to fit a curve having the theoretical slope of -1. Similarly, the actual weight losses of the 12 specimens plotted on logarithmic coordinates versus their average polarization rates also revealed a slope of -1. Thus, once having established the relationship between corrosion current density (from breaks in polarization curves) and polarization rates, $\Delta V/\Delta I$, corrosion current densities can be approximated for other alloys in the particular environment by simply measuring $\Delta V/\Delta I$.

The primary purpose of the laboratory work was to evaluate two polarization techniques as methods for measuring rates of corrosion in an aqueous solution. Of secondary interest to the author was the observation that the biggest benefit in corrosion resistance occurred in changing from 50 to 57 percent Ni. Both the calculated and the actual weight losses revealed a reduction in corrosion of over 80 percent for the 57 Ni alloy over that of the 50 Ni alloy.

The author gratefully acknowledges the cooperation of the personnel of the Research Laboratory, Armco Steel Corporation, Baltimore, Md., who arranged for the fabrication and prepared the alloys.

5. References

[1] W. J. Schwerdtfeger, Corrosion rates of ferrous alloys (Fe-Cr and Fe-Cr-Si) measured by polarization technique, J. Res. NBS **66C** (Engr. and Instr.), No. 3, 245 (July–Sept. 1962).

[2] W. J. Schwerdtfeger and O. N. McDorman, Measurement of the corrosion rate of a metal from its polarizing characteristics, J. Electrochem. Soc. **99,** 407 (1952).

[3] R. V. Skold and T. E. Larson, Measurement of the instantaneous corrosion rate by means of polarization data, Corrosion **13,** 139t (Feb. 1957).

[4] Milton Stern, A method for determining corrosion rates from linear polarization data, Corrosion **14,** 440t (Sept. 1958).

[5] E. H. Phelps, Electrochemical techniques for measurement and interpretation of corrosion, Corrosion **18,** 239t (June 1962).

[6] W. J. Schwerdtfeger and R. J. Manuele, Coatings formed on steel by cathodic protection and their evaluation by polarization measurements, J. Res. NBS **65C** (Engr. and Instr.) No. 3, 171 (July–Sept. 1961).

[7] W. J. Schwerdtfeger, A study by polarization techniques of the corrosion rates of aluminum and steel underground for sixteen months, J. Res. NBS **65C** (Engr. and Instr.) No. 4, 271 (Oct.–Dec. 1961).

[8] W. J. Schwerdtfeger, Current and potential relations for the cathodic protection of steel in a high resistivity environment, J. Res. NBS **63C** (Engr. and Instr.) No. 3, 37 (July–Sept. 1959); Corrosion **16,** 79 (May 1960).

[9] LaQue and Copson, Corrosion Resistance of Metals and Alloys, J. S. Pettibone, Nickel-Iron Alloys p. 459, ACS monograph Series 158 (Reinhold Publishing Corp., New York, N.Y., 1963).

[10] J. S. Marsh, Alloys of Iron and Nickel, Vol. **1** (McGraw-Hill Book Co., Inc., New York, N.Y., 1938).

(Paper 70C3–230)

JOURNAL OF RESEARCH of the National Bureau of Standards—C. Engineering and Instrumentation
Vol. 70C, No. 3, July–September 1966

The Effect of Cold-Drawing on the Creep Behavior of a Nickel-4.2 Percent Aluminum Alloy

William D. Jenkins and William A. Willard

Institute for Materials Research, National Bureau of Standards, Washington, D.C.

(February 21, 1966)

Creep tests were made at 700, 900, and 1200 °F (644, 755, and 921 °K) on a nickel-4.2 percent aluminum alloy (Duranickel) initially as cold-drawn and as cold-drawn and age-hardened. Microstructural changes occurring during creep are correlated with the flow, fracture, and ductility of the specimens. Light and electron microscope observations indicate that increases in creep strength were associated with the formation of rather straight discontinuous slip bands, a well defined subgrain structure, small precipitates of Ni_3Al, and a general distribution of these precipitates throughout the grains. Creep strength at 1200 °F was relatively unaffected by prior cold-drawing or aging. Intercrystalline cracking, accompanied by low ductility, was evident at 900 and 1200 °F and slow creep rates; whereas transcrystalline cracking and high ductility values were observed at 700 °F.

Key Words: Cold-drawing, creep, nickel alloys, Duranickel, nickel-aluminum precipitates, high temperatures, deformation.

1. Introduction

A comprehensive investigation designed to evaluate the influence of stress, strain, strain rate, temperature, and structure on the rheological properties of a precipitation-hardening nickel-4.2 percent aluminum alloy (Duranickel*) has been in progress for the last few years at the National Bureau of Standards. The tensile and creep properties of annealed and annealed and aged Duranickel have been previously published [1, 2].[1] The present phase of the investigation describes (1) the influence of cold-drawing on hardness and creep behavior; (2) the effect of prior aging on creep characteristics; (3) the influence of creep on aging; (4) the role of creep rate and microstructure on crack formation and fracture. In addition, data, previously published [2] describing the temperature dependence of creep behavior of annealed and annealed and aged Duranickel are included for comparison purposes.

2. Material and Testing Procedure

The chemical composition of the metal used in this investigation is given in table 1. All the bars were processed from the same heat as that previously used [1, 2] and were supplied by the Huntington Alloy Products Division of the International Nickel Company in the form of 7/8-in. round rods, approximately 15-ft long. The bars were hot-rolled, descaled, and annealed at 1725 °F (1213 °K), then cold-drawn by the manufacturer to give a tensile strength of 127,000 psi and a hardness of 27 Rockwell "C". Specimens, 1/4 in. in length, were cut from the bar and aged in vacuo for 16 hr at temperatures ranging from 700 to 1250 °F (644 to 948 °K). The specimens age-hardened above 900 °F (755 °K) were cooled at a rate of 25 °F/hr to 900 °F, then furnace cooled to room temperature.

TABLE 1. *Chemical composition (percentage by weight) of the Duranickel used*

Nickel	93.94
Aluminum	4.20
Silicon	0.66
Titanium	.39
Copper	.31
Manganese	.28
Iron	.19
Carbon	.15
Sulfur	.003

Determinations made at the National Bureau of Standards.

Specimens age-hardened at 900 °F and below were also furnace cooled. Room-temperature hardness surveys indicated maximum hardness at 1100 °F (866 °K) was attained with a 16 hr aging time (fig. 1C). Above this temperature at this time the metal appeared to be overaged (fig. 1A). In order to ascertain the effect or rate of cooling on the initial structure and hardness of the cold-drawn metal, specimens were heated in air for 16 hr at temperatures ranging from 700 to 1200 °F (644 to 921 °K) and water quenched (fig. 1A). Room temperature hardness surveys indicated the hardness values for each temperature were lower than those obtained by furnace cooling. Another

*Trade name International Nickel Company.
[1] Figures in brackets indicate the literature references at the end of this paper.

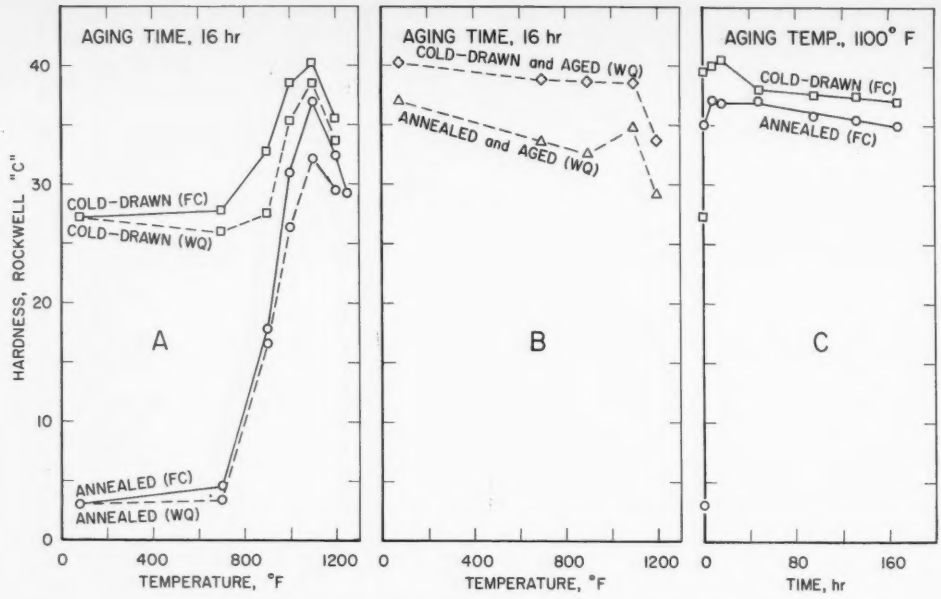

FIGURE 1. *Effect of aging temperature and time and rate of cooling on the hardness of Duranickel.*
FC—furnace cooled; WQ—water quenched.

group of cold-drawn specimens was aged at 1100 °F for 16 hr and furnace cooled. Then they were heated in air to temperatures of 700, 900, 1100, and 1200 °F and held for 16 hr before water quenching. This procedure was used in order to obtain more stable microstructures in the specimens. Room-temperature hardness values indicated a softening effect for the cold-drawn and aged specimens (fig. 1B). The same general trend was also observed for the annealed and aged specimens (fig. 1B).

Cold-drawn rods were cut into specimens 6¼-in. in length for creep testing. These were divided into two groups: one group to be tested in the cold-drawn condition, the other group to be tested in the aged condition (aged at 1100 °F for 16 hr and furnace cooled). Room-temperature tensile properties were determined by the authors for the annealed, cold-drawn and aged specimens (table 2).

The creep specimens had a reduced section of 0.252-in. diam over a 2-in. gage length and the ends were machined with ¾ in. × 10 threads. The reduced section was finished by grinding and then polished in the axial direction, using No. 400 Alumina polishing paper. Before testing, each creep specimen, cold-drawn or cold-drawn and aged, was heated in a tube furnace to the desired temperature and equilibrated at temperature for 16 hr. It was then tested at temperature under constant load. The creep-rupture machines used were of a multiple lever type with motorized jacks to prevent shock loading. They were recently calibrated at room temperature and the errors for the stresses used were less than 0.5 percent. The temperature of each of the specimens was controlled to an accuracy of ±2 °F. Strain-time data were obtained from electric contact follow-up type extensometers attached to shoulders of the specimens. The sensitivity of extension measurement was approximately 0.00005 in.

TABLE 2. *Room temperature tensile properties of Nickel-4.2 percent aluminum alloy*

Condition	Upper yield stress	Lower yield stress	Yield strength (0.2% offset)	Tensile strength	Elongation	Reduction area
	psi	*psi*	*psi*	*psi*	*Percent*	*Percent*
Annealed	45,900	45,700		104,200	47	77
Annealed and aged			122,200	183,000	20	48
Cold-drawn			101,400	126,600	22	65
Cold-drawn and aged			145,500	188,000	18	52

3. Metallography

Most of the specimens tested to fracture in creep were subjected to a metallographic examination. In general, it was observed that transcrystalline cracks having a round or elliptical shape were predominant at 700 °F. A mixture of transcrystalline and intercrystalline cracks was evident at 900 °F. The intercrystalline cracks were more populous at the slower creep rates. At 1200 °F, the cracks were almost exclusively intercrystalline.

Four specimens, two each of the annealed and aged and the cold-drawn and aged metal, were selected for a comprehensive metallographic examination after being tested to fracture in creep. The microstructures are shown in figures 2 to 7. Microstructures of the alloy in the annealed and annealed and aged conditions were previously shown [1].

The basis for selection was (1) these specimens illustrate the effect of cold-drawing on the aged microstructure; (2) they represent the microstructures associated with the extremes of temperatures used (700 and 1200 °F); (3) they show the effects of slow creep rates on changes in microstructure; and (4) they represent microstructures that differed significantly from those previously shown for fast creep rates [1, 2]. Cracks, formed at 700 °F, are illustrated by the photomicrographs in figure 2A and B. Cracks formed at 1200 °F are shown in figure 2C and D. More cracks

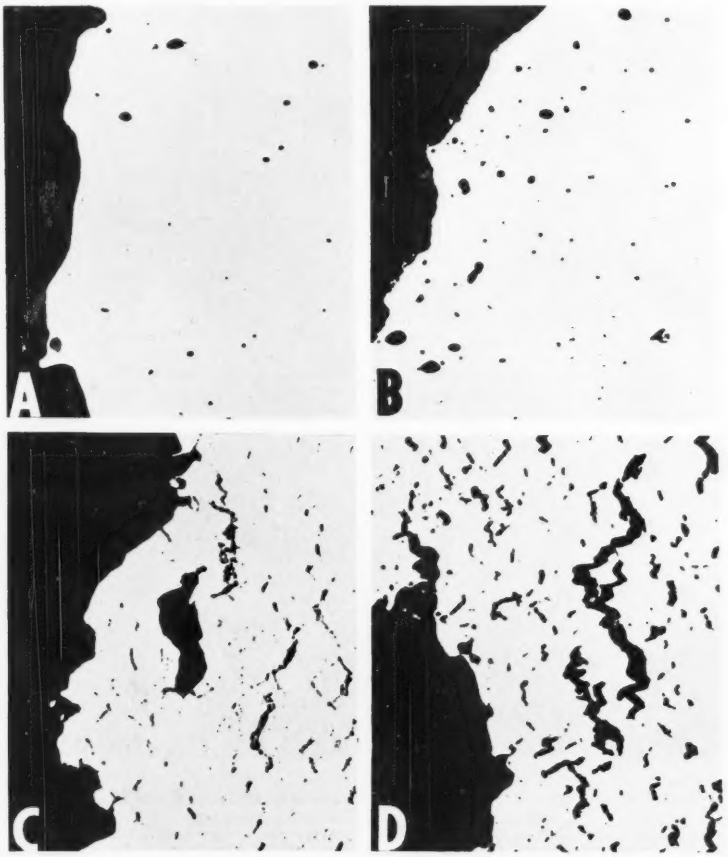

FIGURE 2. *Relation of test conditions to number and distribution of cracks in fractured creep specimens.*
Longitudinal sections, at axis, near fracture, unetched. X 83.

Condition	Test temperature	Fracture time	Reduction of area
	°F	*hr*	%
A Annealed and aged	700	1367.2	5
B Cold-drawn and aged	700	1068	13.5
C Annealed and aged	1200	2059.7	6
D Cold-drawn and aged	1200	2452.7	6.5

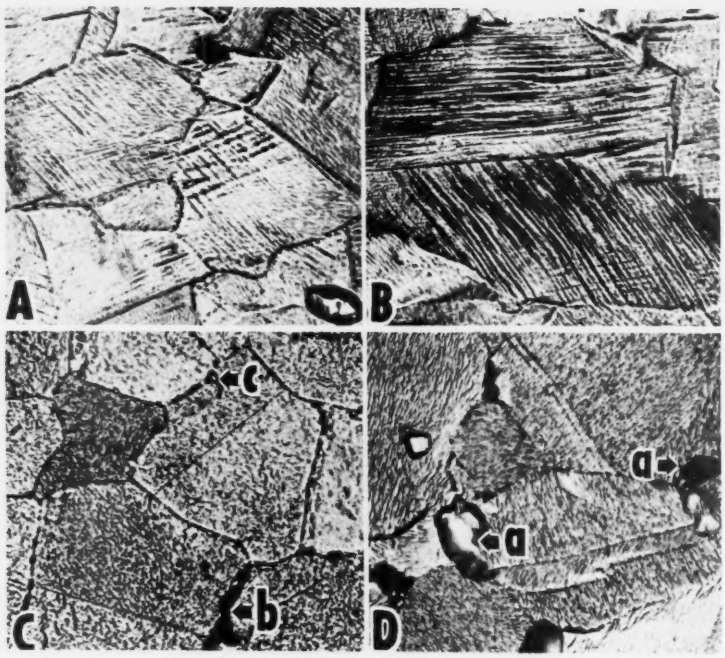

FIGURE 3. *Relation of test conditions to structures of Duranickel after fracture.*
Longitudinal sections, at axis, near fracture. Etched in a solution containing 25 ml each of HNO_3, glacial acetic acid, HCl and water and 3 g of NaOH; X 667. Arrows indicate intercrystalline cracks at "a", "b", and "c".

Condition	Test temperature	Fracture time	Reduction of area
	°F	*hr*	%
A Annealed and aged	700	1367.2	5
B Cold-drawn and aged	700	1068	13.5
C Annealed and aged	1200	2059.7	6
D Cold-drawn and aged	1200	2452.7	6.5

were observed in the specimens that had been cold-worked prior to aging. If it is assumed that a greater number of precipitates were initially present in the cold-drawn and aged metal than in the annealed and aged specimens, these additional precipitates could act as sources for the formation of the cracks as illustrated by the models shown in a previous paper [1, figs. 9 and 10]. The effect of cold-drawing prior to aging on the nature of the substructures within the grains of the fractured specimens is shown in figure 3. Intersecting strain markings were evident in the specimens tested at 700 °F (fig. 3A and B); however, a greater number of curved, wavy markings was observed in the cold-drawn and aged metal (fig. 3B), supporting the hypothesis that more precipitates occurred in the cold-drawn metal. Some of the markings did not traverse the grain from one boundary to the other. Precipitates, subgrain boundaries, and slip bands acted as barriers to the continuous motion of dislocations across the grains as will be illustrated later (fig. 5A) by electron microscopy. A fine structure was observed within the grains of specimens tested at 1200 °F (fig. 3C and D). As will be shown later (figs. 6 and 7) some of this substructure consists of overaged precipitates. Intercrystalline cracks are larger for the cold-drawn and aged specimen (fig. 3Da) than for the annealed and aged specimen (fig. 3Cb). Smaller cracks within the vicinity of the precipitates at the grain boundaries (fig. 3Cc) indicate that voids are nucleated first in these regions, then coalesce to form holes and cracks.

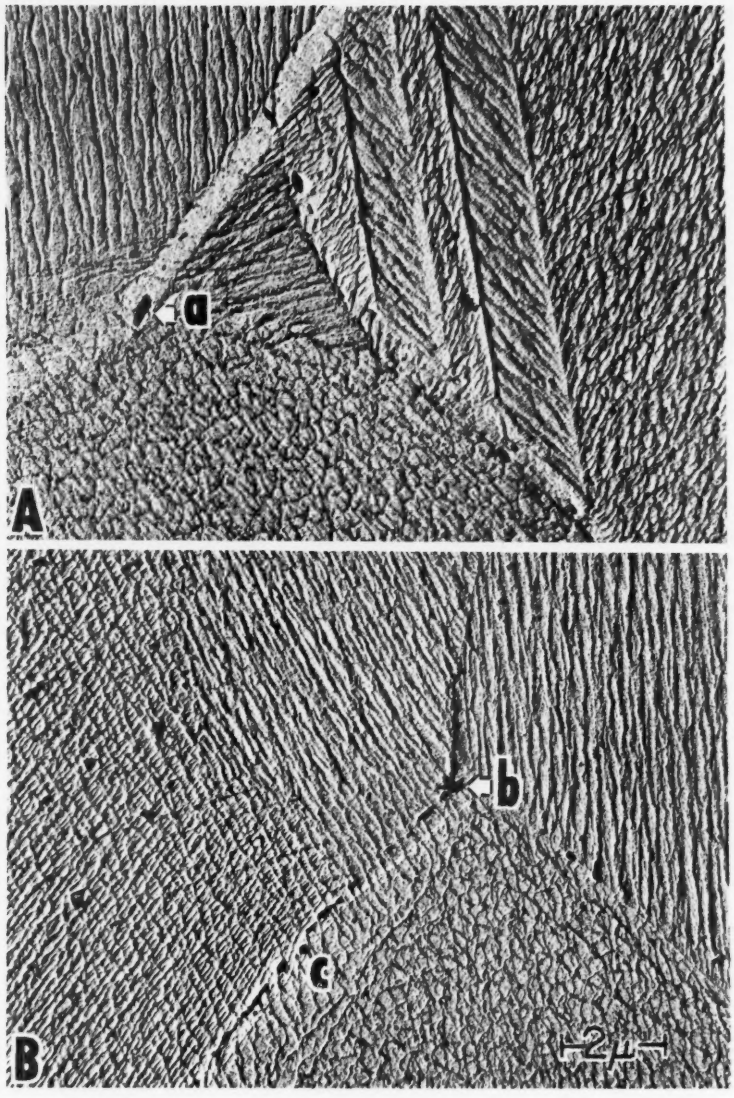

FIGURE 4. *Electron micrographs showing structure of an annealed and aged alloy specimen after fracture in 1367.2 hr at 700 °F.*

Longitudinal sections, near fracture; etched in a solution containing 25 ml each of HNO_3, glacial acetic acid, HCl and water and 3 g of NaOH; X 7,500. Arrows indicate Ni_3Al precipitates at the triple points "a" and "b". "c" indicates substructure near grain boundary.

Electron microscopy replica techniques were used to ascertain more fully the size, number and distribution of the precipitates, subgrains, and strain markings in these specimens. The results are shown in figures 4 to 7. Microstructures of the annealed and aged specimen tested at 700 °F (fig. 4) indicated the presence of annealing twins (fig. 4A), well-defined subgrains, precipitates within some of the grains and an absence of them in other grains. It is probable that most were too small to be resolved at this magnification. Precipitates are also evident at the grain boundaries and appear to be largest at the triple points (fig. 4Aa and Bb). Due to differences in structure of adjacent parent grains, the shape of the subgrains near the boundary is different from that in the interior of the grains (fig. 4Bc). When the microstructures shown in figure 4 are compared with those of the cold-drawn and aged metal, shown in figure 5, it appears that testing

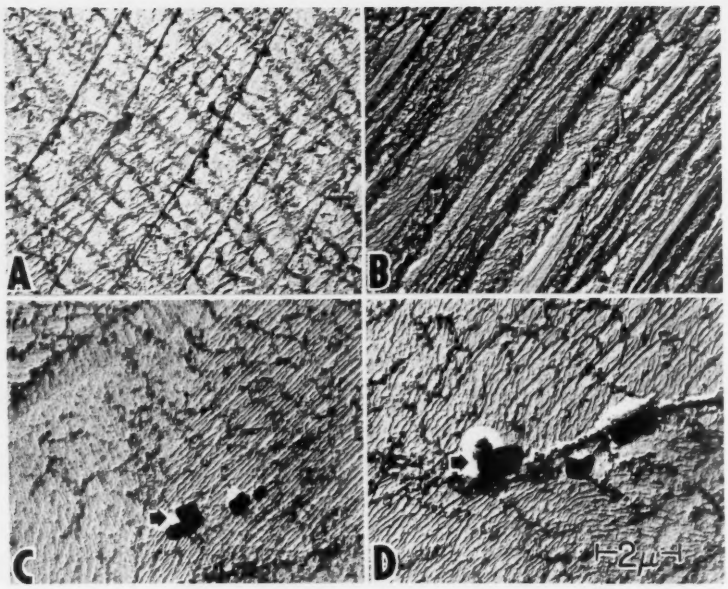

FIGURE 5. *Electron micrographs showing structure of a cold-drawn and aged alloy specimen after fracture in 1068 hr at 700 °F.*

Logitudinal sections, near fracture; etched in a solution containing 25 ml each of HNO_3, glacial acetic acid, HCl and water and 3 g of NaOH; X 6,000. Arrows indicate Ni_3Al precipitates.

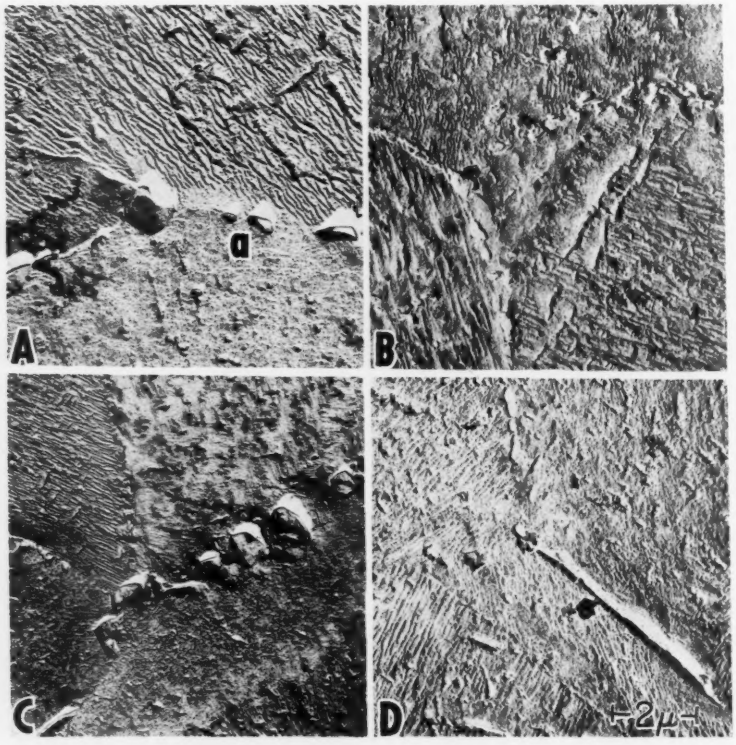

FIGURE 6. *Electron micrographs showing structure of an annealed and aged alloy specimen after fracture in 2059.7 hr at 1200 °F.*

Longitudinal sections, near fracture; etched in a solution containing 25 ml each of HNO_3, glacial acetic acid, HCl and water and 3 g of NaOH; X 6,000. "a" indicates precipitate-free region near grain boundary.

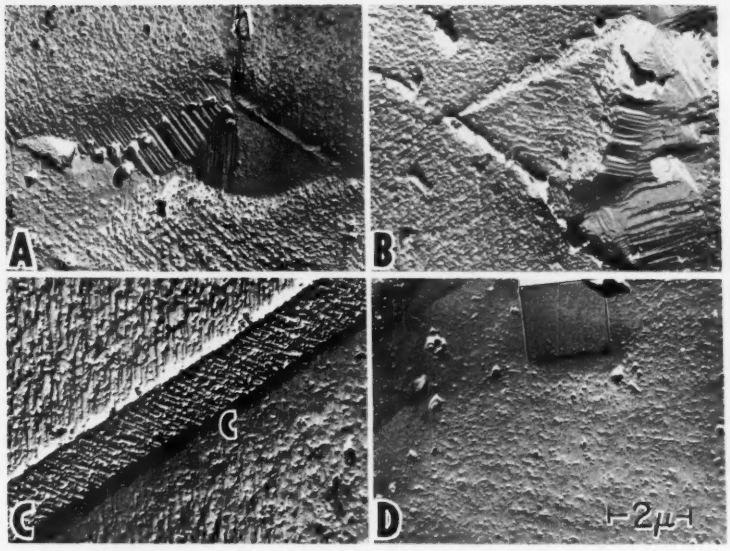

FIGURE 7. *Electron micrographs showing structure of a cold-drawn and aged Duranickel specimen after fracture in 2452.7 hr at 1200 °F.*
Logitudinal sections, near fracture; etched in a solution containing 25 ml each of HNO_3, glacial acetic acid, HCl and water and 3 g of NaOH; X 6,000. "c" indicates precipitate-free region near twin boundary.

the aged metal at 700 °F increases the width of the subgrain boundaries (fig. 5A and C), the size of some of the precipitates (fig. 5C and D, arrows) and the number of slip bands (fig. 5B). The discontinuous nature of some of the strain markings is illustrated in figure 5A. The differences in microstructures had a marked effect on the creep behavior at 700 °F as indicated by the data in figures 8 to 11.

In general, it was found that the size of the precipitates increased with increase in temperature and with increase in time. The size of the precipitates, observed in specimens tested at 1200 °F, was less for the cold-drawn and aged (fig. 7) than for the annealed and aged specimens (fig. 6). Some areas adjacent to the grain boundaries (fig. 6Aa) or twin boundaries (fig. 7Cc) are comparatively free of precipitates. However, precipitation within the grains appears to have taken place on definite preferred planes and the size of these precipitates was less affected by cold-drawing than the size of those at the grain boundary. These differences in microstructures had little effect on the creep behavior at 1200 °F as indicated by figures 9 and 10.

4. Test Data and Discussion

Davies, Richards, and Wilshire [3] studied the effect of prior cold-work on creep and fracture of a nickel-0.1 atomic percent gold alloy. They concluded that, below the recrystallization temperature, creep rate was reduced and rupture life was increased when the prestrain exceeded the initial strain. Their results were interpreted on the basis of varying contributions from the grain interiors and the grain boundary regions. Dennison and Wilshire [4] carried out tests on three grades of nickel and observed that decrease in purity was accompanied by an increase in creep resistance and rupture life. They concluded that impurities impeded grain boundary migration, caused a decrease in ductility and an increase in the occurrence of cracking. The effects of cold-drawing on creep of some nickel-copper alloys were discussed by Jenkins and Willard [5].

Strain-time curves for some of the creep specimens used in the present investigation are shown in figure 8. Cold-drawing has reduced the extent (time and strain) of both the first and second stages of creep below the values for the annealed specimens, previously reported [2]. For the aged material the first stage was practically nonexistent. The shape of the curves are both temperature and stress dependent. Time lag before the initiation of plastic deformation at 1200 °F is believed to be due in part to the blocking of the motion of dislocations by the precipitates that formed at 1200 °F before loading the specimens. These precipitates have been shown both by x-ray and electron diffraction to be predominantly particles of Ni_3Al. The properties of this compound have been studied extensively by Guard and Westbrook [6].

The relation between stress and second stage creep rate[3] is shown in figure 9. A linear relationship be-

[3] The second stage creep rates were obtained from strain-time curves when the data were plotted on a linear scale (not shown).

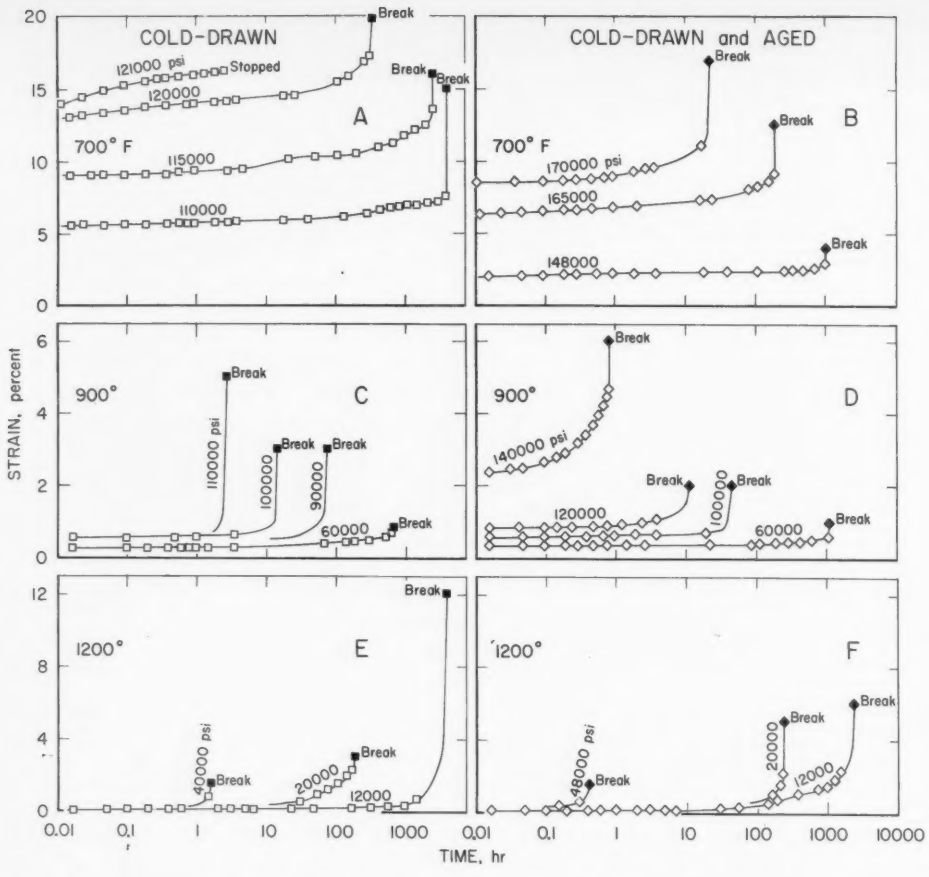

FIGURE 8. *Strain-time relations of cold-drawn and cold-drawn and aged alloy specimens tested at different temperatures.*

tween these variables was not obtained when the data were plotted on linear, log-log, or semilog coordinates. The sigmoidal form of some of the curves indicates the existence of a creep rate for which strain hardening is a maximum. Cold-drawing the metal increased the strength at 700 and 900 °F with the greatest increase occurring at the faster rates (fig. 9A). Furthermore, cold-drawing prior to aging improved the creep strength (fig. 9B) in comparison to the annealed and aged metal. No significant difference in strength is observed at 1200 °F where recrystallization and overaging occurred during the tests.

The effect of stress on time to fracture is shown in figure 10. Obviously, no simple equation could be used to describe the relationship between these variables or between the family of curves for specimens having the same or different heat-treatments. It is observed, at 700 and 900 °F, that strengthening due to cold-drawing or aging is less effective at the longer test times than at the shorter times. Recovery of the strained material is believed to be the major cause of this phenomenon. Although the stress-creep rate and stress-fracture time curves appear to be similar, no consistent relation existed between creep rates and fracture times for either the cold-drawn or cold-drawn and aged specimens.

The interrelationship between second stage creep rate and ductility is shown in figure 11. In general, elongation and reduction of area values increased with increase in creep rate at 700 °F and decreased with increase in creep rate at 1200 °F. A large number of mechanisms, such as strain hardening, recovery, aging, transcrystalline and intercrystalline cracking, accompanied creep at 900 °F and caused the ductility values to vary in the same manner as was observed for annealed and annealed and aged Duranickel [2].

Rockwell hardness tests were made at room temperature on specimens after fracture to ascertain the effect of creep on hardening. Hardness indentations were made on cross sections of both the shoulder and on the deformed (reduced) section near fracture of the cold-drawn and cold-drawn and aged specimens in order to ascertain the effect of plastic deformation on aging characteristics. Small load-free control

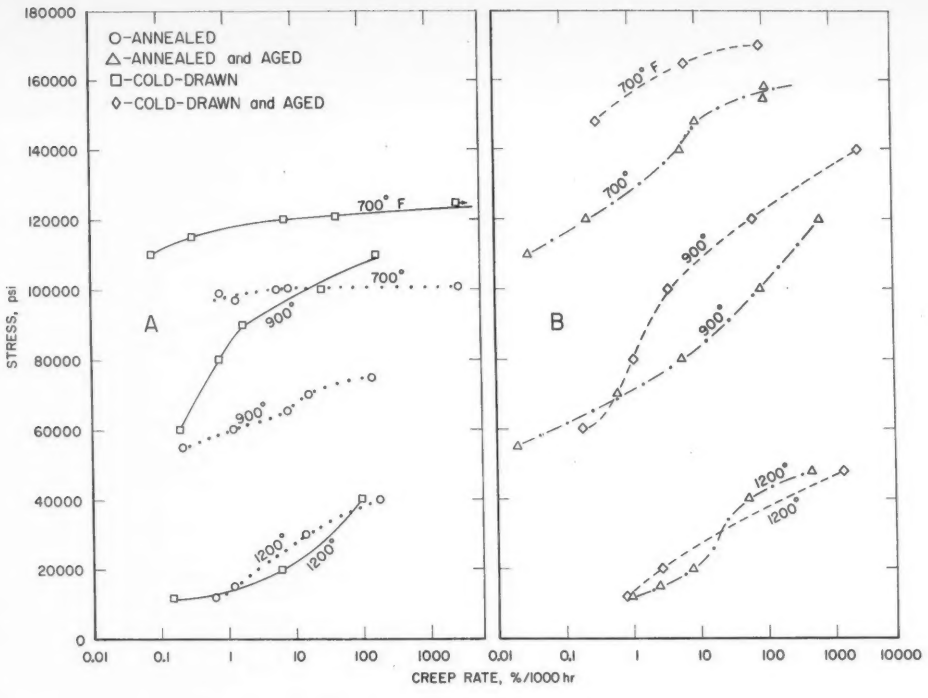

FIGURE 9. *Effect of cold-drawing and aging on the stress-second stage creep rate relations of the alloy.*

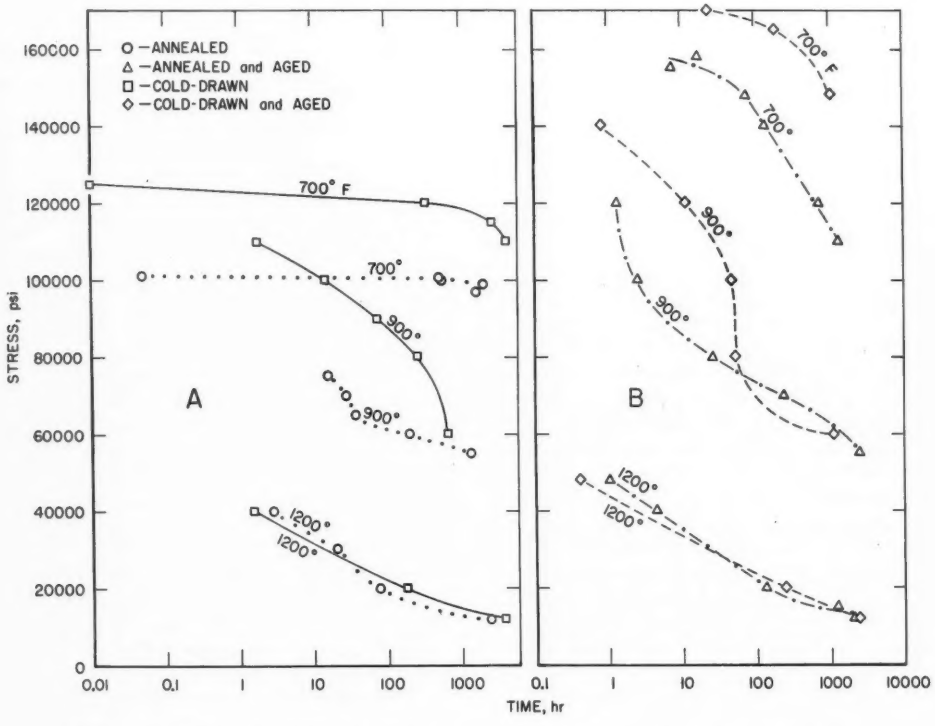

FIGURE 10. *Effect of cold-drawing and aging on the stress-fracture time relations of the alloy.*

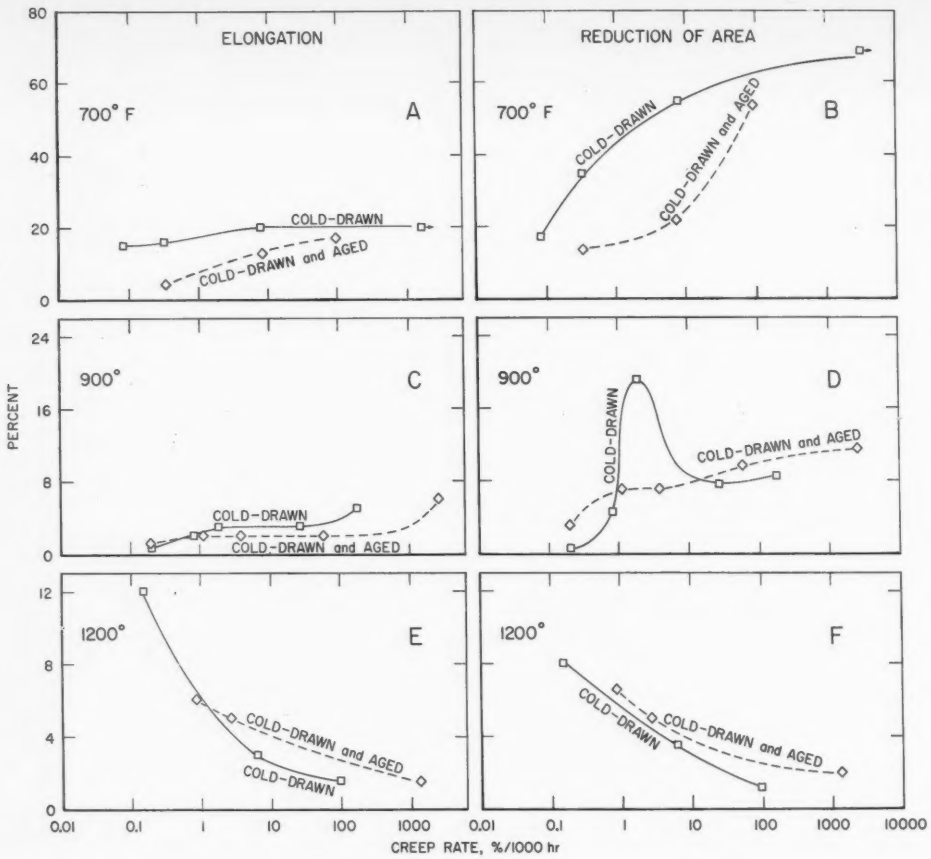

FIGURE 11. *Influence of aging on the ducility-second stage creep rate relations of cold-drawn alloy specimens tested to fracture at different temperatures.*

samples, heat-treated for times corresponding to the various fracture times in the creep tests, were tested for hardness and used for comparison purposes. As indicated by the hardness data for the cold-drawn specimens (fig. 12A, C, and E) precipitation-hardening was more predominant at 900 than at 700 °F. This was evident for the specimens exposed to temperature only (fig. 12A), for unstrained portions of specimens (shoulders) exposed to temperature and stress (fig. 12C), and for the strained portions of the specimens (reduced sections) tested to fracture in creep (fig. 12E). Extensive recovery, recrystallization, and overaging occurred in the specimens tested at 1200 °F as shown by the decrease in hardness with increase in test time. This behavior was also evident for the cold-drawn and aged specimens (fig. 12B, D, and F) tested at 1200 °F; however, test time had only a slight effect on hardness values of the specimens tested to fracture at 700 and 900 °F. These data tend to confirm the general trends associated with the hardness values obtained for the load-free specimens and shown in figure 1.

5. Summary

Creep tests were made at temperatures of 700, 900, and 1200 °F (644, 755, and 921 °K) on a nickel-4.2 percent aluminum alloy initially as cold-drawn and as cold-drawn and age-hardened.

Microstructures and test data obtained in the present investigation are compared to results shown previously for the annealed, and annealed and aged alloy.

The hardness of the alloy was increased by cold-drawing or aging. Additional hardening was induced by aging subsequent to the cold-drawing operation.

Due to the existence and formation of numerous barriers to the motion of dislocations through the crystal lattice, cold-drawing and aging increased the creep strength and decreased the ductility of the alloy at 700 and 900 °F. No significant effect was apparent at 1200 °F, which is slightly above the recrystallization temperature.

Elongation and reduction of area values increased with increase in creep rate at 700 °F and with decrease in creep rate at 1200 °F.

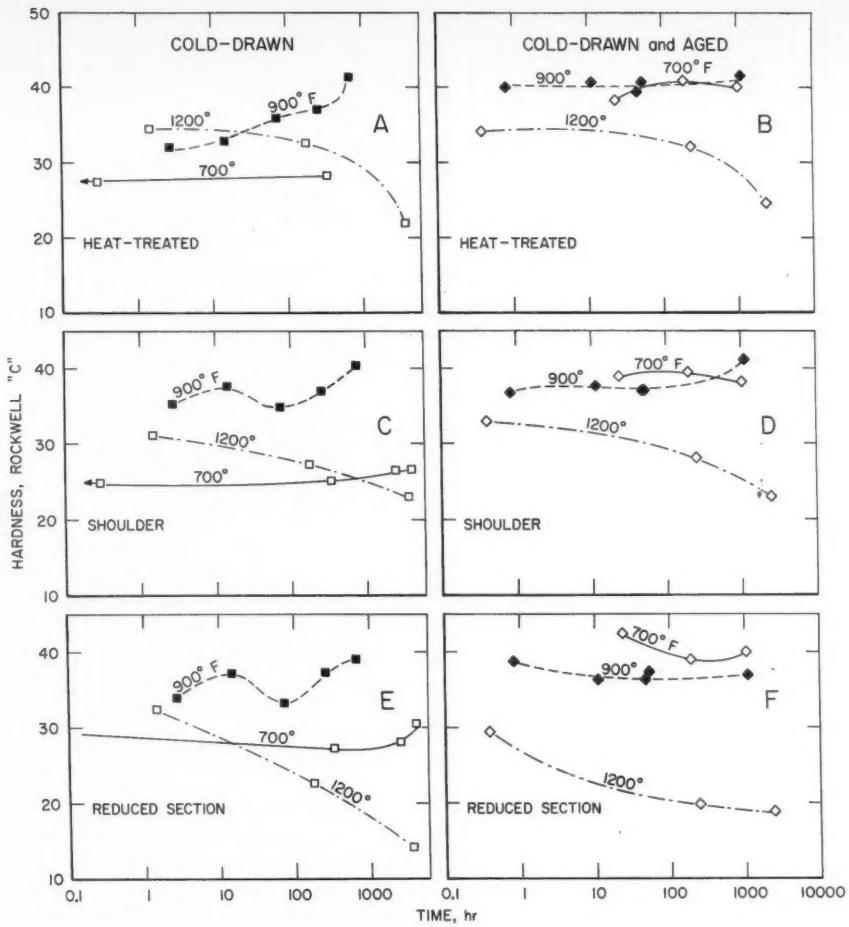

FIGURE 12. *Effect of test temperature and time on hardness, at room temperature, of cold-drawn and cold-drawn and aged alloy specimens.*

A, B, load-free control specimens as heat-treated; C, D, E, F, creep specimens after fracture.

Aging the cold-drawn alloy made it more ductile at 1200 °F and less at 700 °F.

Post-test hardness values decreased with increase in test time at 1200 °F, due to recrystallization. With few exceptions, the hardness after testing at 900 °F was equal to or greater than that after testing at 700 °F.

The tendency toward intercrystalline cracking increased with increase in test temperature. The number of cracks was increased by cold-drawing prior to age-hardening.

Microstructures, associated with high strength and ductility at the lower temperatures indicated the existence of small precipitated particles, small subgrains and rather straight intersecting and nonintersecting strain markings. However, at 1200 °F, few markings were evident and coalesced precipitates appeared predominantly in the grain boundaries. The shape and number of the precipitates appeared to depend on where they are located in the crystal lattice.

(Paper 70C3–231)

The authors gratefully acknowledge the cooperation of James Heywood and David Ballard in carrying out the electron microscopic examination of the specimens.

6. References

[1] W. D. Jenkins and W. A. Willard, The temperature dependence of flow and fracture characteristics of an age-hardenable alloy, Trans. ASM **55,** 580 (1962).

[2] W. D. Jenkins and W. A. Willard, Some factors affecting the creep behavior of an age-hardenable nickel alloy, Trans. ASM **56,** 427 (1963).

[3] P. W. Davies, J. D. Richards, and B. Wilshire, The influence of cold-work on the creep and fracture behavior of a dilute nickel alloy, J. Inst. of Metals **90,** 431 (July 1962).

[4] C. J. P. Dennison and B. Wilshire, Observations on the influence of impurities on the creep and fracture behavior of nickel at 500 and 600 °C. J. Inst. of Metals **91,** 343 (June 1963).

[5] W. D. Jenkins and W. A. Willard, Creep of cold-drawn nickel, copper, 70% nickel-30% copper and 30% nickel-70% copper alloys, J. Res. NBS **66C** (Phys. and Chem.) No. 1, 59 (1962).

[6] R. W. Guard and J. H. Westbrook, Studies of the compound Ni_3Al by high-temperature X-ray methods, Trans. of the Metallurgical Soc. of AIME **215,** 871 (1959).

JOURNAL OF RESEARCH of the National Bureau of Standards—C. Engineering and Instrumentation
Vol. 70C, No. 3, July–September 1966

Magnetic Transformation and the Influence of Plastic Strain on the Shear Modulus of Fe-Cr-Ni alloys

R. P. Mikesell* and R. P. Reed*

Institute for Materials Research, National Bureau of Standards, Boulder, Colo.

(March 31, 1966)

The Fe-18Cr-9Ni and Fe-19Cr-9Ni alloys exhibit a decrease in shear modulus between 76 and 20 °K. Susceptibility measurements confirm that a paramagnetic to antiferromagnetic transition occurs at about 40 °K in these alloys. The shear modulus for the Fe-25Cr-21Ni alloy did not decrease between 76 and 20 °K which was consistent with the fact that the alloy remained paramagnetic to 4 °K. The effect of cold-work on the shear modulus above and below the Néel temperature is discussed.

Key Words: Antiferromagnetic, cold-work, Fe-Ni-Cr alloys, Néel temperature, shear modulus, stainless steel.

1. Introduction

It has been shown that the shear and Young's modulus of a Fe-19Cr-9Ni (weight percent) steel exhibits a decrease between 76 and 20 °K [1].[1] Recently, investigators [2, 3, 4] have reported a paramagnetic to antiferromagnetic transition in certain 18Cr-9Ni steels at about 40 °K. Since it is expected that such a magnetic transition would affect the elastic moduli, a study was made to better understand the effect of the transition on the shear modulus of Fe-Ni-Cr alloys. These alloys were Fe-18Cr-9Ni, Fe-19Cr-9Ni, and Fe-25Cr-21Ni and correspond, respectively, to A.I.S.I. commercial stainless steel grades 303, 302, and 310. In addition, the effect of prior plastic strain at ambient temperatures on the change of shear modulus in the temperature range 295 to 20 °K was documented.

Some data have been reported concerning the combined effects of a magnetic transition and plastic strain on the decrease of elastic moduli on cooling below the transition temperature. Various workers have noted a change in the Young's and shear modulus of materials that have been cooled at zero magnetic field through the ferromagnetic Curie temperature [5–10]. Others have noticed the effect of a paramagnetic to antiferromagnetic transition on the elastic properties of Cr [11, 14, 15] and Cu-Mn alloys [12]. Recently, Roberson and Lipsitt have reported that the Young's modulus and the shear modulus behave differently when Cr is cooled through and below the Néel temperature [16]. They found that the ΔE (the change in modulus on cooling through the transition temperature) for the shear modulus was less than for the Young's modulus. Several investigators have noted that the ΔE effect is less for cold-worked materials than annealed materials in Fe-Ni-Mo [6], Cr [16, 18, 19], and Ni [17].

Many have noted a change in elastic modulus after plastic strain at ambient temperatures. Although some anomalies exist, results on copper, [22, 23, 24, 27–30] aluminum, [20, 21, 25, 26] and silver [27] indicate that the elastic moduli are lowered by as much as 15 percent when the material is previously plastically strained.

Susceptibility measurements described in this paper show that the Fe-18Cr-9Ni and Fe-19Cr-9Ni alloys become antiferromagnetic at 43 and 39 °K, respectively, and that the Fe-25Cr-21Ni alloy remains paramagnetic down to 4 °K. The magnitude of decrease in modulus between 76 and 20 °K for the 18Cr-9Ni and 19Cr-9Ni alloys was found to be inversely related to the amount of prior cold-work.

2. Procedure and Results of Susceptibility Measurements

The susceptibility samples were made from the same bar stock that was used for the modulus specimens. The composition, hardness, condition and grain size of the alloys are listed in table I. The susceptibility was measured by the ballistic method. Values of susceptibility are plotted in arbitrary units; the units of flux change can be converted to susceptibility values through calibration of the apparatus A continuous temperature change of the sample was achieved by allowing the sample to warm from a liquid helium bath. The temperature gradient was less than 1 °K in the sample upon warming. Values of susceptibility were reproducible with ± 1 percent; the temperature was reproducible within ± 1 °K.

*Cryogenics Division, National Bureau of Standards, Boulder, Colo.

[1] Figures in brackets indicate the literature references at the end of this paper.

Table I. Identification of Alloys Tested

Alloy	Chemical Composition (weight %)									Rockwell Hardness (B scale)	Condition	ASTM Grain Size
	C	P	S	Ni	Cr	Mo	Mn	Si	Cu			
19Cr-9Ni (Commercial AISI 302)	0.08	0.02	0.01	8.7	18.6		0.6	0.6		R_B 90	Annealed (~0.5% martensite)	5
										R_B 104	Drawn 14% at room temperature (~13% martensite)	5
18Cr-9Ni (Commercial AISI 303)	0.10	0.03	0.29	8.7	17.6	0.4	1.2	0.6	0.4	R_B 81	Annealed	6
										R_B 87	Drawn 5% at room temperature	6
										R_B 95	Drawn 13% at room temperature	7
25Cr-21Ni (Commercial AISI 310)	0.08	0.02	0.02	20.8	24.8	0.1	1.7	0.7	0.1	R_B 79	Annealed	2
										R_B 89	Drawn 11% at room temperature	2

Results of the susceptibility measurements for 19Cr-9Ni, 18Cr-9Ni and 25Cr-21Ni alloys are shown in figure 1. The annealed 19Cr-9Ni and annealed 18Cr-9Ni were measured with a field of about 1 kG; annealed and 11 percent cold-drawn 25Cr-21Ni were measured with a field of about 0.4 kG. The 19Cr-9Ni specimen, when plastically strained 14 percent, exhibited a partial phase transformation to body-centered cubic martensite. The body-centered cubic phase is ferromagnetic [31]. Therefore, the susceptibility measurements to determine the antiferromagnetic transition were thwarted by the stronger ferromagnetism from the martensite phase. Although the 18Cr-9Ni alloy has similar Cr and Ni content, the amount of other stabilizing elements (see table I) is greater, which explains the lack of detectable amounts of martensite formed by plastic deformation. Since the susceptibility versus temperature measurements for the 18Cr-9Ni cold-drawn specimens were appreciably smeared out, it was difficult to detect a distinct inflection temperature.

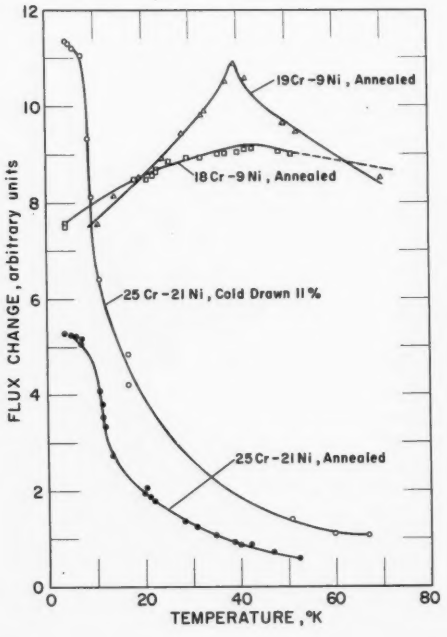

FIGURE 1. *The flux change, proportional to the magnetic susceptibility, as a function of temperature for* 19Cr-9Ni *steel,* 18Cr-9Ni *steel, and* 25Cr-21Ni *steel.*

3. Procedure and Results of Shear Modulus Measurements

The method of determining the shear modulus has been previously described [32]. Briefly, the method consisted of applying small incremental torque loads to carefully machined specimens and measuring the

angle of displacement using an optical lever. The maximum shear stress applied to all the samples was 2900 psi. Measurements were made at three temperatures: 295, 76, and 20 °K. Results are shown in figures 2, 3, and 4.

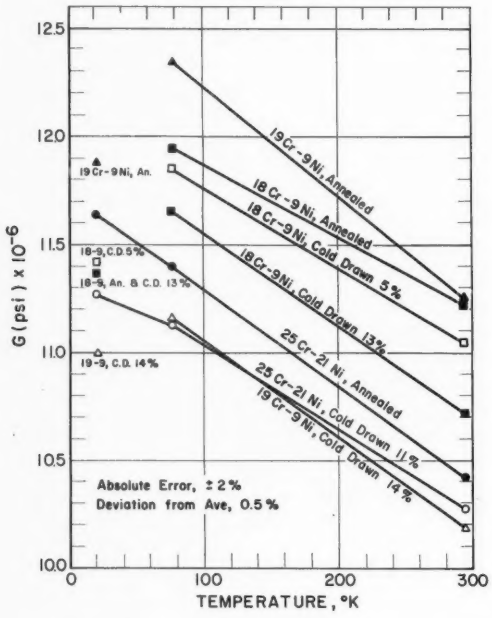

FIGURE 2. *The shear moduli of* 19Cr-9Ni, 18Cr-9Ni, *and* 25Cr-21Ni *steels as a function of temperature.*

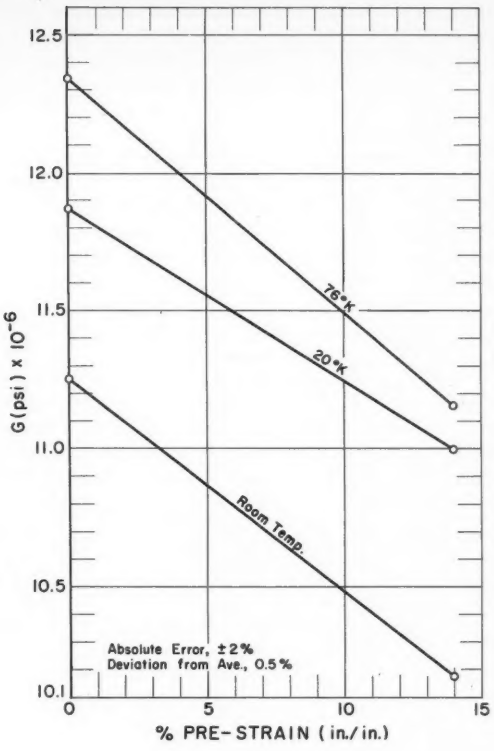

FIGURE 4. *The shear modulus of* 19Cr-9Ni *steel at constant temperature as a function of prior plastic strain.*

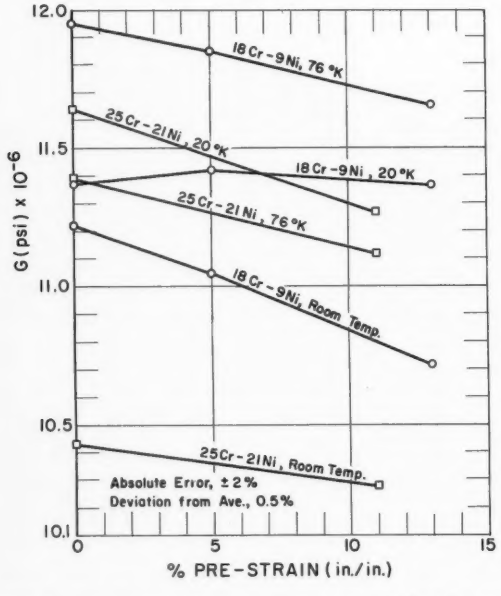

FIGURE 3. *The shear moduli of* 18Cr-9Ni *and* 25Cr-21Ni *steels at constant temperature as a function of prior plastic strain.*

For any one sample and at any one temperature, the deviation from the average value of modulus is 0.5 percent. The maximum absolute error, i.e., the error that occurs either on repeating measurements after removal and remounting of the sample, or on measuring another specimen of the same alloy, is ± 2 percent.

4. Discussion

In figure 1 it is seen that the 19Cr-9Ni and 18Cr-9Ni alloys each show a peak in the susceptibility-temperature curve which is characteristic of a material transforming from a paramagnetic to an antiferromagnetic state. These results are consistent with the modulus curves of figure 2; the 19Cr-9Ni and 18Cr-9Ni alloys exhibit anomalous drops in modulus whereas the 25Cr-21Ni alloy behaves normally down to 20 °K. The decrease in modulus between 76 and 20 °K is due to an additional strain component resulting from antiferromagnetic ordering below the Néel temperature [12, 13].

From the 18Cr-9Ni and 19Cr-9Ni alloy shear modulus curves of figure 2, it is seen that $(G_{76°} - G_{20°})/G_{76°}$ is inversely related to the amount of prior plastic strain: the $\Delta G/G$ for the 18Cr-9Ni alloy is respectively 4.9, 3.6, and 2.6 percent for annealed, 5 percent cold-drawn, and 13 percent cold-drawn conditions; $\Delta G/G$ for the

19Cr-9Ni alloy decreased from 3.6 to 1.4 percent for the annealed to cold-drawn conditions. This decrease indicates that there is less magnetostrictive effect at 20 °K in a cold-worked sample due to internal stresses from defects which influence the redistribution of the domain vectors [35, 6].

The effect of prior plastic strain above the Néel temperature on the shear modulus is illustrated in figures 2 to 4. A decrease of the modulus values, after straining, has been verified. This is expected since many of the dislocations introduced during plastic straining move under very low stresses. In addition, vacancies created by cold-work lower the material density which lowers the modulus. Jongenburger [33] has predicted that materials with low stacking fault energy would exhibit greater sensitivity to cold-work than high stacking fault energy materials, since the stress needed to move extended dislocations should be less. The 18Cr-9Ni alloy is expected to have a lower stacking fault energy than the 25Cr-21Ni alloy [34]. At ambient temperatures the strain sensitivity of the shear modulus for the 18Cr-9Ni alloy is greater; however, at 76 °K their sensitivities are approximately equal. The reason for this temperature trend is not clear.

At 20 °K, notice that the shear modulus of the 18Cr-9Ni alloy is essentially independent of the amount of prior plastic strain. Apparently the ΔE effect and the defect contribution, which serves to lower the overall modulus, just offset each other at this temperature. The much greater reduction of the shear modulus of the 19Cr-9Ni alloy as a function of strain is undoubtedly influenced by the partial transformation to the martensite (body centered cubic) phase during plastic deformation at room temperature.

5. Summary

It has been found that the elastic properties of low stacking fault energy austenitic stainless steels undergo a transition at about 40 °K. This transition produces a decrease in the shear modulus values and is caused by a paramagnetic to antiferromagnetic transformation. The decrease of the modulus values between 76 and 20 °K is inversely related to the amount of prior cold-work at ambient temperature. The shear modulus at temperatures above the Néel temperature is influenced by previous cold-work, decreasing up to 10 percent for 10 to 15 percent plastic strain.

The authors thank J. J. Gniewek for informal discussions regarding the work in this paper.

(Paper 70C3–232)

6. References

[1] R. P. Reed and R. P. Mikesell, Adv. in Cryogenic Engr. **10,** 46 (Plenum Press, New York, 1964).
[2] E. I. Kondorskii and V. L. Sedov, J. Exptl. Theoret. Phys. (USSR) **35,** 1579 (1958); Soviet Physics JEPT **35** (8), 1104 (1959).
[3] W. H. Meikeljohn, J. Appl. Phys. **32S,** 274S (1961).
[4] U. Gonser, C. J. Meedhan, A. H. Muir, and H. Wiedersich, J. Appl. Phys. **34,** 2373 (1963).
[5] O. Engler, Ann. Physik. **31,** 145 (1938).
[6] M. E. Fine and W. C. Ellis, Trans. A.I.M.E. **188,** 1120 (1950).
[7] M. E. Fine and W. C. Ellis, Trans. A.I.M.E. **191,** 761 (1951).
[8] K. P. Belov, G. I. Kataev, and R. Z. Levitin, J. Exptl. Theroet. Phys. (USSR) **37,** 670 (1959).
[9] G. I. Kataev and Z. D. Sirota, J. Exptl. Theoret. Phys. (USSR) **38,** 747 (1960).
[10] G. I. Kataev, Fiz. Metal. Metalloved. 11, No. 3, 375 (1961); Phys. of Metals and Metallography **11,** No. 3, 53 (1961).
[11] M. E. Fine, E. S. Greiner, and W. C. Ellis, Trans. A.I.M.E. **191,** 56 (1951).
[12] R. Street and J. H. Smith, J. Physique et le Radium **20,** 82 (1959).
[13] R. Street, J. Appl. Phys. 31S, 310S (1960).
[14] D. I. Bolef and J. de Klerk, Phys. Rev. **129,** 1063 (1963).
[15] M. E. de Morton, Phys. Rev. Letters **10,** 208 (1963).
[16] J. A. Roberson and H. A. Lipsitt, J. Appl. Phys. **36,** 2843 (1965).
[17] W. Köster, Z. Metallkunde **35,** 57 (1943).
[18] R. Street, Phys. Rev. Letters **10,** 210 (1963).
[19] M. J. Klein, A. H. Clauer, and R. E. Maringer, J. Appl. Phys. **35,** 1994 (1964).
[20] M. Kornfeld, Phys. Z. Sov. **6,** 329 (1934).
[21] W. Koster, Z. Metallkunde **32,** 382 (1940).
[22] A. D. N. Smith, Phil Mag. **44,** 453 (1953).
[23] M. Cook, T. Richards, and G. F. Bidmead, J. Inst. Met. **83,** 41 (1954–55).
[24] E. C. Crittenden, Jr., and H. Dieckamp, Phys Rev. **91,** 232(A) (1953); **94,** 1421(A) (1954).
[25] J. Friedel, C. Boulander, and C. Crussard, Acta Met. **3,** 380 (1955).
[26] M. J. Hordon, B. S. Lement, and B. L. Averbach, Acta Met. **6,** 446 (1958).
[27] M. J. Druyvesteyn, O. F. Z. Schannen, and E. C. J. Swaving, Physica. **25,** 1271 (1959).
[28] G. A. Alers and D. O. Thompson, J. Appl. Phys. **32,** 283 (1961).
[29] W. Lems, Physica. **28,** 445 (1962).
[30] W. F. Druyvesteyn and B. S. Blaisse, Physica. **28,** 695 (1962).
[31] R. P. Reed and R. P. Mikesell, Adv. in cryogenic Engr. **4,** 84 (Plenum Press, New York, 1958).
[32] R. P. Mikesell and R. M. McClintock, Adv. in Cryogenic Engr. **7,** 509 (Plenum Press, New York, 1961).
[33] P. Jongenburger, Acta Met. **11,** 992 (1963).
[34] J. F. Breedis, Acta Met. **13,** 239 (1965).
[35] R. M. Bozorth, Ferromagnetism (Van Nostrand, New York, 1951).

JOURNAL OF RESEARCH of the National Bureau of Standards—C. Engineering and Instrumentation
Vol. 70C, No. 3, July–September 1966

Publications of the National Bureau of Standards*

Selected Abstracts

Thermal relaxation and Brillouin scattering in liquids, R. D. Mountain, *J. Res. NBS* **70A3** (*Phys. and Chem.*), *No. 3, 207–220* (*May-June 1966*).
Weak coupling of internal degrees of freedom of molecules to the translational degrees of freedom of a fluid results in additional modes of motion for density fluctuations. These new modes affect the spectral distribution of light scattered by density fluctuations so that the Landau-Placzek ratio is not satisfied. The case of thermal relaxation with a single relaxation time is worked out in detail. Formulas for the spectral distribution of the scattered light, for the ratio of the intensities of the central (Rayleigh) to the Brillouin components and for the phonon velocity are derived and applied to carbon disulfide and carbon tetrachloride. The data for carbon tetrachloride are shown to be inconsistent with the single relaxation time model for thermal relaxation.

Calibration of germanium resistors at low temperatures (2–20 °Kelvin), G. Cataland and H. H. Plumb, *J. Res. NBS* **70A3** (*Phys. and Chem.*), *No. 3, 243–252* (*May-June 1966*).
Two germanium resistors, C and D, have been referenced to values of temperature determined by the NBS acoustical thermometer. The resistance-temperature calibration data for these resistors have been fitted to a function of the form $\log_{10} R = \sum_{n=0} A_n (\log_{10} T)^n$ and the results are presented. The resistors C and D that are used as secondary standards maintain the scale, NBS Provisional Scale 2 to 20 (1965), to which public calibrations of germanium thermometers are referenced.
The calibration apparatus and measurement techniques that are employed in calibrating submitted resistors are described in detail. Additionally, data of three typical calibrations and their treatment by polynomial fitting are included to demonstrate the characteristics of some commercially available germanium resistors.

Mechanical relaxation in polyethylene crystallized with various degrees of lamellar orientation, J. M. Crissman and E. Passaglia, *J. Res. NBS* **70A3** (*Phys. and Chem.*), *No. 3, 225–232* (*May–June 1966*).
The mechanical relaxation behavior of a set of well-characterized samples of polyethylene crystallized with different degrees of lamellar orientation is reported. The various samples ranged in morphology from unoriented isotropic samples to ones which showed a high degree of orientation of the *b*-axis along the sample growth direction. The mechanical measurements were made using a torsion pendulum apparatus of standard design, the direction of shear being normal to the *b*-axis for the oriented samples. The temperature range covered was from 100 to 400 °K. No definite effects attributable to orientation were observed for either the γ or β relaxation process, whereas for the α relaxation results for G'' indicate that a slight decrease in peak height resulted from the presence of lamellar orientation, particularly on the high temperature side of this peak. Data for the real and imaginary parts of the complex shear compliance are also discussed.

On a sequence of points of interest for numerical quadrature, S. Haber, *J. Res. NBS* **70B2** (*Math. and Math. Phys.*), *No. 2, 127–136* (*Apr.–June 1966*).
The distribution of 2 sequences of points, originally discussed by van der Corput and by K. F. Roth, is studied in detail. The results obtained disprove a conjecture of J. H. Halton and suggest a conjecture on the improvement of a theorem of Roth.

Treatment of outliers in samples of size three, F. J. Anscombe and B. A. Barron, *J. Res. NBS* **70B2** (*Math. and Math. Phys.*), *No. 2, 141–147* (*Apr.–June 1966*).
Let X be a space of functions, say $X \subset C(K)$, K locally compact Hausdorff, let $l \epsilon X^*$ be an integral on X and let $M^* \subset X^*$ be a given subspace of "simple" functionals, then it is desired to obtain an $l \epsilon M^*$ for given n, $l \epsilon M_n^* \subset M^*$; M_n^* being a suitable n dimensional subspace determined so that l if $l - l$ annihilates a given finite dimensional subspace $X_1 \subset X$. In this general context, the abstract analyses of numerical intergration is developed and certain specific applications are made.

Radio meteorology, B. R. Bean and E. J. Dutton, *NBS Mono. 92* (*Mar. 1, 1966*). *$2.75.*
This volume brings together the work done in radio meteorology over the past ten years at the National Bureau of Standards' Central Radio Propagation Laboratory (CRPL). This decade has seen the development, on an international scale, of great emphasis upon the effects of the lower atmosphere on the propagation of radio waves. The CRPL group has concentrated upon the refraction of radio waves as well as the refractive index structure of the lower atmosphere on both synoptic and climatic scales. These are the areas of radio meteorology that are treated in this volume, with additional chapters on radio-meteorological parameters and the absorption of radio waves by the various constituents of the lower atmosphere.

Copper wire tables, *NBS Handb. 100* (*Feb. 21, 1966*). *50 cents. Supersedes Circ. 31.*
This Handbook is a revision of the Copper Wire Tables previously published as NBS Circular 31. It reflects changes in the nominal diameters of gages 45 and smaller and extends the tables to 56 gage. The changed diameters and extended range were established in 1961 by the Committee on Wires for Electrical Conductors of the American Society for Testing and Materials and were published as ASTM Standard B258–61. They have also been approved as American Standard C7.36–1961 by the American Standards Association. To reduce internal inconsistencies, tables 5 through 14 were completely recomputed by the ASTM Committee on Wires for Electrical Conductors.
The first edition of Circular 31 was published in 1912 at the request of the American Institute of Electrical Engineers. Subsequent editions appeared in 1914 and 1956.

OMNITAB. A computer program for statistical and numerical analysis, J. Hilsenrath, G. G. Ziegler, C. G. Messina, P. J. Walsh, and R. J. Herbold, *NBS Handb. 101* (*Mar. 4, 1966*). *$3.00.*
This user's manual gives the characteristics and application of a general-purpose interpretive program for the generation of physical and mathematical tables on the digital computer using FORTRAN. The vocabulary and sentence structure permit (with only a few simple rules) the translation of a mathematical statement into text understandable both to the user (not necessarily a programmer) and to the machine. The basic vocabulary of slightly over 250 English words is given. These cover the arithmetic and mathematical operations such as ADD, DIVIDE, MULT, SUBTRACT, LOGE, EXP; the elementary and special mathematical functions: SIN, TAN, COSH, TANH, orthogonal polynomials, Bessel functions, elliptic integrals, etc; and various manipulative operations on columns of numbers and on entire arrays.
Detailed instructions are given also for applying the program to: matrix calculations, statistical analysis of experimental data, least-squares curve fitting, linear and nonlinear interpolation, numerical differentiation and integration, solutions of systems of equations, and location of zeros and maxima and minima of algebraic and transcendental functions.
Numerous examples are given of applications of the program to scientific calculations covering a wide spectrum of problems encountered in a research and development organization. Aside from the comprehensive repertoire of mathematical functions and operations, the important features which are stressed are the flexible format-free input and output provisions and curve plotting facility.

Procedures for precise determination of thermal radiation properties, November 1963 to October 1964, J. C. Richmond, S. T. Dunn, D. P. DeWitt, and W. D. Hayes, Jr., *NBS Tech. Note 267 (Dec. 17, 1965). 45 cents.*

A laser-source integrating sphere reflectometer was designed and built to measure the reflectance of specimens at high temperatures. The sphere was calibrated for linearity of response at 0.632μ by means of a shallow cylindrical cavity with a variable depth-to-radius ratio, having a lining of known reflectance. Preliminary tests showed that the flux emitted by a hot specimen at temperatures up to 2500 °K will not invalidate the reflectance measurement. An ellipsoidal mirror reflectometer was calibrated for all known errors in the 1 to 7.5μ range. A preliminary analysis indicates that the errors in measurement of absolute reflectance with this equipment should not exceed 2 percent. A review of the literature on relation of thermal radiation properties to other properties of materials is presented, together with a summary of the work done in an effort to compute the spectral emittance of rhodium.

Earth's field static calibrator for accelerometers, P. S. Lederer and J. S. Hilten, *NBS Tech. Note 269 (Feb. 1, 1966). 20 cents.*

This paper describes a simple, relatively inexpensive system for the precise static calibration of accelerometers in the earth's gravitational field with an estimated limit of error of ± 0.0004 g. The system consists of a precision machinists dividing head on a surface plate and a precision level. Experimental results obtained during the calibtation of three types of accelerometers are shown to indicate the capabilities and usefulness of the system.

Radiochemical analysis: Activation analysis, instrumentation, radiation techniques, and radioisotope techniques, July 1964 to June 1965, ed. J. R. DeVoe, *NBS Tech. Note 276 (Jan. 7, 1966), $1.00.*

This is the second summary of progress of the Radiochemical Analysis Section of the Analytical Chemistry Division at the National Bureau of Standards.

Arrangements for the new facilities at the reactor building and Linac are in their final stages of completion. Additional work is described on the electronics for the handling of data from pulse height analyzers as well as the use of digital computers for processing these data.

A Mössbauer spectrometer which uses optical interferometry in the Doppler drive, and the mechanical design for the electromechanical drive described in last years report are presented. A description of chemical shift of iron compounds is given. The use of a correction factor for certain source detector geometries are described for Mössbauer spectroscopy. A new source of Sn^{119m} in palladium which produces a very narrow line width is also described.

For the first time a trace element has been certified in a Standard Reference Material with the assistance of the activation analysis technique. Flux measurements for the NRL reactor are given. A number of special analyses for various NBS projects by activation analysis are described (e.g., argon in silicon, chlorine in polystyrene, hafnium in zirconium). A beta-gamma sum coincidence gamma-ray spectrometer is described.

A constant potential electrochemical method of analysis using radioisotopic tracers is presented which has potential high sensitivity. A method of using radioisotopic tracers in heterogeneous equilibrium between an aqueous medium of cobalt to be analyzed and manganese dioxide impregnated filter paper is described. Some results on the precision of the substoichiometric radioisotope dilution analysis of silver and iron are presented.

A peak ac-dc voltage comparator for use in a standards laboratory, L. A. Marzetta, *NBS Tech. Note 280 (Jan. 17, 1966).* 25 cents.

An increased availability of high-precision a-c and d-c power sources has allowed routine electrical measurements to be made in the field with a precision previously possible only in the standards laboratory. Ac-dc comparisons are being made on the basis of the peak, rms, and average value of the sine wave source. The peak ac-dc voltage comparator described in this report was developed for use in the standards laboratory to help meet the increasing demand for the certification of new field instruments. The described instrument is capable of establishing the ac-dc error of other peak comparators at frequencies from 50 to 2400 hz with an imprecision of less than 15 ppm.

Keypunch controls for string-punching of statistical data, M. J. Brennan, *NBS Tech. Note 282 (Feb. 11, 1966). 25 cents.*

This note describes controls for a keypunch machine used to key statistical data with "string-punching techniques." Since the data are punched into cards that do not contain fixed field sizes, an identification code is punched for each data entry. To avoid a split field (part on one card and the remainder on another), the keypunch machine is programed to provide a justification zone in which an answer identification code or a "delete" code cannot be keyed. The cards are automatically serialized for each questionnaire and an arrangement is provided to punch an end-of-questionnaire code in the last card for the questionnaire.

An outline for cooperative action on the determination of x-ray mass attenuation coefficients in the wavelength range from 0.5 to 100 Å (25 to 0.12 keV), K. F. J. Heinrich, *NBS Tech. Note 284 (Feb. 21, 1966). 15 cents.*

Sources of information on x-ray mass attenuation coefficients and the present status of data in this area are reviewed. Many gaps are observed in the existing data and some values derived by interpolation may be of questionable accuracy. Because of the importance of accurate mass attenuation coefficients, the extension and improvement of these measurements is proposed together with a plan for coordination of effort and exchange of information.

Computation of the permeability and permittivity of a relatively small ring sample in a toroidal coil, E. G. Johnson, Jr., *NBS Tech. Note 311 (Jan. 25, 1966). 30 cents.*

The derivation and the *FORTRAN* machine program are presented for a formula which gives the *impedance* of a partially filled *toroid coil*. This formula shows the relationship of the *complex permeability and permittivity* of the ring material, the dimensions of the coil and sample, and the frequency of the applied electromagnetic field. Limitations of the formula due to proximity of the ring and coil, range of permeability and permittivity of the ring, and uniformity of the coil winding are considered. The cost of the program in terms of computer time is also considered. The principal value of the formula is to accurately determine the permeability and permittivity of ferrites.

A 100 kW 2–25 Mc/s distributed amplifier, designed for use with 10 kW ionospheric sounders, W. B. Harding, M. W. Woodward, and J. C. Carroll, *NBS Tech. Note 331 (Feb. 15, 1966). 20 cents. (Formerly Central Radio Propagation Laboratory of the National Bureau of Standards, now Environmental Science Services Administration, Boulder, Colo.).*

The principles of distributed amplification have been known for many years and have been applied to fast rise time pulse and oscilloscope amplifiers for small-signal applications [Percival, 1935–37; Pettit and McWhorter, 1961]. This paper describes the design, construction, and testing of an r-f distributed amplifier intended for ionospheric sounding and backscatter applications. The amplifier has a power gain of 10 dB and a rated output of 100 kW peak pulse power, over a range of 2 to 25 Mc/s. A feature of this amplifier is the elimination of input and output transformers.

Restoration of complete dentures inadvertently warped by the patient: Report of case, J. B. Woelfel and G. C. Paffenbarger, *J. Am. Dental Assoc.* **71,** *866–870 (Oct. 1965).*

A set of Hydro-Cast dentures that had given satisfactory service for over 5 years was accidently warped when the patient poured hot water over them. The warpage was manifested by a molar-to-molar shrinkage of 0.43 mm. on the upper and 0.5 mm. on the lower denture. The corresponding flange-to-flange shrinkages were 1.35 mm. on the upper and 0.67 mm. on the lower. These changes rendered the upper denture unusable. Both dentures were satisfactorily altered by selectively grinding areas of the denture base which were in hard contact with the supporting tissues. The apposition of the tissues and the dentures was determined with patterns produced on the tissue-bearing surfaces of the dentures by

a thin coating of a pressure-indicator paste. After four trial adjustments with the upper denture and three with the lower denture, they fitted satisfactorily, were comfortable and functioned well as evidenced by the patient's ability to chew such foods as celery and to play the trumpet regularly. The supporting tissues had a normal appearance after the adjustments.

Spectrophotometric determination of bromine and hydrogen bromide, E. C. Creitz. *Anal. Chem.* **37,** *1690–1692 (Dec. 1965).*
A method is described for determination of Br_2 and HBr in the concentration range zero to one microgram Br per ml. The analysis depends on oxidation of o-tolidine by Br_2 and subsequent colorimetric determination of the yellow oxidation product. Total bromine was determined by measurement of the optical absorption of AgBr suspensions, and HBr obtained by difference. An overall reproducibility of about 2 absorbance units (approximately 70 nanograms per ml) was obtained. Some oxidizing or reducing substances may produce interferences.

Comment on obscurities of oscillator noise, L. Fey, W. R. Atkinson, and J. Newman, *Proc. IEEE Letter* **52,** *104–105 (Jan. 1964).*
Because of the need for knowledge of oscillator noise characteristics and because other published results conflict with those in a recent paper by the present authors, a separate analysis of this published data was made in order to ascertain whether any alternative conclusions might be reasonable. This analysis showed that the data might also be interpreted to imply flicker type noise, as reported by the present authors for oscillators which they examined, rather than noise of a thermal origin as suggested in the original publication.

Cryogenic fluid, two-phase critical flow studies related to reactor systems, R. V. Smith, H. S. Isbin, H. K. Fauske, M. Petrick, C. H. Robbins, and F. R. Zuludek, *Proc. 3d United Nations Intern. Conf. Peaceful Uses of Atomic Energy, Geneva, Switzerland, Aug. 31-Sept. 9, 1964.*
This paper reviews the applications where critical two-phase flow of cryogenic fluids is possible in reactor systems and summarizes the analytical and experimental work that has been done with respect to this problem.

Field strength calibration techniques at the NBS, H. E. Taggart, *IEEE Trans. Electromag. Compatability* **EC-7,** *No. 2, 163–169 (June 1965).*
Instrumentation utilized by the National Bureau of Standards to calibrate field strength meters and standards in terms of absolute field strength at frequencies from 10kHz to 1 GHz are described. Two basic techniques are used: (1) the standard-field method for loop antennas at frequencies from 30 kHz to 30 MHz and (2) the standard-antenna method for horizontally-polarized dipole antennas at frequencies from 30 to 1000 MHz. The accuracy and the limitations of each technique are discussed. Present loop antenna calibration uncertainties vary from 3 to 5 percent depending on the frequency. Dipole antenna uncertainties are presently 12 persent. Various other antenna calibration techniques that have been studied are mentioned, pointing out their limitations. The instrumentation used to calibrate the field strength receiver characteristics is described. These measurements include the calibration of the signal attenuators, calibration of the overall linearity of the receiver, and calibration of the receiver as a two-terminal rf voltmeter.
Future plans of the NBS field strength and noise calibration services are discussed. Improved uncertainties and extended services are planned for antennas from 30 Hz to 1000 MHz. New noise calibration services are planned; these include the calibration of random noise generators at selected frequencies from 30 to 1000 MHz, and the calibration of impulse generators in terms of their spectral density.

Field-strength measurements in a multipath field, C. C. Watterson, *Proc. 4th Natl. IEEE Symp. Radio Frequency Interference, San Francisco, Calif., June 28–29, 1962.*
Field-strength measurements made in the VHF–UHF portion of the spectrum often have limited accuracy and are ambiguous because of the prevalence of multipath propagation. This paper describes a method of making field-strength measurements in a multipath field from which it is possible to calculate the amplitude, polarization, relative time phase, and direction of arrival of each of the multipath components. The method is basically an aperture-synthesis technique which requires that the amplitude and phase of the signal from a moving antenna be measured as the antenna is moved successively along three orthogonal straight-line paths. Three antenna orientations are used on each of the three paths. From the measurements of the signal amplitudes and phases it is necessary to solve nine parallel, similar problems, one for each of the nine combinations of antenna orientation and measurement path. The nine solutions are combined to provide the final solutions for each multipath component: The amplitude and relative time phase of the horizontal electric field component, the amplitude and time phase of the "vertical" electric field component, and the azimuthal and elevation angles of arrival.

Gearing errors as related to alinement techniques of the rotary-vane attenuator, W. Larson, *19th Annual IEEE Conference and Exhibit on Instrumentation and Measurements, New York, N.Y., Oct. 12–15, 1964, Preprint No. 12–5–2–64 (Sept. 1965); IEEE Instr. Meas.* **IM–14,** *No. 3, 117–123 (Sept. 1965).*
The rapid advancement of microwave techniques in the measurement of attenuation, power, noise, and impedance has increased the need for a precision rf variable attenuator. The rotary-vane attenuator appears to be potentially capable for use as a high-precision rf attenuator or attenuation standard. An analysis of the measured errors of a large number of rotary-vane attenuators has shown that the systematic error present is correlated with vane misalinement. Also, a study of the gear mechanism used to drive the rotating vane has revealed another systematic error for which corrections can be made.
Graphs are used to illustrate the readout scale error in decibels at various magnitudes of the drive-gear eccentricity and driven gear pitch diameter. An electrical alinement technique utilizing a correction equal to the "average vane angle error," which is determined from calibration data, is used to aline the rotating vane to an accuracy of $\pm 0.0012°$. Vane alinement by this technique can reduce the systematic error of vane misalinement by an order of magnitude and decrease the deviation in attenuation at high values of attenuation as much as two orders of magnitude.

Optical instrumentation for the biologist, J. R. Meyer-Arendt, *Appl. Opt.* **4,** *No. 1, 1–9 (Jan. 1965).*
A great variety of optical instruments have been developed for use in biology. The microscope and its many special types are part of them. In this article, a survey is given of the history, development, current status, and future outlook of general microscopy, microspectroscopy, interference microscopy, and electron and X-ray microscopy.

The NBS cryogenic data center, *Proc. XI Intern. Congress Refrigeration, Munich, Germany, Aug. 28, 1963, pp. 110–114 (1965).*
A brief description is given of the two principal activities of the Cryogenic Data Center, namely: the evaluation and compilation of data on low temperature properties of materials; and the acquisition, handling and dissemination of technical literature. A program for thorough evaluation and the compilation of thermodynamic and transport properties of cryogenic fluids and selected solids is mentioned. Four functions of the literature service are outlined and typical pictures of the operation included.

Timing and space navigation with an existing ground based system, G. Hefley, R. F. Linfield, and R. H. Doherty, *AGARD Navigation Systems for Aircraft and Space Vehicles, pp. 490–506 (Pergamon Press Inc., New York, N.Y., 1962).*
New time synchronization techniques have been developed with accuracies which make feasible the use of an inverse hyperbolic system for determining the position of space vehicles.
The National Bureau of Standards has developed a Loran-C clock which provides timing and synchronizing accuracies of one microsecond or better and stabilities of 0.1 microseconds or better anywhere within a Loran-C navigation chain. Synchronization of other chains could provide base line lengths equal to an earth's diameter.

Having established a common time base, short pulse transmissions from space vehicles are measured relative to this base. Differences in the time of arrival of these pulses at various ground stations permit space fixes at great ranges.
The time synchronization scheme is discussed along with fix accuracies obtainable as a function of synchronization accuracy and system geometry.

22 ISCC–NBS centroid colors of maximum contrast, K. L. Kelly, *Color Engr.* **3,** *No. 6, 26–27 (Nov.-Dec. 1965).*
Sets of colors having maximum contrast with one another are often needed for color coding. The number of colors required will depend upon the application. Twenty-two ISCC–NBS centroid colors have been selected and arranged in such an order that maximum contrast is obtained by taking the required number of colors from the top of the list.

Elastic stress-strain relations in perfect elastic fluids, B. Bernstein, E. Kearsley, and L. Zapas, *Trans. Soc. Rheol.* **9,** *Pt. 1, 27–39 (1965).*
The theory of perfect elastic fluids deals with the nonequilibrium thermodynamics of finite viscoelastic deformation. The thermodynamics of finite elastic strain and of perfect elastic fluids are discussed. It is shown that the stress-strain relations for perfect elastic fluids may be written in a way which appears formally identical to those in elasticity theory, but the form of this dependence depends on past history.

A stable arc source of high ultraviolet radiance, C. R. Yokley, *Proc. Symp. Solar Radiation Simulation, Los Angeles, Calif., Jan. 18–20, 1965, pp. 107–110 (1965).*
A high pressure argon arc with an intense continuum has been developed as a possible source in ultraviolet radiometry. The wall-stabilized, continuously operating arc exhibits radiance temperatures of about 5000 °K at 2400 Å. Typical operating conditions are currents from 50 to 100 amperes and pressures from 5 to 25 atmospheres. Reproducibility of spectral radiance calibration is about 3 percent when argon flow, arc current, and chamber pressure are regulated within prescribed limits. Short term reproducibility over a period of several hours is about 1 percent in spectral radiance. The spectral radiance is approximately proportional to the square root of the pressure with an upper stability limit of 375 psia for 50-ampere arcs. The arc design, stabilizing and operating techniques along with typical spectral radiance calibrations from 2200 Å to 7000 Å is given.

Coherent Raman effect in the off-axis Raman resonator, D. A. Jennings and H. Takuma, *Appl. Phys. Letters* **4,** *No. 11, 185–186 (June 1964).*
The ruby *Q*-switched laser has been used to excite coherent Raman oscillation in a separate optical resonator. The Raman effect was excited by the 20 MW ruby laser through a hole in one of the mirrors of the Raman resonator. The Raman resonator was placed at a small angle relative to the ruby laser beam axis. Experimental evidence is given to show that the Raman output is a build-up of oscillations along the axis of the Raman resonator.

Estimation of the parameters of the Hyper-Poisson distribution, E. L. Crow and G. E. Bardwell, (*Proc. Symp. Classical and Contagious Discrete Distribution, Montreal, Canada, Aug. 15–20, 1963), Chapt. V, pp. 127–140 (Statistical Publ. Soc., Calcutta, India, 1965).*
The hyper-Poisson family of discrete distributions, a two-parameter generalization of the Poisson distributions, was introduced recently by the authors (Journal of the American Statistical Association, 59, March 1964). In this paper six different pairs of estimators (including four proposed in the previous paper) for the two parameters are presented and discussed: maximum likelihood, two moments, three moments, two moments plus zeroth frequency, mean plus first two frequencies, and two frequencies only. Three of these pairs are given by simple explicit formulae. Asymptotic variances are obtained for the three-moment estimators, and empirical variances for the three pairs of explicit estimators. Some of the estimators are applied to five examples of experimental or survey data.

Generalized variational principles for electromagnetic junctions. Vibrations: application to the theory of waveguide, *Proc. Symp. Electromagnetic Theory and Antennas, Copenhagen, Denmark, June 1962, ed. E. C. Jordan, pp. 253–260 (Pergamon Press Inc., New York, N.Y., 1963).*
Generalized variational principles are stated for the elements—and for the associated electromagnetic fields—of the immittance matrices of waveguide junctions. The formulation applies to junctions containing arbitrary dissipative and anisotropic media, for which the underlying differential equations are not self-adjoint; and, by the use of bilinear (rather than quadratic) functional forms, permits direct treatment of off-diagonal elements of the immittance matrices.

Infrasonic observations of the May 16, 1964, volcanic explosion on the island of Bali, V. H. Goerke, J. M. Young, and R. K. Cook, *J. Geophys. Res.* **70,** *No. 24, 6017–6022 (Dec. 15, 1965).*
The volcanic eruption of Mount Agung on the Island of Bali reached explosive proportions on May 16, 1963. Perturbations generated in the atmosphere traveling at sonic velocities were recorded in Boulder, Colo., 14,700 km distant, both via the short great-circle path and via the long great-circle path through the antipodes and around the world. In Boston, Mass., 16,200 km distant, and in Washington, D.C., 16,300 km distant, sound waves were received via the short great-circle path. The average transit velocity for the short path was 17 m/sec less than for the long path. The effect of wind velocities at mesospheric heights on the transit velocities is discussed.

On the use of thermopiles for absolute radiometry in the far ultraviolet, R. G. Johnston, and R. P. Madden, *Appl. Opt.* **4,** *No. 12, 1574–1580 (Dec. 1965).*
Thermopiles used for absolute radiometry in the far ultraviolet spectral region are generally calibrated with visible and near infrared radiation. Three possibilities for the failure of the sensitivy of thermopiles to be independent of wavelength have been investigated. It was found that gold-black typical of that used on thermopiles for far ultraviolet applications reflectivity scattered 2 to 4 percent of the incident far ultraviolet radiation. Since the same gold-black scattered a similar fraction of incident visible and near infrared radiation, the correction for this effect was small. An analysis of surface sensitivity maps indicated that a thermopile of 0.04-sec time constant showed no wavelength variation of sensitivity when either dc detection or ac synchronous detection with 13 cps chopping was used. The most significant wavelength-dependent phenomenon was found to be the photoelectric effect. Ejected electrons carry a significant amount of energy away from gold-blacked thermopiles in the spectral region below 1600 Å. The maximum correction determined for a particular thermopile was 5.2 percent at λ 735 Å.

Solute nuclear magnetic resonances in primary lead alloys, L. H. Bennett, R. M. Cotts, and R. J. Snodgrass (*Proc. XIIIth Colloque and Relaxation in Solids), Book, Nuclear Magnetic Resonance and Relaxation in Solids, ed. L. V. Gerven, pp. 171–180 (North Holland Publ. Co., Amsterdam, The Netherlands, 1965).*
The nuclear magnetic resonances of In^{115}, Bi^{209}, Tl^{205}, Hg^{199}, and Sb^{121} as solutes in fcc primary lead solid solutions have been measured. The room temperature Knight shifts for these solutes at low concentration in Pb are: In^{115}, $k=0.86\%$; Bi^{209}, $k=1.15\%$; Tl^{205}, $k=1.93\%$; Hg, $k=2.41\%$ and Sb^{121}, $k=0.66\%$. In all cases the change of Knight shift with temperature, magnetic field, or concentration, if any, is small. Quadrupole effects, if any, are small. From the temperature dependence of the linewidth for Tl^{205}, T_1 is found to be about 7 μ sec, compared with 7.3 μ sec found by use of the Korringa relation. Comparison of the solute shifts is made both with the solvent shift, and with the shift of the solute in itself, assuming a free electron model.

Brush cathode plasma—a well behaved plasma, K-B. Persson, *J. Appl. Phys.* **36,** *No. 10, 3086–3094 (Oct. 1965).*
Results of probe, spectroscopic and microwave studies are used to describe properties of a novel cold cathode discharge. The use of a brush cathode greatly exaggerates some of the usual cold cathode mechanisms, thus determining the interesting features of

the plasma produced. The cathode fall is about an order of magnitude larger than for the corresponding normal cold cathode. The brush cathode generates a uniform electron beam in the energy range 1 to 10 kilovolts and a corresponding negative glow with a longitudinal dimension (reaching distance of the beam) one to two orders of magnitude larger than for the normal cathode. The large dimensions of the negative glow and the fact that it is extremely well-behaved (no instabilities and no striations) make it ideal for a whole series of investigations in plasma physics and spectroscopy. The electron density in the helium plasma is in the range 10^{10} to 10^{14} cm^{-3}, the electron temperature in the range 0.05 to 0.10 eV. The negative glow is beam generated (essentially field free) and recombination dominated making it a practically uniform plasma ideal for the study of rate and transport coefficients. Preliminary measurements of the particle balance give a recombination rate of 5×10^{-10} cm^3 sec^{-1} at 1100 °K and an electron density of 3×10^{12} cm^{-3} in excellent agreement with the collisional-radiative recombination theory developed by Bates, Kingston, and McWhirter. The recombination light emitted by the plasma is sufficiently strong to make spectroscopic methods very useful for measurements of the electron density and the electron temperature. Lines in the series $2s^3S - np^3P^0$ are observed up to the quantum level $n = 30$.

The realization and use of the international practical temperature scale of 1948, J. P. Evans, *ISA 20th Annual Conference and Exhibit, Los Angeles, Calif., Oct. 4–7, 1965), ISA Preprint 14.3–1–65 (1965).*
This paper describes the International Practical Temperature Scale of 1948, the methods and accuracy with which it is realized, and the current efforts being made to improve the scale. Methods of transferring the scale to temperature measuring instruments are also discussed.

Topside sounding as a tool for global ionosphere studies, R. W. Knecht, *IEEE Trans. Ant. Prop. Programs Digest, pp. 21–23 (1963).*
With the advent of the successful Alouette topside sounding satellite, a powerful new technigue has become available for exploration and mapping of the ionosphere. Observations of the ionosphere from above by means of satellite-borne sounders offers the possibility of the rapid collection of synoptic ionospheric data on a global basis. Given data storage on the satellite and appropriate ground data transmission facilities, short-term ionospheric mapping may be possible. Results so far obtained from the Alouette satellite regarding the structure and variability of the topside ionosphere will be presented.

Thermal conductivity and viscosity of simple fluids, J. V. Sengers, *Intern. J. Heat Mass Transfer* **8,** *1103–1116 (1965).*
The behavior of the thermal conductivity and viscosity coefficient of simple fluids as a function of pressure, density and temperature is surveyed. Particular attention is given to the behavior of the transport coefficients in the critical region. In a previous paper [1] it was shown that the thermal conductivity coefficient exhibits a pronounced maximum in the critical region. Additional information confirming the existence of such a maximum is presented.
Theoretical predictions of the transport coefficients in dense systems are often based on the theory of Enskog. A survey is presented showing to what extent the theory of Enskog describes the density dependence of the transport coefficients in monatomic fluids. Finally, the transport mechanism leading to the anomalous rise of the thermal conductivity in the critical region is indicated.

International comparison on dielectric measurements, E. Rushton, G. Russell, B. W. Petley, H. E. Bussey, J. E. Gray, E. C. Bamberger, and D. Morris, *IEEE Trans. Instr. Meas.* **IM–13,** *No. 4, 305–311 (Dec. 1964).*
Three materials, namely fused silica, glass, and alumina, were selected for comparison based on known or expected homogeneity, isotropy, and stability. Measurements were made by the three international laboratories, both in the radio frequency range using capacitor type holders either with or without an air gap, and at microwave frequencies using either cavity resonance methods or transmission line impedance methods. The results show agreement among the three laboratories of better than one per cent for the real part of the permittivity. Also, the dispersion from 9 GHz to 1 MHz is reasonable. The agreement on loss tangent is less satisfactory and is being investigated. A second round of measurements is in progress and with the expectation that closer agreement will result.

Lightning characteristics as derived from sferics, W. L. Taylor, *(Proc. 3rd Intern. Conf. Atmospheric and Space Electricity, Montreus, Switzerland, May 1963), Book, Problems of Atmospheric and Space Electricity, ed. S. C. Coroniti, pp. 388–404 (Elsevier Publ. Corp., Amsterdam, The Netherlands, 1965).*
Lightning discharges emit electromagnetic signals, called atmospherics or sferics, that usually attain a spectral peak within the VLF region; i.e., 3 to 30 kc/s. Primary emphasis is placed on this band of frequencies for describing lightning discharge characteristics. The important problems and limitations in utilizing atmospherics are discussed with reference to particular research areas. These areas include: 1) measurements of the radiation field from lightning discharges, 2) determination of VLF and ELF propagation characteristics, 3) observations of atmospherics for specialized purposes such as study of the thunderstorm mechanisms and detecting and tracking thunderstorms, and 4) radio interference from lightning discharges.

New developments in dental materials: A world-wide survey, G. C. Paffenbarger, *Intern. Dental J.* **15,** *No. 3, 311–422 (Sept. 1965).*
General discussion of a symposium prepared by the moderator, G. C. Paffenbarger, chairman, Commission on Dental Materials, Instruments, Equipment and Therapeutics of the Federation Dentaire Internationale.

MAGIC—A machine for automatic graphics interface to a computer, D. E. Rippy and D. C. Humphries, *Proc. Fall Joint Computer Conf., Nov. 20–Dec. 2, 1965, Los Vegas, Nevada, pp. 819–830 (Spartan Books, Inc., Wash., D.C. 1965).*
This report describes a machine which has been developed within the Computer Technology Section of the National Bureau of Standards as a research tool for the investigation of man-machine communication techniques. This machine has been designated MAGIC (Machine for Automatic Graphics Interface to a Computer) and consists of large-diameter cathode-ray displays combined with a small, specially designed, programmable digital computer. It is intended to operate as a remote display station connected to a large ADP system via voice-quality communication lines.
MAGIC is subdivided into two basic units: the processor unit and the display unit. The display unit consists of two CRT displays termed primary and secondary. The processing unit is also subdivided into a control processor and four subordinate list processors. Three of these subordinate list processors operate directly on data displayed by the primary display, utilizing list processing techniques. Described is the software repertoire and hardware design of MAGIC, particularly that which pertains to the subordinate list processors. Conclusions are drawn with respect to the adequacy of the original system design. Future plans for MAGIC, and the proposed design and construction of a Model II MAGIC are discussed.

The NBS time scale and its relation to other time scales, J. A. Barnes and R. C. Mockler, *(Proc. XIV General Assembly of URSI, Tokyo, Japan, 1963), Book, Progress in Radio Science 1960–1963. Vol.* **I.** *Radio Standards and Measurements, ed. R. W. Beatty, p. 41 (Elsevier Publ. Co., Amsterdam, The Netherlands, 1965).*
Newman, Fey and Atkinson established an atomic time scale using the time pulses of WWV and based on the United States Frequency Standard (USFS) in Boulder, Colorado. The hyperfine structure separation was assumed to be 9192631770.00 . . . cps. The rate of the WWV clock is determined by comparison with VLF transmissions from Boulder which are in turn referred to the USFS. NBS atomic time was assigned to WWV time pulses beginning in October 1957. These assignments were compared with similar assignments by the U.S. Naval Observatory according to their A. 1 time scale. The NBS atomic time was made to agree with A. 1 time on January 1, 1958. Since that date the two scales have diverged at an average rate of about 1×10^{-10} sec/sec.
More recently atomic clocks have been placed in operation at Boulder also based on the USFS. The precision of these clocks is

normally about 0.3 microseconds per day (3×10^{-12}). The absolute time differences between this clock at Boulder, the clock at WWV, the clock at the U.S. Naval Observatory and the clock at the Loran-C master station at Cape Fear, North Carolina, were determined by carrying a portable clock between these various stations. The absolute time difference between these clocks was known to $\pm 5\mu$ sec. at the time of the measurement, April 24, 1963. The results of this experiment yielded experimental values for the composite propagation and receiver delays between these stations. With these results the Loran-C time pulses are now used to continuously compare the clock times of NBS-A and the U.S. Naval Observatory time A. 1.

Annual report of the National Bureau of Standards, C. E. Moore, *Astron. J.* **70,** *No. 9, 637–639 (Nov. 1965).*
This report is furnished annually to the Astronomical Journal in order to present to astrophysicists the spectroscopic work that they are particularly interested in. It is published with the Observatory Reports and provides a brief summary of activity at the NBS.

A review of zinc oxide-eugenol type filling materials and cements, G. M. Brauer, *Rev. Belge. Med. Dent.-Belg. Tijds. Tandheelk* **20,** *No. 3, 323–364 (1965).*
A review is given of the status of zinc oxide-eugenol type cements as well as modifications of these materials developed in this laboratory and elsewhere. The mechanism of the setting reaction and the physical, histological and clinical properties of these cements are discussed. Zinc oxide-eugenol cement is decidedly superior to other materials in its palliative effect on the pulp and in patient comfort. Whereas, solubility is low and initial adaptation to the cavity walls unusually good, its low strength and lack of resistance to abrasion confine its use to restorations not involving high stress or attrition. Properly formulated, it is the cement of choice for selected restorations.
Recent investigations have explored the possibilities of improving the desirable physical properties. Incorporation of *o*-ethoxybenzoic acid has led to materials that appear promising as bases and cementing materials for inlays and crowns. Further studies should lead to stronger, more adhesive and more permanent restorative materials that are impermeable to moisture.

Separation of pyrenediones by column chromatography, A. J. Fatiadi, *J. Chromatog.* **20,** *319–324 (1965).*
The 1,6- and 1,8-pyrenedione were separated directly on a column of silica gel by means of glacial acetic acid as the eluant. The final purification of 1,6-pyrenedione was accomplished on a column of activated alumina by use of benzene as the solvent. The IR and UV spectra of purified 1,6-, 1,8-, and 4,5-pyrenedione and of 1-oxo-6,7-phenalenedicarboxylic acid anhydride were recorded.

The thermal degradation mechanism of polystyrene, L. A. Wall, S. Straus, J. H. Flynn, D. McIntyre, and R. Simha, *J. Phys. Chem.* **70,** *No. 1, 53–62 (Jan. 1966).*
New and extensive measurements of (1) the rates of volatilization and (2) the molecular weights as a function of the extent of pyrolysis are reported for various polystyrene samples, in particular, fractions spanning a broad range of molecular weights. The experimental observations are shown to be described quite well by the results of computer calculations based on the theory of free-radical degradation and a mechanism involving four elementary reactions – initiation, depropagation, intermolecular transfer, and termination by disproportionation. Certain characteristics of the volatilization rates are sensitive to intermolecular transfer, which is required together with pure end initiation in order to match theory with experiment. "Weak links" appear to be absent although introduction of a relatively slight amount of random scission, which would be important at large molecular weights, may improve the agreement. A tendency toward higher than theoretical weight-average degrees of polymerization during pyrolysis may be indicative of a small amount of termination by combination, diffusion-controlled rates, and a failure of the molecular weight relationship.

Zone refiner with temperature control, F. Ordway, *Anal. Chem.* **37,** *1178–1180 (Aug. 1965).*
The sample tube is heated and cooled by fluids of controlled temperatures, circulating through successive chambers in a carrier that slides along the rotating sample tube. Mixing and loss of the fluids are substantially eliminated by use of commercial shaft seals to separate the chambers.

A simple method for making stereoscopic drawings, F. Ordway, *Am. Mineralogist* **50,** *1496–1498 (1965).*
Stereoscopic pairs of drawings are made on a film-measuring device that has a cursor movable along a graduated scale. One drawing is fixed to the scale, the other to the cursor. Points are plotted simultaneously on both by using carbon paper or a needle point, after setting the cursor for the required parallax distance.

A system for accurate direct and alternating voltage measurements, F. L. Hermach, J. E. Griffin, and E. S. Williams, *IEEE Trans. Instr. Meas.* **IM-14,** *No. 4, 215–224 (Dec. 1965).*
A system for calibrating and using a group of dc and ac standards has been developed at NBS to meet increasing needs for greater accuracy in the measurement of direct and rms alternating voltages at audio frequencies. With a group of saturated cells, a universal ratio set as a potentiometer, a simplified self-calibrating volt box, and a new differential-thermocouple ac-dc comparator, an accuracy of 10 ppm can be obtained for direct voltage measurements and 40 ppm for rms alternating voltage measurements between 20 and 20,000 c/s, in terms of the direct volt and the ac-dc transfer standards maintained at NBS.

Effect of surface roughness on emittance of non-metals, J. C. Richmond, *J. Opt. Soc. Am.* **56,** *No. 2, 253–254, (Feb. 1966).*
It has been observed experimentally, both at NBS and elsewhere, that the emittance of polished metals can be markedly increased by roughening the surface, by as much as a factor of 2 or 3. For non-metals and particularly white ceramic materials, on the other hand, the emittance appears to be essentially independent of surface roughness, at least for wavelengths below 7 or 8 microns. This apparent anomaly is explained on the basis of the differences in the optical properties of the two types of materials.

Comparison of uncertainty ellipses calculated from two spectrophotometric colorimetry methods by an automatic-computer program, I. Mineroff, *J. Opt. Soc. Am.* **56,** *No. 2, 230–237 (Feb. 1966).*
The parameters and equations for calculating uncertainty of chromaticity coordinates in spectrophotometric tristimulus colorimetry have already been derived for the 10°-field standard-observer system. From the variability data for eleven optical filters obtained from two methods of spectrophotometric tristimulus colorimetry, standard-observer-system method and actual-observer method, two sets of chromaticity uncertainty ellipses are derived and intercompared. The similarity between corresponding ellipses of these two sets of ellipses leads to the conclusion that the system-derived uncertainty ellipses, based on the variances and covariances of the spectral tristimulus values of the large-field standard-observer system, can be used to estimate observer-derived chromaticity-uncertainty ellipses.
The equations which are the basis of the automatic-computer program and with which to compute uncertainty ellipses are given to aid anyone who wishes to arrange such a program in his laboratory. The fixed combinations of the spectral tristimulus values of their variances and covariances can be readily prepared by researchers who may wish to use desk calculators to compute uncertainty ellipses for actual-observer data or for standard-observer-system data, respectively.

An international comparison of current-ratio standards at audio frequencies, B. L. Dunfee and W. J. M. Moore, *IEEE Trans. Instr. Meas.* **IM-14,** *No. 4, 172–177 (Dec. 1965).*
The results and analysis of an intercomparison between the National Research Council (NRC), Canada and the National Bureau of Standards (NBS), Washington, of two contrasting types of current ratio standards (current comparator and current transformer) are presented. The agreement achieved between the two laboratories when their respective designs and methods of measurement were quite different is emphasized. To this end, the basic theories underlying the design and operation of the current comparator and current transformer are contrasted; the origin and significance of their respective errors are summarized; the $(N+1)$ method used at NBS

to measure the errors of the multi-range transformer standards up to 10 kHz is contrasted with the $N+1$ method (one of several) used at NRC in calibrating the comparator standards. The comparison circuit used at NRC to compare the respective standards of the two laboratories is described. The errors of the transformers as measured at NBS and NRC are presented and contrasted in both tabular and graphical forms.

The design and performance of multirange current transformer standards for audio frequencies, B. L. Dunfee, *IEEE Trans. Instr. Meas.* **IM-14,** *No. 4, 190–204 (Dec. 1965).*
The design, construction, and performance of two nearly identical, multi-range current transformers for operation 400 Hz to 16 kHz and with errors of only a few ppm are discussed. A general discussion of the parameters that influence the performance of single-stage transformers and their consideration in effecting minimum errors throughout a wide frequency band is included. Construction of the two standards having consecutive ratios 1/1 to 6/1 and operating at a rated secondary current of 5 amperes is described with the aid of line drawings. Circuit diagrams are presented and used to describe (1) the self-calibration circuit for measuring the errors of the 1/1 ratios and (2) the $(N+1)$ circuit together with an auxiliary circuit for measuring the errors of ratios > 1. Balance equations are derived in an Appendix. Measured values are presented in tabular form and include, in addition, the results obtained at the National Research Council Canada, during an international comparison and described in a companion paper. The effects of polarization at low frequencies is particularly emphasized by utilizing the 400 Hz data together with information obtained in supplementary experiments; also, the role of winding and interwinding capacitances and the necessity for a more explicit definition of current ratio at the higher frequencies is high-lighted.

High-frequency elastic moduli of simple fluids, R. Zwanzig and R. D. Mountain, *J. Chem. Phys.* **43,** *No. 12, 4464–4471 (Dec. 15, 1965).*
This article presents a calculation of the infinite-frequency elastic moduli of monatomic fluids. When the intermolecular potential has the standard Lennard-Jones form, the elastic moduli are shown to be related to the pressure and internal energy of the fluid. Numerical values of the elastic moduli at various densities and temperatures are presented in tabular and graphical form. An identity is derived relating the shear and bulk moduli of any isotropic material in which particles interact by means of two-body central forces; this is a generalization of the familiar Cauchy identity occurring in the theory of elasticity of solids. The approach is based on analysis of the high-frequency limit of exact time-correlation function expressions for shear and bulk viscosity.

Photometry, L. E. Barbrow, *Book, Encyclopedia of Physics, pp. 516–519 (Reinhold Publ. Corp., New York, N.Y. 1966).*
The photometric quantities luminous intensity and flux, illuminance and luminance, and luminous reflectance, transmittance, directional reflectance factor, and directional transmittance factor are defined, the methods of measuring them are briefly described, and the factors which affect the accuracy of the measurements are discussed. Included is a table of the currently internationally agreed-upon symbols for the photometric and related radiometric quantities and units.

Adhesive bonding of various materials to hard tooth tissues. V. The effect of a surface-active comonomer on adhesion to diverse substrates, R. L. Bowen, *J. Dental Res.* **44,** *No. 6, 1369–1373 (Nov.-Dec. 1965).*
A surface-active comonomer or coupling agent (NPG-GMA, the addition-reaction product of *N*-phenylglycine and glycidyl methacrylate) has been found to improve significantly the bond strength between a direct-filling resin and fluorapatite. Since fluorapatite surfaces contain no organic material, this demonstrates that the collagen and other organic constituents of enamel and dentin are not essential to the improvement of bonding produced by the NPG-GMA. It does not follow, however, that the organic constituents play no role in the bonding. The objectives of the present investigation were primarily to observe the effects of NPG-GMA on the bonding to unmineralized collagen and keratin and secondarily to learn more about NPG-GMA and its behavior in bringing about improved bonding between a methacrylate resin and hard tooth tissues.

Chemical analysis, G. M. Brauer and G. M. Kline, *Encyclopedia of Polymer and Technology* **3,** *633–665 (John Wiley & Sons Inc., New York, N.Y., 1965).*
The chemical analysis of polymeric materials is reviewed. Preparation of the sample, physical tests, thermal degradation techniques and chemical procedures such as analysis for functional and end groups and characterization tests are discussed. Instrumental techniques that are employed in the analysis of polymers are described and systematic schemes for the analysis of high molecular weight compounds are outlined.

Viscosity and density of boron trioxide, A. Napolitano, P. B. Macedo, and E. T. Hawkins, *J. Am. Ceramic Soc.* **48,** *No. 12, 613–616 (1965).*
Extensive and accurate viscosity values for molten B_2O_3 are reported over the continuous range from 20 poises (at 1400 °C) to 10^{10} poises (at 318 °C). The measurements were made with a wide range rotating cylinder viscometer. The melts were pretreated by bubbling super dry nitrogen through them to insure that the water content was at a minimum. Densities were also determined between 1400 and 400 °C. Above 800 °C the temperature dependence of the viscosity curve was Arrhenius, below this it had a smooth curvature showing no breaks. At the low temperatures, although its curvature decreased, the viscosity curve was not Arrhenius.

Comparison of xenon and carbon arcs as radiation sources for laboratory weathering of asphalts, K. G. Martin, P. G. Campbell, and J. R. Wright, *Am. Soc. Testing Mater. Proc.* **65,** *809–830 (1965).*
The xenon- and carbon-arc weatherometers were compared as radiation sources for the laboratory weathering of coating-grade asphalts using aluminum-backed asphalt films of 25 mils thickness and unsupported films of 25 microns (1 mil) thickness. The 25-mil films were exposed to the ASTM Daily Cycle A and degradation was measured by the spark-probe technique. The 25-micron films were irradiated at a controlled humidity level, but were not exposed to the cold water spray. Photooxidation was measured by infrared spectroscopy.
Since the xenon source operated on a near continuous basis, it required less total time to cause failure of the 25-mil films than did the carbon-arc machine, although the latter degraded asphalts about 1.2 times faster per hour of exposure. The order of durability of asphalts, from a given source group, was reversed for the carbon arc compared to the xenon arc, but when asphalts of similar source were considered in groups to the overall correlation between the two weatherometer types was good. The spark-probe test method was found to influence greatly the durability results from both weatherometers. Thermal shock, alone, had little effect. Photooxidation rates of the 25-micron films were of the same order for xenon and solar sources, but a different order for carbon-arc exposures.

Proposed standard for measuring and reporting physical properties of optical materials, G. W. Cleek, F. J. P. Consitt, and W. D. Lawson, *Infrared Phys.* **5,** *141–160 (Dec. 1965).*
For some time there has been evidence of a lack of data on the properties of optical materials, particularly as a function of temperature. This has been particularly apparent to designers of optical equipment which has to operate in unusual environments e.g., in space vehicles, or which has to withstand severe conditions during critical periods of operation e.g., during rocket launch. For instance refractive indices have in general been measured only around room temperature but optical instruments with complex lens systems may be required to function at either much higher or much lower temperatures.
Another problem arises through different manufacturers of optical materials using different methods and specimens for measuring physical properties and presenting the data differently. This frequently makes it difficult for a user to compare directly optical materials from different sources and in general he does not wish to set up and carry out comparative measurements himself. Thus

the development of a joint set of standards on methods of measuring and reporting the properties of optical materials was considered highly desirable.
With the needs of the optical designer in mind the authors have attempted to list specific properties of interest, outline standard methods of measuring these properties, and suggest standard methods of presenting the results. We have used for illustration, in Appendix C, the data on synthetic sapphire listed in the manufacturer's data sheets.

Techniques for detection of high-altitude nuclear explosions, A. G. Jean, C. E. Hornback, R. H. Doherty, J. R. Winkelman, and R. T. Moore, *Proc. IEEE* **53,** *No. 12, 2088–2098 (Dec. 1965).*
The Central Radio Propagation Laboratory (CRPL) is conducting a study for the Advanced Research Projects Agency (ARPA) project VELA of ground based techniques for detecting geophysical effects produced by nuclear explosions at altitudes above about 20 km and in space. This activity is called HANDS for High Altitude Nuclear Detection Studies. A substantial amount of experimental data exists on effects produced by high-altitude explosions and theoretical predictions have been made of effects expected from explosions in space. The ability to record and identify these signatures is limited by knowledge of the natural background. The objective of the HANDS is to acquire data on natural background required in the design of future detection systems. The experimental facility for collecting background data at conventional and more rapid rates from a collection of colocated geophysical sensors is described.

The analysis, synthesis, and description of biological images, L. E. Lipkin, W. C. Watt, and R. A. Kirsch, *Ann. N.Y. Acad. Sci.* **128,** *No. 3, 984–1012 (Jan. 31, 1966).*
There may be distinguished two approaches to characterizing the properties of biological images: the statistical approach traditionally used for mechanized image-processing, and the articular approach generally used among biologists. We discuss both approaches, but focus attention on the second, for we hold that an articular approach allows the expression of much that is effectively impossible to express in the form of numerical measurements; and we know of no inherent reason why a computer cannot deal with information of a nonquantitative nature.
The articulation of biological images necessarily takes place on two fronts: the imposition of an articular structure on the image itself; and the expression of this construal in English sentences. We will study both kinds of articulation, and we will suggest how they may be brought together, in the form of linked pictorial and linguistic *grammars.* The computer system which this paper envisions will be able to analyze a presented image with respect to a pictorial grammar, and to formulate and accept descriptions of that image, in English sentences, with respect to a linguistic grammar. It will be able to present pictorial instances of English descriptions, and in other ways to respond to English directives.

Multivibrator provides bidirectional output pulses, F. C. Ruegg, *Electronics* **38,** *No. 17, 87 (Aug. 8, 1965).*
A bipolar flip-flop with variable output levels has been designed. The circuit can be used to test the frequency response of many transistor circuits, and there are many applications in the field of logic circuitry.

Precision of cubic lattice parameter measurements by the Kossel technique, H. Yakowitz, *Trans. Symp. Electron Probe Analysis, Oct. 12–15, 1964, Wash., D.C., pp. 417–438 (John Wiley & Sons, Inc., New York, N.Y., 1966).*
The major factors affecting the precision of cubic lattice parameter measurement by means of the Kossel technique are considered. It is shown that three special cases can be solved rigorously for projection distortion effects and that obtaining these cases is not difficult. The fact that a lens ratio method should be employed to reduce measured lengths on the film to lattice parameter values is emphasized. General formulae for the lattice parameter and the geometric sensitivity are presented. Correction and minimization of errors resulting from refractive index effects and temperature variations is indicated to be possible. An example of the determination of the lattice parameter of LiF is given. The indicated sensitivity of the method expresses the relative standard error of the mean lattice parameter of LiF, is given by $\frac{\Delta a}{a_{LiF}} = 2.54 \times 10^{-6}$.

Status of linear relations among heats of transport, R. E. Howard and A. B. Lidiard, *J. Chem. Phys.* **43,** *No. 11, 4158–4160 (Dec. 1, 1965).*
It is shown that previously derived linear relations among the heats of transport contain no physical information, but serve only to complete the definition of these quantities in situations where the fluxes of the various components of the system are not linearly independent. Other defining equations are possible but physical predictions are unaffected by the choice so presented. This resolves the paradox of the apparent inconsistency of these linear relations with kinetic theories of heats of transport.

Stress-strain properties of textile yarns subjected to rifle bullet impact, C. A. Fenstermaker and J. C. Smith, *J. Appl. Polymer Sci.* **1,** *125–146 (1965).*
If a flexible filament is struck transversely by a rifle bullet, and the motion observed by flash photography, data can be obtained on the resulting strain distribution and on the time required to break the filament. The theory and experimental procedure for obtaining these data are described and test data are given for a sample of polyester yarn. These data include strain distributions at various times after impact and at various impact velocities, and a plot of breaking time versus impact velocity. Data analysis shows that although creep and stress relaxation occurred within 50 μ sec after impact, during the next 150 μ sec the creep and relaxation effects were too small to be observed. At an impact velocity of 174 m/sec the strain at the point of impact changed from an initial value of 1.08 percent to a 50 μ sec value of 1.27 percent, and the corresponding stress from 15.26 g/tex to 14.51 g/tex. The yarn sample broke within 10 μ sec when impacted at 620 m/sec velocity, but required 100 μ sec to break at an impact velocity of 420 m/sec.

The effect of humidity on ionization measurements with cavity and free-air chambers, T. P. Loftus, B. Petree, and J. T. Weaver, J. *Radiology* **86,** *No. 1, 149 (Jan. 1966).*
Measurements are described that show the effect of humidity on the measurement of gamma radiation with cavity ionization chambers. It is found that the chamber current does not vary by more than 0.06 percent as the relative humidity is changed by more than 50 percent. A calculation, based on the assumption that the air and its moisture produce ionization independently, predicts a decrease of about 0.4 percent for the measurement in moist air. The discrepancy is believed to be connected with the value used for the average energy required to produce an ion pair in moist air.
Similar results were obtained with a free-air chamber exposed to 60 kVcp x rays. A current increase of only 0.03 percent was observed when the relative humidity was changed from 48 to 13 percent, although the calculated increase is 0.3 percent.

Other NBS Publications

J. Res. NBS 70A3 (Phys and Chem.), No. 3 (May–June 1966), $1.00

Thermal relaxation and Brillouin scattering in liquids. R. D. Mountain (See above abstracts).
Density of polyethylene crystals grown from solution. G. M. Martin and E. Passaglia.
Mechanical relaxation in polyethylene crystallized with various degrees of lamellar orientation. J. M. Crissman and E. Passaglia. (See above abstracts).
Pentafluorophenyl alkyl and vinyl ethers. W. J. Pummer and L. A. Wall.
Calibration of germanium resistors at low temperatures (2–20 °Kelvin). G. Cataland and H. H. Plumb. (See above abstracts).
Dissociation pressure of aluminum carbide using a rotating Knudsen cell. E. R. Plante and C. H. Schreyer.
Determination of intermolecular potential functions from macroscopic measurements. M. Klein.

J. Res. NBS 70B2 (Math. and Math. Phys.), No. 2 (Apr.–June 1966), 75 cents.

On a sequence of points of interest for numerical quadrature. S. Haber. (See above abstracts.)

On abstract numerical integrations. J. J. Sopka.

Treatment of outliers in samples of size three. F. J. Anscombe and B. A. Barron. (See above abstracts.)

A note on contaminated samples of size three. T. A. Willke.

Realizing the distance matrix of a graph. A. J. Goldman.

Pairs of nonsingular matrices. K. Goldberg.

Upper bounds for the determinant of a row stochastic matrix. K. Goldberg.

Groups preserving ordering in vectors. K. Goldberg.

A table of radiation characteristics for uniformly spaced optimum endfire arrays with equal sidelobes, M. T. Ma and D. C. Hyovalti, NBS Mono. 95, (Dec. 10, 1965), 45 cents.

Quarterly radio noise data September, October, November 1964, W. Q. Crichlow, R. T. Disney, and M. A. Jenkins, NBS Tech. Note 18–24 (Feb. 10, 1966), 50 cents. (Formerly the Central Radio Propagation Laboratory of the National Bureau of Standards, now Environmental Science Services Administration, Boulder, Colo.)

Materials for PLACEBO V, W. C. Watt, NBS Tech. Note 281 (Jan. 17, 1966), 50 cents.

An atlas of solar flare effects in the ionosphere observed with a high-frequency Doppler technique, September 1960–December 1962, D. M. Baker, NBS Tech. Note 326 (Dec. 1, 1965), 60 cents. (Formerly the Central Radio Propagation Laboratory of the National Bureau of Standards, now Environmental Science Services Administration, Boulder, Colo.)

The seasonal variation of nightglow NaI 5890–96 A, [01] 5577 A and [01] 6300 A in the tropics, L. L. Smith and R. W. Owen, NBS Tech. Note 329 (Jan. 10, 1966), 35 cents. (Formerly the Central Radio Propagation Laboratory of the National Bureau of Standards, now Environmental Science Services Administration, Boulder, Colo.)

Computations of the antenna cut-back factor for LF radio waves, D. C. Hyovalti, NBS Tech. Note 330 (Nov. 26, 1965), 30 cents. (Formerly Central Radio Propagation Laboratory of the National Bureau of Standards, now Environmental Science Services Administration, Boulder, Colo.)

Deuterium isotope effect in vacuum-ultraviolet absorption coefficients of water and methane, A. H. Laufer and J. R. McNesby, Can. J. Chem. **43,** No. 12, 3487–3490 (Dec. 1965).

Electrochemical methods, J. K. Taylor, E. J. Maienthal, and G. Marinenko, Book, Trace Analysis: Physical Methods, ed. G. H. Morrison, chapt. 10, pp. 377–433 (Interscience Publ. Inc., New York, N.Y., 1965).

Interaction of oxygen with platinum, A. J. Melmed, J. Appl. Phys. **36,** No. 11, 3691–3692 (Nov. 1965).

Proton transfer reactions occurring in the gas-phase radiolysis, P. Ausloos and S. G. Lias, Discussions Faraday Soc. **39,** 36–44 (1964).

Solid-vapor equilibrium in the system hydrogen-methane, M. J. Hiza and R. N. Herring, (Proc. 1964 Cryogenic Engineering Conf., Philadelphia, Pa., Aug. 17–21, 1964), Book, International Advances in Cryogenic Engineering, ed. K. D. Timmerhaus, 10, Sec. Q, pp. 182 (Plenum Press, Inc., New York, N.Y., 1965).

A bounded automorphic form of dimension zero is constant, M. I. Knopp, J. Lehner, and M. Newman, Duke Math. J. 32, No. 3, 457–460 (Sept. 1965).

Density distribution of polymer segments in the vicinity of an absorbing interface, C. A. J. Hoeve, J. Chem. Phys. **43,** No. 9, 3007–3008 (Nov. 1, 1965).

Error bounds for asymptotic solutions of second-order differential equations having an irregular singularity of arbitrary rank, F. W. J. Olver and F. Stenger, J. SIAM, Ser. B. **2,** No. 2, 244–249 (1965).

Generalized functions of symmetric matrices, M. Marcus and M. Newman, Proc. Am. Math. Soc. **16,** No. 4, 826–830 (Aug. 1965).

Inequalities for permanents and permanental minors, R. A. Brualdi and M. Newman, Proc. Camb. Phil. Soc. **61,** 741–746 (Jan. 1966).

Normal subgroups of the modular group which are not congruence subgroups, M. Newman, Proc. Am. Math. Soc. **16,** No. 4, 831–832 (Aug. 1965).

On the asymptotic solutions of second-order differential equations having an irregular singularity of rank one, with an application to Whittaker functions, F. W. J. Olver, J. SIAM, Ser. B. **2,** No. 2, 225–243 (1965).

Real two-dimensional representations of the modular group and related groups, J. Lehner and M. Newman, Am. J. Math. **87,** No. 4, 945–954 (Oct. 1965).

The fundamental solution and Huygens' principle for decomposable differential operators, J. E. Lagnese, Archive Rat. Mech. Anal. **19,** No. 4, 299–307 (Jan. 22, 1965).

A latitude survey of the night airglow, T. N. Davis and L. L. Smith, J. Geophys. Res. **70,** No. 5, 1127–1138 (Mar. 1965).

A theoretical study of the Martian and Cynthian ionospheres, R. B. Norton, Natl. Aeronautic. Space Admin. Tech. Note TN D–2333 (1964).

Atomic lifetimes in neon I, J. Z. Klose, Phys. Rev. **141,** No. 1, 181–188 (Jan. 7, 1966).

Comment on the "Difference between a non-LTE, and a pure absorption, model for the line-blanketing effect," R. N. Thomas, Astrophys. J. **141,** No. 1, 333–335 (Jan. 1965).

Flare importance ratings—some hope for improvement, C. S. Warwick, Proc. Natl. Aeronautics Space Admin. Flare Conf. The Physics of Solar Flares, pp. 27–28 (1964).

Generalized master equation for arbitrary initial states, J. Weinstock, Phys. Rev. **140,** No. 1A, A98–A99 (Oct. 4, 1965).

Interaction of 350-keV polarized neutrons with oriented ^{165}Ho nuclei, R. Wagner, P. D. Miller, T. Tamura, and H. Marshak, Phys. Rev. **139,** No. 1B, B29–B46 (July 12, 1965).

Nonanalyticity of transport coefficients and the complete density expansion of momentum correlation functions, J. Weinstock, Phys. Rev. **140,** No. 2A, A460–A465 (Oct. 18, 1965).

Nonlinear ambipolar diffusion across a magnetic field, K. B. Persson and E. R. Mosberg, Phys. Fluids **7,** No. 11, 1829–1833 (Nov. 1964).

Nuclear size determination by neutral-pion photoproduction, R. A. Schrack, Phys. Rev. **140,** No. 4B, B987–B904 (Nov. 22, 1965).

Phonon induced nuclear dipole transitions, R. J. Mahler (Proc. XIIIth Colloque and Relaxation in Solids), Book, Nuclear Magnetic Resonance and Relaxation in Solids, ed. L. V. Gerven, pp. 202–209 (North Holland Publ. Co., Amsterdam, The Netherlands, 1965).

Remarks on a paper by T. Makino "On the cosmic-ray cut-off rigidities and the earth's magnetic Field," H. H. Sauer, Report of Ionosphere and Space Research in Japan **19,** No. 1, 54–55 (1965).

Spectra of C_2 in solidified gases at 4° and 20 °K, R. L. Barger and H. P. Broida, J. Chem. Phys. **43,** No. 7, 2371–2376 (Oct. 1, 1965).

Spectra of C_3 in solidified gases at 4° and 20 °K, R. L. Barger and H. P. Broida, J. Chem. Phys. **43,** No. 7, 2364–2370 (Oct. 1, 1965).

Spectrum of stationary homogeneous magnetohydrodynamic turbulence, C. M. Tchen, Phys. Fluid **8,** No. 9, 1659–1667 (Sept. 1965).

Suppression at high temperature of effects due to statistics in the second virial coefficient of a real gas, S. Y. Larsen, J. E. Kilpatrick, E. H. Keb, and H. F. Jordan, Phys. Rev. **140,** No. 1A, A129–A130 (Oct. 1965).

The relationship of a.c. resonant probes to resonant scattering, W. M. Leavens, Physics Letters **19,** No. 2, 118–120 (Oct. 1, 1965).

A study of auroral absorption events at the south pole: 2. Conjugate properties, J. K. Hargreaves and H. J. A. Chivers, J. Geophys. Res. **70,** No. 5, 1093–1102 (Mar. 1965).

Characteristic variations in the antarctic ionosphere, V. L. Peterson, G. Stonehocker, and J. W. Wright, Antarctic Research Series, Am. Geophys. Union, Geomagnetism and Aeronomy **4,** 47–75 (1965).

Interrelations of sporadic *E* and ionospheric currents, S. Matsushita, Book, Ionospheric Sporadic-*E*, Ed. E. K. Smith and S. Matsushita, chapt. II, pt. C, No. 5, 344–375 (Pergamon Press Inc., New York, N.Y., 1962).

Long term characteristics for air-ground propagation in band nine, R. S. Kirby, IEEE Antenna Propagation Intern. Symp. Digest, pp. 43–47 (July 9–11, 1963).

On the continuity equation for electron density in the ionosphere, T. Shimazaki, J. Atmospheric Terrest. Phys. **27,** 593–604 (1965).

Studies of Alouette observations at the CRPL, W. Calvert, H. Rishbeth, and T. Van Zandt, Trans. American Geophysical Union, IG Bull. **45,** No. 2, 398–401 (June 1964).

Gas phase radiolysis and vacuum ultraviolet photolysis of 2- and 3-pentanone, A. Scala and P. Ausloos, J. Phys. Chem. **70,** No. 1, 260–269 (Jan. 1966).

Quenching of the triplet state of acetone and biacetyl by various unsaturated hydrocarbons, R. E. Rebbert and P. Ausloos, J. Am. Chem. Soc. **87,** No. 24, 5569–5572 (Dec. 20, 1965).

Vacuum-ultraviolet photolysis of ethane at high temperature. II. Collisional deactivation of excited ethylene, R. F. Hampson, Jr., and J. R. McNesby, J. Chem. Phys. **43,** No. 10, 3592–3596 (Nov. 15, 1965).

Foreword, R. G. Scott, Book, Cryogenics, pp. V (Reinhold Publ. Corp., New York, N.Y., 1964).

Oxygen metastable atom production through photodetachment, L. M. Branscomb, S. J. Smith, and G. C. Tisone, J. Chem. Phys. **43,** No. 8, 2906–2907 (Oct. 15, 1965).

The current revision of the solar spectrum table λ 2935 Å to λ 8770 Å, C. E. Moore, Proc. Utrecht Symp. Solar Spectrum, Utrecht, The Netherlands, August 26–31, 1963, ed. C. DeJager, pp. 89–101 (D. Reidel Publ. Co., Dordrecht, The Netherlands, 1965).

Total cross section for 14 MeV neutrons using alined ^{165}Ho nuclei, H. Marshak, A. Richardson, and T. Tamura, Phys. Rev. Letters **16,** No. 5, 194–197 (Jan. 31, 1966).

Influence or irregular terrain on propagation, J. W. Herbstreit (Proc. XIV General Assembly of URSI, Tokyo, Japan, 1963), Book, Progress in Radio Science 1960–1963. Vol. **II.** Radio and Troposphere, ed. F. du Castel, pp. 141–156 (Elsevier Publ. Co., Amsterdam, The Netherlands, 1965).

Application of a high-intensity, multi-slit Raleigh interferometer to sedimentation studies, I. H. Billick and R. J. Bowen, J. Phys. Chem. **69,** 4024–4030 (1965).

Crystal and molecular structure of $C_4B_{20}H_{22}$, bis (o-dodecacarborane), L. H. Hall, A. Perloff, F. A. Mauer, and S. Block, J. Chem. Phys. **43,** No. 11, 3911–3917 (Dec. 1965).

Dissociation of ammonium ion in methanol-water solvents, M. Paabo, R. G. Bates, and R. A. Robinson, J. Phys. Chem. **70,** No. 1, 247–251 (1966).

Electrochemistry, W. J. Hamer, Book, Encyclopedia of Physics, pp. 200–203 (Reinhold Publ. Corp., New York, N.Y., 1966).

'Kinetics of the hydroxyl radical in aqueous solution, F. Sicilio, R. E. Florin, and L. A. Wall, J. Phys. Chem. **70,** No. 47, 47–52 (Jan. 1966).

Manganese-hydrogen bond distance in $HMn(CO)_5$, T. C. Farrar, W. Ryan, A. Davison, and J. W. Faller, J. Am. Chem. Soc. **88,** 184 (Jan. 5, 1966).

Matrix-isolation infrared spectrum of the free radical CCO, M. E. Jacox, D. E. Milligan, N. G. Moll, and W. E. Thompson, J. Chem. Phys. **43,** No. 10, 3734–3746 (Nov. 1965).

Matrix-isolation infrared spectrum of the free radical NH_2, D. E. Milligan and M. E. Jacox, J. Chem. Phys. **43,** No. 12, 3487–4493 (Dec. 15, 1965).

Matrix isolation study of the photolysis of cyanogen azide. The infrared and ultraviolet spectra of the free radical NCN, D. E. Milligan, M. E. Jacox, and A. Bass, J. Chem. Phys. **43,** No. 9, 3149–3160 (Nov. 1, 1965).

Patterns of thinking in searching patent applications by manual and machine-assisted methods, J. R. Cornog and P. P. Ellis, J. Chem. Doc. **5,** 215–225 (Nov. 1965).

Photolysis of cyclobutane at photon energies below and above the ionization energy, R. D. Doepker and P. Ausloos, J. Chem. Phys. **43,** No. 11, 3814–3819 (Dec. 1, 1965).

The effect of gamma-irradiation on a polyamide, V. J. Kransnansky, M. S. Parker, and R. E. Florin, J. Phys. Chem. **70,** No. 1, 40–46 (Jan. 1966).

Color, D. B. Judd, Book, Encyclopedia of Physics, pp. 113–116 (Reinhold Publ. Corp., New York, N.Y., 1966).

Deposition of energy by neutrons in spherical cavities, R. S. Caswell, Radiation Res. **27,** No. 1, 92–107 (Jan. 1966).

Initiation of spherulite growth: The case of concurrent homogeneous and heterogeneous nucleation, F. Gornick, J. Appl. Phys. **36,** No. 10, 3012–3014 (Oct. 1965).

Limits on calorimetric residual entropies of glasses, A. B. Bestul and S. S. Chang, J. Chem. Phys. **43,** No. 12, 4532–4533 (Dec. 15, 1965).

Nuclear moments of Pm^{147}, J. Reader, Phys. Rev. **141,** No. 3, 1123–1128 (Jan. 1966).

Erratum-Nuclear magnetic moment of Pr^{141} from the hyperfine structure of doubly ionized praseodymium, J. Reader and J. Sugar, Phys. Rev. **140,** No. 7AB, AB3 (Dec. 27, 1965).

Two-dimensional probability distribution in a turbulent field, F. N. Frenkiel and P. S. Klebanoff, Phys. Fluids **8,** No. 12, 2291–2293 (Dec. 1965).

Relativistic electron precipitation into the mesosphere at subauroral latitudes, D. K. Bailey and M. A. Pomerantz, J. Geophys. Res. **70,** No. 23, 5823–5830 (Dec. 1, 1965).

Absolute-velocity mossbauer spectrometer, J. J. Spijkerman and F. C. Ruegg, Trans. Am. Nucl. Soc. **8,** No. 2, 344 (1966).

A simple device for adjusting dental interferometers, H. J. Caul and J. W. Kumpula, J. Dental Res. **44,** No. 6, 1412 (Nov.-Dec. 1965).

Determination of trace amounts of cadmium and silver by substoichiometric radioisotopic dilution analysis, A. R. Landgrebe, L. T. McClendon, and J. R. DeVoe, Trans. Am. Nucl. Soc. **8,** No. 2, 315–316 (1966).

Dissociation of acetic acid-d_3 in aqueous solution and related isotope effects from 0 to 50°, M. Paabo, R. G. Bates, and R. A. Robinson, J. Phys. Chem. **70,** 540–543 (1966).

Magnesium isotope ratios in natural samples, E. J. Catanzaro and T. J. Murphy, J. Geophys. Res. **71,** No. 4, 1271–1274 (Feb. 15, 1966).

NMR studies of inorganic fluorides. I. High-resolution ^{19} F spectra of Si_2F_6 and $(SiF_3)_2$ O, R. B. Johannesen, T. C. Farrar, F. E. Brinckman, and T. D. Coyle, J. Chem. Phys. **44,** No. 3, 962–964 (Feb. 1, 1966).

On the limiting shape of the distribution function of lengths of a single polymer molecule with excluded-volume effects, J. Mazur, J. Chem. Phys. **43,** No. 12, 4354–4356 (Dec. 15, 1965).

Propagation of electromagnetic pulses in terrestrial waveguides, J. R. Wait, IEEE Trans. Ant. Prop. **AP–13,** No. 6, 904–918 (Nov. 1965).

The low temperature removal of small quantities of nitrogen or methane from hydrogen gas by physical adsorption on a synthetic zeolite, A. J. Kidnay and M. J. Hiza, A.I.Ch.E.J. **12,** No. 1, 58–64 (Jan. 1966).

Departures from local thermal equilibrium in a magnetically-driven shock wave, K. L. Eckerle and R. W. P. McWhirter, Phys. Fluids **9,** No. 1, 81–89 (Jan. 1966).

Effect of normal-fluid motion on third sound in liquid-helium films, G. L. Pollack, Phys. Rev. **143,** No. 1, 103–109 (Mar. 4, 1966).

Mossbauer line broadening in SnO_2, R. H. Herber and J. Spijkerman, J. Chem. Phys. **42,** No. 12, 4312–4314 (June 15, 1966).

Precision of cubic lattice parameter measurements by the Kossel technique, H. Yakowitz, Trans. Symp. Electron Probe Analysis, October 12–15, 1964, Washington, D.C., pp. 417–438 (John Wiley & Sons, Inc., New York, N.Y., 1966).

Radiative corrections. I. High-energy bremsstrahlung and pair production, K. Mork and H. Olsen, Phys. Rev. **140,** No. 6B, B1661–B1674 (Dec. 20, 1965).

Random-walk calculations of diffusion coefficients, R. E. Howard, Proc. 5th Intern. Symp. Reactivity of Solids, Munich, Germany, 1964, pp. 250–255 (Elsevier Publ. Co., Amsterdam, The Netherlands, 1965).

Relative transition probabilities for prominent Ni I and Ni II lines in the near-ultraviolet, G. D. Bell, D. R. Paquette, and W. L. Wiese, Astrophys. J. **143,** No. 2, 559–572 (Feb. 1966).

Resonances in the elastic and inelastic electron scattering from N_2, H. G. M. Heideman, C. E. Kuyatt, and G. E. Chamberlain, J. Chem. Phys. **44,** No. 1, 355–358 (Jan. 1, 1966).

The correction factor for fast neutron reactions on sulfur and oxygen in the manganous-sulfate-bath calibration of neutron sources, W. M. Murphey, Nucl. Instr. Methods **37,** No. 1, 13–21 (1965).

An investigation of concentric ring antennas with low sidelobes, C. O. Stearns and A. C. Stewart, IEEE Trans. Ant. Prop. **AP–13,** No. 6, 856–863 (Nov. 1965).

On radiation of electromagnetic and electroacoustic waves in plasma. Part II, J. R. Wait, Appl. Sci. Res. **12,** Sect. B, 130–138 (1965).

**Publications for which a price is indicated are available by purchase from the Superintendent of Documents, U.S. Government Printing Office, Washington, D.C., 20402 (foreign postage, one-fourth additional). The NBS nonperiodical series are also available from the Clearinghouse for Federal Scientific and Technical Information, Springfield, Va., 22151. Reprints from outside journals and the NBS Journal of Research may often be obtained directly from the authors.*

U.S. GOVERNMENT PRINTING OFFICE : 1966 OL—217-689

UNITED STATES
GOVERNMENT PRINTING OFFICE
DIVISION OF PUBLIC DOCUMENTS
WASHINGTON, D.C. 20402

OFFICIAL BUSINESS

POSTAGE AND FEES PAID
U.S. GOVERNMENT PRINTING OFFICE

JOURNAL OF RESEARCH of the National Bureau of Standards Vol. 70C, No. 3 July–September 1966
C. Engineering and Instrumentation

Contents

Page

Some harmonic properties of an oscillating Fabry-Perot interferometer. M. Gaussen and H. M. Williams. 159

Precise reflection coefficient measurements with an untuned reflectometer. W. E. Little and D. A. Ellerbruch. 165

A versatile ratio instrument for the high ratio comparison of voltage or resistance. Alfred E. Hess. 169

Console for the rapid and precise comparison of volt boxes. Patrick H. Lowrie, Jr. 173

Corrosion rates of binary alloys of nickel and iron measured by polarization methods. W. J. Schwerdtfeger. 187

The effect of cold-drawing on the creep behavior of a nickel-4.2 percent aluminum alloy. William D. Jenkins and William A. Willard. 195

Magnetic transformation and the influence of plastic strain on the shear modulus of Fe-Cr-Ni alloys. R. P. Mikesell and R. P. Reed. 207

Publications of the National Bureau of Standards. 211

Library of Congress Catalog Card Number: 62–3900

For sale by the Superintendent of Documents, U.S. Government Printing Office, Washington, D.C., 20402. Price 75¢ (single copy). Subscription price: $2.75 a year; 75¢ additional for foreign mailing.
UNITED STATES GOVERNMENT PRINTING OFFICE, WASHINGTON : 1966